SISSA ISAS

SCUOLA INTERNAZIONALE SUPERIORE DI STUDI AVANZATI
INTERNATIONAL SCHOOL FOR ADVANCED STUDIES

Hubbard U enhanced superconductivity

Thesis submitted for the degree of

Doctor Philosophiæ

Candidate:
Evgeny Plekhanov

Supervisors:
Prof. Michele Fabrizio
Prof. Sandro Sorella

October 2003

Summary

We present a study of the superconducting properties of models containing the Hubbard repulsion term. This strong on-site repulsion is considered as a key ingredient of the high temperature superconductivity. Though the fact that for the normal, low temperature superconductors, repulsion destroys superconducting order, it is argued in the present thesis, that for the pairing of the d-wave symmetry in the strongly correlated electronic systems its effect is to enhance and may be to cause superconductivity. Various methods such as Variational Monte Carlo, Gutzwiller Approximation, Time Dependent Hartree-Fock and Fixed Node Approximation have been used to investigate $t-U-W$ model, $t-U-J-V$ and pure Hubbard models.

In this thesis, by considering correlations contribution to the BCS condensation energy due to the Hubbard U it is shown that the latter lowers the total energy of a d-wave superconductor in the weak coupling limit, thus enforcing the stability of such superconductor. This effect appears to be mainly due to the enhancement of the spin fluctuations near the nesting vector $\vec{Q} = (\pi, \pi)$.

It is then studied the crossover from weak to strong coupling regimes in $t-U-J-V$ model by increasing U. Remarkably in this model an order of magnitude growth of the superconducting order parameter is found and explained as being due to the Hubbard repulsion. We find also, that the pairings, originally induced by spin or charge fluctuations upon increase of U are differently renormalized, being the former enhanced, while the latter suppressed.

In the final part of the thesis the superconductivity in the pure Hubbard model is carefully studied by means of Variational Monte Carlo and related numerical methods aimed to improve variational results. We observe the onset of strong coupling superconductivity at $U/t \sim 7$ within the Fixed Node Approximation in the systems of large size and compare our results for small clusters with those of Lanczos diagonalization. We show that Variational Monte Carlo, though overestimating the quasiparticle weight ($Z_{\mathrm{VMC}} > Z_{\mathrm{exact}}$) succeeds in reproducing the correct pairing between quasiparticles.

Contents

Introduction

Superconductivity represents a remarkable phenomenon where quantum coherence effects appear at macroscopic scale. The theoretical bases of this unusual state of matter were put forward by Bardeen, Cooper and Schrieffer [1], who introduced in 1957 a variational many-body wave-function, thereafter called BCS wave-function, which provided a unique framework able to explain the key features of superconductivity, like the Meissner or the isotope effects. BCS theory was built out of several fundamental observations: first the isotope effect which pointed to a relevant role played by the electron-phonon coupling, secondly the overscreening of the Coulomb repulsion among the electrons which, thanks to the electron-phonon coupling, turns into an attraction at energy-transfer smaller than a typical phonon frequency and thirdly the just discovered Cooper-phenomenon which showed the instability of the Fermi sphere towards formation of bound-pairs of electrons in the presence of attraction [2]. Therefore, even though the mean-field BCS Hamiltonian only involved electronic degrees of freedom, yet phonons were a key ingredient built into the theory to describe the attraction between electrons, which stabilize the BCS wave function.

Soon after however the deep meaning of the BCS wave function as well as of superconductivity itself, independently of the precise microscopic details, was unveiled mainly by Anderson [3]. It became clear that the superconducting properties, especially the perfect diamagnetism, are microscopic manifestations of the spontaneous breakdown of one of the fundamental symmetries of matter, namely the U(1) gauge symmetry. That property allowed to separate at the conceptual level the phenomenon of superconductivity from the microscopic models which may display such a behavior, which also played an important role for instance in extending the BCS analysis to superfluid ^{3}He.

Indeed the discovery of High-T_c superconductors in cuprates by Bednortz and Muller [7] in 1986 has demonstrated that superconductivity is a phenomenon which goes beyond the conventional microscopic explanation provided by BCS as well

from its improvement by the Migdal-Elishberg theory [4, 5]. Macroscopically, High-T_c superconductivity is not that different from conventional Low-T_c one: perfect diamagnetism, absence of residual resistivity, flux quantization of charge $2e$. Yet, by more careful inspection, the whole microscopic foundations on which BCS theory was built on can not be used to explain cuprate superconductivity. That seems to us not only because cuprates lack relevant isotope effect, which can still be fit into BCS theory by assuming that the mediators of attractions are not phonons, but because of more fundamental reasons. The conventional BCS theory identifies superconductivity as an instability of the Fermi sea. That assumes the existence of a normal Landau-Fermi-liquid which forms well above T_c, which eventually turns into a superconductors below T_c due to (a) a residual attraction among low-lying quasiparticles which overcomes the Coulomb repulsion, efficiently screened by higher-energy excitations; (b) the Cooper instability of a Fermi sea of quasi-particles. In cuprates there is an overwhelming evidence that superconductivity does not appear as an instability of a Landau-Fermi liquid but rather of an anomalous metal. Apart from the well known non-Fermi liquid temperature behavior of transport properties [6], the most striking anomaly is the pseudo-gap [8] which is observed in the under-doped normal phase. Evidently that can not be compatible with a conventional Fermi liquid.

It is widely accepted that the key feature of cuprates, which was emphasized soon after their discovery by Anderson, is the strong-correlation. This shows up manifestly in the fact that un-doped cuprates are Mott antiferromagnetic insulators, and it is also the main reason why, almost twenty years after their discovery, they are still a puzzle for theorists. Indeed there is not even consensus on the mechanism driving superconductivity. It has for instance been proposed that the strong-repulsion itself provides this mechanism, either emphasizing the nature of the non-Fermi liquid normal phase which might emerge by doping an antiferromagnetic Mott insulator [9, 11], or the role of antiferromagnetic fluctuations as mediator of paring [10, 12]. Otherwise it has been argued that strong-correlations, by suppressing electron motion, pushes the system into an unstable state very sensible to any kind of charge/spin ordering. In this almost critical state superconductivity might emerge as a response to huge quantum fluctuations [13, 14]. Yet, in spite of all the fascinating theoretical proposal, the final theory of High-T_c superconductivity is still lacking.

In this Thesis we hope to shed some light on this controversial issue, without any pretension to propose the nth theory of superconductivity, but just with the purpose to understand better the physical properties of most common models for cuprates: the Hubbard and the t-J models.

It was first proposed by Anderson [18] that the Hubbard model correctly captures the relevant physics for superconductivity which emerges in the CuO_2 planes. This model has been known from early sixties when Hubbard has introduced it to describe the Mott-insulating phase in the transition metal oxides. The single-band Hubbard model is probably the simplest many-body model for correlated electrons; apart from a free tight-binding term it contains a short-range interaction piece which prevents doubly occupied sites. Despite its simplicity, there are no analytic solutions for the Hubbard model apart from one dimension. First-principle calculations predict that in cuprates the electron-electron on-site repulsion U is strong as compared with the hopping parameter t : $U/t \sim 4 \div 12$. In this case simple mean field theory fails, since the interaction cannot be treated as a small perturbation, and only non-perturbative techniques may be of help.

Numerous analytic approaches have proposed to treat the repulsive Hubbard model. Weak coupling Renormalization Group studies [19] seem to reveal an instability in the Cooper channel with $d_{x^2-y^2}$ symmetry, compatible with the gap-symmetry in cuprates. Kohn-Luttinger instability may also be a route to superconductivity in the weak coupling limit [20]. Fluctuation exchange approximation - an attempt to go beyond Hartree-Fock theory, obeying local conservation laws - also shows some tendency towards $d_{x^2-y^2}$-wave superconductivity [21]. In the strong coupling limit more appropriate for cuprates, the Hubbard model maps onto $t-J$ model, which i) possesses an explicit pairing mechanism provided by the spin-exchange and ii) it is indeed known from numerical calculations to be superconducting. This fact might support the weak coupling evidences, and suggests a d-wave superconducting ground state all the way from weak Hubbard U, with a Kohn-Luttinger small T_c, to strong U, with a much larger T_c.

The simplest analytic approximation which goes beyond Hartree-Fock is the so called Random Phase Approximation (RPA). It only takes into account the quantum fluctuations around the Hartree-Fock solution. At the mean-field level, the Hubbard repulsion does not compete with $d_{x^2-y^2}$-wave superconductivity, since the on-site pair amplitude is zero, but only with hopping. One is therefore legitimated to examine the role of repulsion in a d-wave superconductors as opposed to a normal metal within RPA. The comparison between the quantum fluctuations corrections to the energy in both the above cases, the so called exchange-correlation energy, may provide an alternative indication of how the Hubbard interaction affects $d_{x^2-y^2}$-wave superconductivity.

Along with analytical treatments, numerical methods developed in the past few

decades represent a valuable source of information. In particular Lanczos technique provides an unbiased information on the ground state energy and wave function, which can be then used to estimate the accuracy and check the validity of any given approximation. It is restricted however to systems of extremely small sizes, since the Hilbert space of the problem grows exponentially with the size.

Quantum Monte Carlo methods allow to study bigger sizes. They are in principle exact if it were not for the sign problem. For the repulsive Hubbard model, however, this is not the case and the most interesting regions of U, doping and temperature remain still unreachable for quantum Monte Carlo. Several approximate Monte Carlo methods have been proposed, among them the variational Monte Carlo technique (VMC), which we are going to use in the present work. VMC provides not only an upper bound for the exact ground state energy but also it possesses the so called zero-variance property: the variance of a variational state is the smaller the closer this state is to the exact one, becoming zero if the two coincide. Thus, comparing the variance of different variational states one can estimate how close they are with respect to the exact one. Moreover it is even possible to make a variance extrapolation of physical quantities, thus having at least two distinct variational estimates for their ground state values. Among the advantages of variational Monte Carlo is its relative simplicity, which allows a careful analysis of nontrivial results and the possibility of a comparison between different phases. It can be efficiently implemented by sampling the electronic configurations with the Metropolis algorithm, using the square of the wave function as the probability density.

The results of variational Monte Carlo depend drastically on the choice of the trial function, which needs therefore to be properly chosen. As it was pointed out above, the Green's function Monte Carlo can not be efficiently implemented for the Hubbard model with large U and away from half filling. This is because the fermionic wave function can have regions of positive and negative sign and hence the weights of the configurations in the weighted average can change sign, which leads to a well defined mean value but with enormous fluctuations. The simplest workaround from this problem, used in the present thesis is the so called Fixed Node (FN) approximation [22], when the nodes of the exact ground state are approximated by the nodes of a variational guess, called guiding function. FN is known to improve significantly the variational state in a controlled way, since its energy is also variational, i.e. an upper bound to the exact one. Using variational Monte Carlo simulations, Gros [23] indeed found an enhancement of the $d-$wave superconductivity, but tentatives to improve the wave function by going beyond variational approach have led to controversial

conclusions, confirming [24, 25] or denying [26] the presence of superconductivity.

In the first Chapter of this thesis we review and compare some aspects of Low-Temperature and High-Temperature superconductivity, which are relevant for our work. We also introduce the lattice models often used to describe the physics of High-T_c cuprates and which we study in the present thesis: the one-band Hubbard as well as the $t-J$ models.

In the second Chapter we introduce the general methodology of quantum Monte Carlo (QMC) as well as variational Monte Carlo (VMC) and Fixed Node approximation (FN), which will be used in the succeeding chapters.

In Chapter 3 we study within random phase approximation (RPA) the one-band Hubbard model in the small U limit and in the presence of a small W term, proportional to the square of the kinetic energy. This additional term provides an explicit attraction between electrons. It is shown therein that the Hubbard repulsion U, although irrelevant at the BCS level, lowers the condensation energy within RPA, thus favoring $d_{x^2-y^2}$ superconductivity.

In Chapter 4 we study the crossover from weak to strong coupling in $t-J-U$ model at fixed J and varying U within the variational Monte Carlo. At $U=0$ we have a $t-J$ model without the constraint of no double occupancy. At small J, this model is undoubtedly a weak coupled BCS superconductor. By increase of U, the strong suppression of double occupancies occurs, which we find leads to a growth of the variational gap by even one order of magnitude. A comparison with Gutzwiller approximation is made, and the behavior of the long-range order parameter is analyzed respect to that of the variational gap.

In Chapter 5 we investigate the possibility of the superconductivity in the pure Hubbard model within variational Monte Carlo and FN approximations. An unexpectedly large variational gap is found for the region of $U > 8 \div 15t$ and doping $\delta = 16\%$. This effect is then analyzed as a function of system size and doping. long range order parameter and condensation energy are also calculated. A comparison with the exact Lanczos diagonalization results for the condensation amplitude is made for the 18 site system.

Chapter 1

Superconductivity

1.1 Low-T_C versus High-T_C

1.1.1 BCS theory

Since its discovery by Kamerling Onnes at the beginning of twentieth century [27] *superconductivity* remained an unexplained phenomenon over almost 50 years. Indeed superconductors display unusual properties in comparison with conventional metals in their normal phase, most notably

- the Meissner effect, *i.e.* perfect diamagnetism, for not too strong magnetic fields;

- the absence of resistivity.

The explanation of the above phenomenon had to wait until Bardeen, Cooper and Schrieffer [1] proposed a variational wave-function, thereafter called BCS wave-function, on the basis of relevant physical arguments which they successfully screened out of the rich phenomenology of superconductors. Here we do not intend to discuss the theory of conventional superconductors, for which we make reference to very popular books [28, 29], but just to introduce some aspects which are pertinent to our work.

The BCS wave-function

BCS in their original work introduced a variational wave-function of the form:

$$|\Psi_{BCS}\rangle = \prod_k \left(u_k + v_k c^\dagger_{k,\uparrow} c^\dagger_{-k,\downarrow}\right)|0\rangle, \tag{1.1}$$

emphasizing the tendency to form zero-momentum singlet pairs of electrons which was put forward by Cooper [2]. as a key ingredient to understand superconductivity. The variational parameters are chosen as those which minimizes the expectation value of a model Hamiltonian:

$$H_{BCS} = \sum_{k,\sigma} \varepsilon_k c^\dagger_{k,\sigma} c_{k,\sigma} + \sum_{k,k'} V(k,k') c^\dagger_{k,\uparrow} c^\dagger_{-k,\downarrow} c_{-k',\downarrow} c_{k',\uparrow} \tag{1.2}$$

subject to the condition that the average number of particles is fixed:

$$N_0 = \frac{1}{V}\sum_k \langle n_k \rangle. \tag{1.3}$$

u_k and v_k are not independent in (1.1), they are related by normalization condition: $u_k^2 + v_k^2 = 1$. Thus it is more convenient to introduce another variable, θ_k, such that $\cos\theta_k = v_k$ and $\sin\theta_k = u_k$. After minimization we have for θ_k:

$$\sin 2\theta_k = \frac{\Delta_k}{E_k}, \quad \cos 2\theta_k = -\frac{\xi_k}{E_k}. \tag{1.4}$$

In (1.4) $\xi_k = \varepsilon_k - \mu$, being μ the chemical potential, Δ_k is the order parameter and $E_k = \sqrt{\xi_k^2 + \Delta_k^2}$. μ and Δ_k are determined self-consistently from the following self-consistency equations (BCS equations):

$$\begin{cases} \Delta_k &= -\frac{1}{V}\sum_{k'} V(k,k') \sin 2\theta_{k'} \\ N_0 &= \frac{1}{V}\sum_{k'} \cos 2\theta_{k'}. \end{cases} \tag{1.5}$$

Several remarks should be made concerning the above equations:

i) An obvious solution exists when $\theta_k = 0$ inside the Fermi surface and $\theta_k = \pi/2$ otherwise and corresponds just to Fermi gas. Thus our wave function (1.1) includes it as a trivial solution.

ii) It follows that $V(k,k')$ must be negative, especially for $k \sim k'$ (attraction among electrons) to get non-trivial solution. One can show that such solution exists for arbitrarily small attraction and has lower free energy respect to the Fermi gas. The latter is thus unstable with respect to superconducting pairing.

iii) Since in (1.1) we assumed spin-singlet pairing, then $\Delta_k = \Delta_{-k}$. We can expand Δ_k into components having definite lattice symmetry. Thus we can speak about s-wave, d-wave, etc., superconductivity. The symmetry of Δ_k is determined by the symmetry of the interaction $V(k,k')$.

For instance, the solution of (1.5) assuming an attraction V constant in the vicinity of Fermi surface within some cutoff ω_c and zero outside reads:

$$\Delta = 2\omega_c \exp\left(-\frac{1}{\rho_0 V}\right), \tag{1.6}$$

being ρ_0 the density of states at Fermi surface. The inverse exponential dependence upon interaction strength shows that the phenomenon is highly non perturbative in V. In conventional superconductors, as we will mention, ω_c is proportional to the typical phonon energy, $\omega_c \to \hbar\omega_D$, which provides an explanation for the observed isotope effect.

An important quantity measuring the spatial correlation between Cooper-paired electrons is the *correlation length*, defined as:

$$\xi = \frac{\hbar v_F}{\pi\Delta}. \tag{1.7}$$

In conventional superconductors ξ ranges from $50\mathring{A}$ to $10^4\mathring{A}$.

The energy gain with respect to the best Fermi-liquid state is called *condensation energy* and for the model solution (1.6) can be easily calculated:

$$E_{SC} - E_{FL} = -\frac{\rho_0\Delta^2}{2}. \tag{1.8}$$

Finally, another quantity which will be of interest in this thesis is defined by adding two electrons in the states $\mathbf{k}$, $\uparrow$ and $-\mathbf{k}$, $\downarrow$ to the wave-function with N average number of particles. The probability amplitude for obtaining the state with $N+2$ particles will is:

$$Z_2 \equiv \langle \Psi_{BCS}(N+2)|c^\dagger_{k,\uparrow}c^\dagger_{-k,\downarrow}|\Psi_{BCS}(N)\rangle = \frac{\sin 2\theta_k}{2}. \tag{1.9}$$

Z_2 is called *condensation amplitude.*

Origin of the attractive interaction

The crucial point of BCS theory is the existence of an attractive interaction among electrons, which may not seem obvious for electrons in metals interacting by Coulomb repulsion. Indeed, it was first realized by Frölich [30] the importance of phonons to explain the net attractive interaction. Lately this assumption was confirmed experimentally by the discovery of the *isotope effect* i.e. the proportionality of T_c to $M^{-1/2}$ for isotopes of the same element, which is taken into account in BCS theory by the above mentioned relation $\omega_c \propto \omega_D$.

A sketch example of how the phonons can turn the sign of the net interaction is provided by the jellium model [31], in which the solid is approximated by a fluid of electrons and point-like positive ions, hence completely neglecting crystal structure effects. As shown e. g. in [32] the jellium model predicts a screened interaction between electrons of the form

$$V(q,\omega) = \frac{4\pi e^2}{q^2+q_{TF}^2} + \frac{4\pi e^2}{q^2+q_{TF}^2}\frac{\omega_q^2}{\omega^2-\omega_q^2}. \tag{1.10}$$

Here the first term is the electron-screened Coulomb repulsion and the second one is the phonon-mediated interaction. The frequency ω_q is the screened plasma frequency of the ion fluid, which is transformed by the electron-ion interaction into an acoustic branch, $\omega_q \sim cq$. The net interaction thus is attractive for $\omega < \omega_D$, being the Debye frequency the characteristic phonon energy, Clearly this model is too oversimplified and it lacks all the specific material features, but it is still useful to draw some generic remarks. In the framework of Landau Fermi-liquid theory, which is essentially at the hearth of BCS theory, the high frequency repulsion is absorbed into the so-called Landau parameters, assuming that quasi-particles form well above ω_D. What is left is the low-frequency attraction cut-off by ω_D plus a residual repulsion, the Coulomb pseudo potential, μ_* (see Chapter 5). If the former overcomes the strength of the latter, superconductivity occurs.

It is worth to mention, that though in conventional superconductors attraction is provided by phonons, the BCS pairing theory only requires an attractive interaction.

Thus different mechanisms, involving exchange of bosons other then phonons may be responsible for superconductivity in other materials.

To conclude this brief discussion on the conventional BCS theory, let us summarize what seem to be the key ingredients:

- a boson-mediated interaction which is attractive below some typical energy ω_c;
- Landau quasi-particles which form well above ω_c so that their residual repulsion, μ_*, is smaller than the boson-mediated attraction.

As we are going to discuss, in High-T_c cuprate superconductors either the bosons which may mediate the attraction are not well identified and there are no evidences of Landau quasi-particles above T_c. This is the reason why High-T_c superconductivity asks for a profound revision of BCS theory, which presently is still lacking.

1.1.2 Cuprates

High temperature superconductors were discovered by Bednorz and Muller in a ceramic copper oxide material $La_{2-x}Ba_xCuO_4$ in 1986 [7]. In the succeeding few years dozens of "high-T_c" compounds have been synthesized and currently a mercury-based material has the highest confirmed critical temperature of 133 K [33].

This discovery has stimulated an incredible amount of research activity, aimed on understanding this phenomenon. Nevertheless even now, after almost twenty years of extensive studies, one still lacks a satisfying explanation. The practical importance of these materials is determined by their high critical temperature, which for many of them lies above the boiling temperature of nitrogen (70 K). For theorists high-T_c materials represent an example of complex system with many unusual properties (see below), most of which needs to be understood.

Structure

Crystal structure of cuprates is quite complicated (a unit cell of $YBa_2Cu_3O_6$ is shown on Fig.1.1 as an example) and differs from one compound to another. However, the key elements of all cuprates are strikingly the same. These are: CuO_2 planes, whose number per unit cell varies from one, as in La_2CuO_4, two, as in $YBa_2Cu_3O_6$ or three,

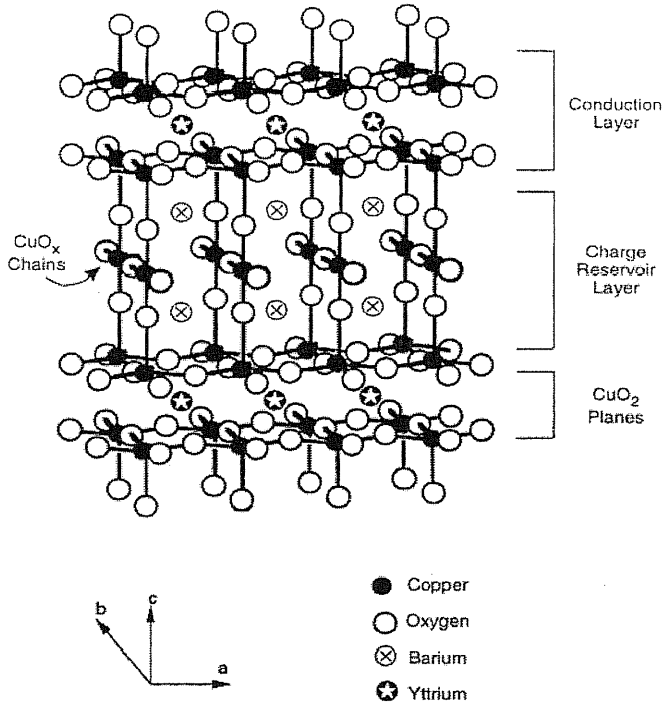

Figure 1.1: Crystal structure of $YBa_2Cu_3O_{6+x}$. Taken from [34].

as in $Bi_2Sr_2YCu_3O_8$, and the so called *charge reservoirs*, which reside in between the CuO_2 planes. The formers are believed to host those electronic excitations which are most relevant for superconductivity, while the latter serve as the instruments for fine tuning of the carriers concentration - *doping* - in the planes. In $YBa_2Cu_3O_{6+x}$ it occurs by adding oxygen atoms to the charge reservoir, while e.g. in $La_{2-x}Sr_xCuO_4$ - by replacing La^{3+} with Sr^{2+}.

The charge carriers in High-T_c cuprates are holes, and the parent compounds, e.g. those with normal stoichiometry, are anti-ferromagnetic insulators (below a Neél temperature T_N) [35] due to the strong holes localization on Cu^{2+} ions. Upon doping, holes start to move giving rise to a superconductor or a metal phase, depending to the temperature and the doping concentration.

Phase diagram

Above some critical doping δ (see in the Fig. 1.2), cuprates become superconductors below T_c. This superconductivity depends strongly on doping, and the maximum T_c occurs at some doping called *optimal*. It is well established that below T_c Cooper-

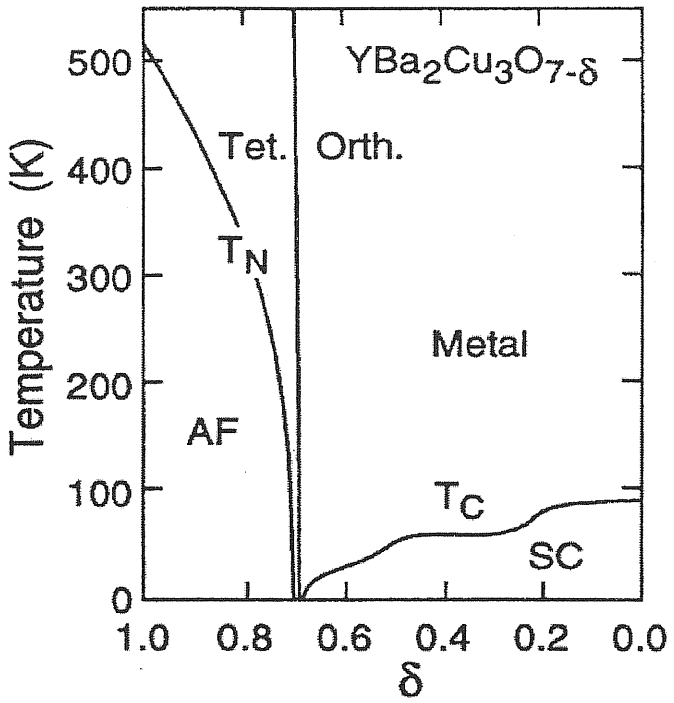

Figure 1.2: Phase diagram of $YBa_2Cu_3O_{6+x}$. Taken from [36] and [37].

pairs of charge $2e$ exist, yet there is no relevant isotope effect [38, 39, 40]. The former evidence favors a conventional pairing hypothesis but the latter discourages any explanation based on electron-phonon interaction. The NMR, Raman scattering and ARPES experiments [41] have revealed a $d_{x^2-y^2}$ symmetry of the superconducting gap. In addition, the anomalously small value of the coherence length (ξ of the order of $12 \div 15\mathring{A}$ contrary to conventional superconductors, where $\xi \sim 50 \div 10^4\mathring{A}$) and large value of the ratio $2\Delta/T_c \sim 6 \div 8$ at the optimal doping (for BCS $2\Delta/T_c = 3.52$) imply strong coupling superconductivity.

It is widely believed, that understanding the normal-state properties of the high-T_c will also shed light on the mechanisms underlying the superconductivity. The basis for this expectation resides in the unusual normal-state properties of these materials. For example, strong anisotropies are observed, mainly caused by the two-dimensional nature of the problem, and magnetic phases exist close to the superconducting regions. In addition, there are properties of the cuprates that deviate from a Landau Fermi-liquid description of the normal state, thus posing serious problems to a conventional BCS explanation. Indeed, it is known that in a normal Fermi-liquids the magnetic susceptibility and the Hall coefficient are temperature independent, the resistivity grows like T^2 at low temperatures, and the NMR re-

laxation is proportional to temperature ($1/T_1 \sim T$). This behaviors have not been observed in the cuprates [42], [43]. In the under-doped regime, below a crossover temperature T^* the cuprates are characterized by the opening of a large *pseudo-gap* in the single-particle excitation spectrum and in the spin response function, as observed in angle-resolved photoemission, tunneling and specific heat [8]. Although in this state there is a single-particle gap of $d_{x^2-y^2}$-like symmetry, no long-range order is observed [44, 45] and the system is still metallic.

1.2 Models for strongly correlated cuprates

1.2.1 $t-J$ model

The holes in CuO_2 reside mainly on $d_{x^2-y^2}$ orbitals of copper. Thus a simple tight-binding Hamiltonian could be constructed, in which the holes are allowed to hop between copper and oxygen ions, being the system a metal at half-filling. This picture, however, lacks a very important ingredient of real cuprates: the strong Coulombic repulsion between holes in the same copper orbital. In fact, the latter should force the system to become instead strongly correlated antiferromagnet at half-filling. Following this type of reasoning there was proposed [46] three-band Hubbard model to describe physics of CuO_2 plane:

$$\begin{aligned} H_{3b} = & - t_{pd} \sum_{<ij>} p_j^\dagger (d_i + \text{H.c.}) - t_{pp} \sum_{<jj'>} p_j^\dagger (p_{j'} + \text{H.c.}) \\ & + \epsilon_d \sum_i n_i^d + \epsilon_p \sum_i n_i^p + U_d \sum_i n_{i\uparrow}^d n_{i\downarrow}^d \\ & + U_p \sum_j n_{j\uparrow}^p n_{j\downarrow}^p + U_{pd} \sum_{<ij>} n_i^d n_j^p \end{aligned} \tag{1.11}$$

where p is the hole creation operator in oxygen $p-$orbital, d is the same for $d-$orbital on Cu and the Hamiltonian constants can be obtained from electronic structure calculations [47]:

$\epsilon_p - \epsilon_d$	t_{pd}	t_{pp}	U_d	U_p	U_{pd}
3.6 eV	1.3 eV	0.65 eV	10.5 eV	4 eV	1.2 eV

At half-filling, the model is a so-called charge-transfer Mott insulator. The holes localize, mainly on Cu d-orbitals, and the hybridization with the oxygens generate a super-exchange responsible for the anti-ferromagnetic order. Additional holes doped

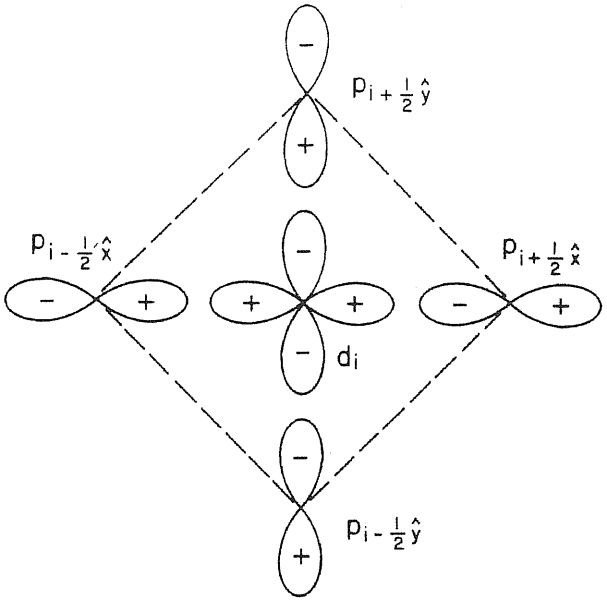

Figure 1.3: Schematic diagram of the hybridization of the O hole ($2p^5$) and Cu hole ($3d^9$). The signs + and - represent the phase of the wave functions. Taken from [48].

into the system will instead prefer to sit on the oxygen orbitals rather then on the copper ones, since $U_d > \epsilon_p - \epsilon_d$. Yet the system gains energy from *hybridization* of the holes between oxygen and copper sites. In general a hole can occupy whatever of four oxygen orbitals surrounding a copper site (see Fig 1.3) and form singlet or triplet spin states with the hole localized on the copper. It appears, however [48, 49], that the singlet configuration, containing the copper orbital and the $d_{x^2-y^2}$-like *combination* of four oxygen orbitals, surrounding it, has much smaller energy scale respect to other singlet or triplet combinations. If one is interested only in the low energy physics of the model (1.11), then it is a good approximation to identify the motion of the doped hole with the motion of such *Zhang-Rice singlet.* As a consequence, the oxygen orbitals become excluded from the consideration and one arrives to an effective one-band model called $t-J$ *model*:

$$H_{t-J} = -t \sum_{<ij>,\sigma} \left(\tilde{c}^{\dagger}_{i\sigma} \tilde{c}_{j\sigma} + \text{H.c.} \right) + J \sum_{<ij>} \left(\vec{S}_i \cdot \vec{S}_j - \frac{1}{4} n_i n_j \right), \tag{1.12}$$

originally proposed by Anderson [50]. Here $\tilde{c}^{\dagger}_{i\sigma} = c^{\dagger}_{i\sigma}(1 - n_{i,-\sigma})$ are the fermion operators, projected on the subspace of non-doubly occupied sites and $\vec{S}_i$ are the spin operators on site i. The superexchange constant is given by:

$$J = \frac{4t_{pd}^4}{(\Delta_{pd} + U_{pd})^2}\left[\frac{1}{U_d} + \frac{2}{2\Delta_{pd} + U_p}\right], \tag{1.13}$$

where $\Delta_{pd} = \epsilon_p - \epsilon_d$ and describes antiferromagnetic type interaction between holes on copper sites. Using the data from [47] one gets $J \sim 0.2 \div 0.6t$. The hopping term in (1.12) describes the process when a singlet moves from site i to j and simultaneously a hole moves from j to i, to preserve the single occupancy of the copper sites. Zhang-Rice singlet represents thus the absence of the hole on copper site, and for the latter we have the *constraint of no double occupancy*. The hopping amplitude for nearest neighbor sites, see Ref. [48], is $t \approx 1.5t_{pd}^2/(U_d - \Delta_{pd}) \sim 0.3 \div 0.4eV$.

Contrary to the Hubbard model (see below), the $t - J$ one without constraint of no-double occupancy already at BCS level exhibits the possibility of d-wave superconductivity (along with the extended s). To see that, it is enough to rewrite the bare J interaction of (1.12) in the form:

$$V^J(k, k', q) \sim -J\left[\psi(k + \frac{q}{2})\psi(k' + \frac{q}{2}) + \varphi(k + \frac{q}{2})\varphi(k' + \frac{q}{2})\right], \tag{1.14}$$

where $\psi(k) = \cos k_x + \cos_{k_y}$ and $\varphi(k) = \cos k_x - \cos_{k_y}$. In Hartree-Fock BCS-theory only contributions with $q = 0$ survive, hence V^J indeed have extended s or $d_{x^2-y^2}$ symmetries. The numerical evidences support a scenario in which this mean-field behavior is even enforced by the *no double occupancy* constraint[51].

1.2.2 Hubbard model

Another model which is often considered as relevant for cuprates is the one-band Hubbard model [52] (or just Hubbard model), known from the theory of transition metals oxides:

$$H_{1b} = -t \sum_{<ij>,\sigma} \left(c_{i\sigma}^\dagger c_{j\sigma} + \text{H.c.}\right) + U \sum_i n_{i\uparrow} n_{i\downarrow}$$

where $U > 0$ (repulsion) now tries to mimic the charge transfer gap between Cu and O bands, (see the Fig. 1.4) $U \sim \epsilon_p - \epsilon_d$ and t is the same as for $t - J$. Numerical fitting of the excitation spectra of one-band Hubbard model (1.15) to that of the

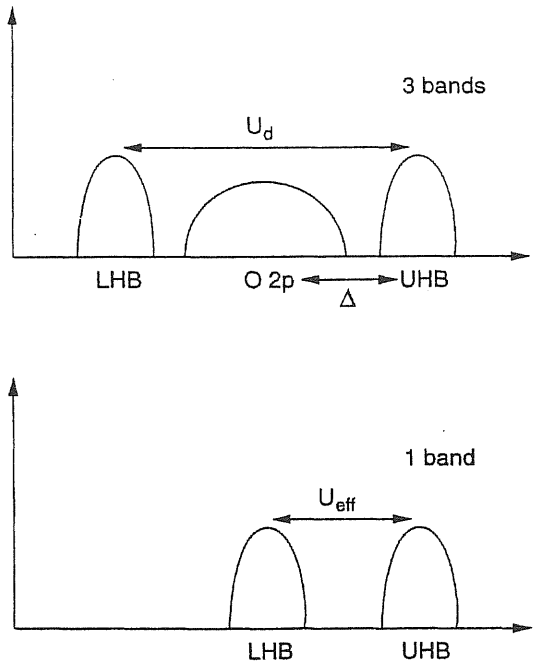

Figure 1.4: Schematic band structure of the CuO_2 planes. U_d is the Coulombic repulsion at the copper ions, while Δ is the difference in energy between copper and oxygen orbitals. The lower part of the figure represents the one-band Hubbard model that simulates the charge-transfer gap by a Hubbard gap using an effective U_{eff}. Taken from [54].

three-band one (1.11), made e.g. in [53] for the above shown parameters, yields: $t = 0.43 \div 0.50eV$, $U = 2.3 \div 2.7eV$.

The Hubbard model remains one of the most popular models in the scientific community as far as the high-T_c are concerned. The reason for this is its relative simplicity, which allows the application of several analytical and numerical methods. One has to remind, however, that even for such simple model in two dimensions an exact solution is not known. Moreover, there is a lot of controversy even about the possibility of superconducting state in any region of phase diagram of repulsive Hubbard model (see Chapter 6). Indeed, even though the Hubbard model does not include any explicit attraction, it is known that in the large U/t limit it can be mapped onto the $t - J$ model[55], having $J = 4t^2/U$. Rigorously speaking the mapping is not fully exact, since *three-site terms*, i.e. couplings involving three sites, appear. Yet the $t - J$ model contains an explicit inter-site attraction, as we mentioned, although supplemented by the *no double occupancy* constraint. This observation suggests that in the strong coupling limit d-wave superconductivity may actually appear also in the Hubbard model, even though at weak coupling there is

not strong evidence of that (see however [21, 19, 20]). Indeed, in large U/t limit, there are indications (see below) that the Hubbard model does superconduct. Due to the strong repulsion, one is however led to go beyond BCS mean-field theories and study the properties of Hubbard interaction in some non-perturbative way. Luckily numerical methods developed in the past few decades offer the possibility for such study either exactly, on small size clusters, or approximately by a variety of approaches, such as quantum Monte Carlo, DMRG, DMFT etc.

Chapter 2

Quantum Monte Carlo

2.1 Monte Carlo Integration and Metropolis algorithm

Extraordinary grow of computer power in the last few decades gave rise to the development of numerical methods. Among those stay apart a large group of methods known as Monte Carlo. The common feature for all these methods is the use of the concept of a stochastic variable - a number generated randomly by computer in a way to sample a given distribution function.

Consider a (multidimensional) integral:

$$I = \int_{\Omega} F(x)G(x)dx \tag{2.1}$$

where I is taken over the domain Ω and $F(x)$ is positively definite on Ω and

$$\int_{\Omega} F(x)dx = 1. \tag{2.2}$$

$F(x)$ has then all the properties of the probability density. I can be viewed of as a mean value of the function $G(x)$ on Ω with the distribution function $F(x)$. A Monte Carlo approximation to I is constructed in a following way:

1. A sequence of points x_i, $i = 1, \ldots N$ in Ω is generated so that to sample $F(x)$.
2. An estimate to I is calculated as

$$I_N = \frac{1}{N}\sum_i G(x_i) \tag{2.3}$$

In the limit of $N \to \infty$, $I_N \to I$. For finite N the deviation from the exact value can be estimated as a variance of $G(x)$:

$$\sigma_N = \sqrt{\frac{1}{N}\sum_i (G^2(x_i) - I_N^2)} \tag{2.4}$$

One can see from (2.4) that σ goes as $1/\sqrt{N}$ for large N. In general, if one has just an integral

$$\int_\Omega H(x)dx \tag{2.5}$$

then the function $H(x)$ can be always decomposed into a product of the kind (2.1) with $F(x)$ satisfying the condition (2.2) and $G(x) = H(x)/F(x)$. This choice is not unique but can be made such that $F(x)$ to be as close as possible to the integrand $H(x)$, hence generating the sequence of x_i, that is located in the regions which contribute mostly to I. This choice is called *importance sampling* and is known to reduce significantly the number of points N needed to obtain a given accuracy. Usually the number of points of d-dimensional quadrature needed to obtain a given accuracy grows exponentially with d while for Monte Carlo it is just independent of d. Monte Carlo represents thus a clever way to explore the large Hilbert space of a complex problem, choosing the points making the most contribution to the integral.

When treating a physical system, one usually knows the dynamics and aims to find the equilibrium distribution function. The main idea of *Metropolis algorithm* (MA) [56], is to reverse this problem - imposing some artificial dynamics, constraint the system to arrive to a given equilibrium distribution $F(x)$. MA allows to sample an arbitrary distribution function in the same way. An important remark should be made, which restricts the class of dynamics used in this approach. Suppose that $A(x, y)$ is the transition probability to arrive to point x from point y. Then, in equilibrium, the system should be on average as likely to move in x from y as to move exactly in the reverse direction:

$$A(x, y)F(y) = A(y, x)F(x) \tag{2.6}$$

This condition is called *detailed balance*. Starting from a point x_i, the next point of the sequence x_{i+1} is accepted if a random number ξ, uniformly distributed between 0 and 1, is greater than the ratio $F(x_{i+1})/F(x_i)$ otherwise $x_{i+1} = x_i$. Here we used

the most popular form of $A(x,y) = \min(1, F(x)/F(y))$. On each step i, x_i are distributed according to some distribution function $\phi_i(x)$. As such random walks proceed, a recursive relationship develops between succeeding $\phi_i(x)$. Namely, there are two contributions to $\phi_{i+1}(x)$: one that we come to x_{i+1} from some point x' and another that we stay in the same x since the last step (last step has been rejected), hence:

$$\phi_{i+1}(x) = \sum_{x'} A(x,x')\phi_i(x') + \phi_i(x)(1 - \sum_{x'} A(x',x)) \tag{2.7}$$

or

$$\phi_{i+1}(x) = \phi_i(x) + \sum_{x'}(A(x,x')\phi_i(x') - \sum_{x'} A(x',x)\phi_i(x)) \tag{2.8}$$

Notice that $F(x)$ is the fixed point of (2.8) i.e. if $\phi_i(x) = F(x)$ then $\phi_{i+1}(x) = F(x)$ using (2.6). One can prove [57] that $F(x)$ will be the asymptotic distribution for x.

2.2 Variational Monte Carlo

To estimate the ground state energy of quantum Hamiltonian the *variational principle* is used very often. It states that the ground state wave function minimizes the functional:

$$\langle \Psi \left| \hat{H} \right| \Psi \rangle \tag{2.9}$$

where E_0 is the ground state energy and the corresponding Euler equation is just the Schrödinger one. Given a trial wave function $|\Psi_G\rangle$ the expectation value of Hamiltonian is:

$$E_G = \frac{\langle \Psi_G | \hat{H} | \Psi_G \rangle}{\langle \Psi_G | \Psi_G \rangle} \geq E_0. \tag{2.10}$$

Notice that equality in (2.10) occurs only when Ψ_G coincides with Ψ_0. In simulations of many-body systems on lattice, usually the integration on x has a meaning of summation over the electron configurations - x - the states with definite positions

and spins of electrons. The set of all the configurations $\{x\}$ constitutes obviously a complete set of orthogonal states. With this notations (2.10) rewrites as follows:

$$E_G = \frac{\langle \Psi_G | \hat{H} | \Psi_G \rangle}{\langle \Psi_G | \Psi_G \rangle} = \frac{\sum_{x,x'} \Psi_G(x) H_{x,x'} \Psi_G(x')}{\sum_x \Psi_G^2(x)} \tag{2.11}$$

where $H_{x,x'} = \langle x | \hat{H} | x' \rangle$ are the matrix elements of the Hamiltonian between the states x and x' and $\Psi_G(x) = \langle x | \Psi_G \rangle$ is the value of many body wave function $|\Psi_G\rangle$ on a given configuration x. Making the sum in (2.11) would require an exponentially large number of terms (typically $\sim 4^N$, where N is the number of sites in the system) and is not accomplishable for systems of realistic size. Instead, one can make use of the procedure (2.3) to build up an approximation to E_G. We cast as $F(x)$ the normalized square of $\Psi_G(x)$:

$$F(x) = \frac{\Psi_G^2(x)}{\sum_y \Psi_G^2(y)} \tag{2.12}$$

and the remainder

$$G(x) = \frac{\sum_y H_{y,x} \Psi_G(y)}{\Psi_G(x)} \equiv E_x \tag{2.13}$$

is the so-called local energy. Then a Monte Carlo estimate to E_G is given simply by the mean value of local energy:

$$E_G = E_N \pm \sigma_N, \text{ where } E_N = \frac{1}{N} \sum_x E_x \text{ and } \sigma_N = \sqrt{\frac{1}{N} \sum_x (E_x^2 - E_N^2)}. \tag{2.14}$$

The expectation value of any other observable $\hat{O}$ can be obtained in a similar way, namely substituting in (2.13) $H_{x,x'}$ with $O_{x,x'}$. For non-hermitian operators the approach is more complicated and an example of such case will be given in Appendix B.

2.3 Green function Monte Carlo

Variational Monte Carlo uses stochastic sampling of a trial variational wave function. There is, however, another way to implement Monte Carlo in resolving many-body

Hamiltonian which allows, in principle, to sample exact ground state . This is called the *Green function Monte Carlo* (GFMC). It is based on *power method*, which consists in repetitive application of the Green function $\hat{G} = \Lambda - \hat{H}$ on a state, which has non zero overlap with ground state:

$$|\Psi_n\rangle = G^n|\Psi_0\rangle, \text{ and } |\Psi_{n+1}\rangle = G|\Psi_n\rangle. \tag{2.15}$$

Here the constant Λ, called shift, is positive and chosen to be larger then the largest positive eigenvalue of H. If we expand the initial wave function $|\Psi_0\rangle$ in the basis of eigenstates of H,

$$|\Psi_0\rangle = \sum_i \alpha_i |\Phi_i\rangle \tag{2.16}$$

then after n steps:

$$G^n|\Psi_0\rangle = (\Lambda - E_0)^n \left[\alpha_0|\Phi_0\rangle + \sum_{i\neq 0} \alpha_i \left(\frac{\Lambda - E_i}{\Lambda - E_0}\right)^n |\Phi_i\rangle\right] \tag{2.17}$$

It is obvious from (2.17) that, provided $\alpha_0 \neq 0$, $G^n|\Psi_0\rangle$ will converge exponentially to the ground state as $n \to \infty$.

To implement the power method stochastically one needs to decompose the Green function:

$$G_{x,x'} = s_{x,x'} p_{x,x'} b_{x'}. \tag{2.18}$$

Here $s_{x,x'}$ is the sign of a given matrix element, $p_{x,x'} = |G_{x,x'}|/b_{x'}$ is the so-called *stochastic matrix* which defines the transition probability from x' to x and $b_{x'} = \sum_x |G_{x,x'}|$. The basic element of GFMC is called *walker* and consists of a configuration x and a weight w. The goal of GFMC is to construct a sequence of walkers which have, as a distribution function, the ground state. This is done by means of an iterative procedure. We are going to build up a *Markov chain* of walkers in following three steps:

1. Given the walker (w, x), change the weight by scaling it with b_x:

$$w \to b_x w. \tag{2.19}$$

2. Generate randomly a new configuration x' according to the stochastic matrix $p_{x',x}$.

3. Finally multiply the weight of the walker by $s_{x',x}$:

$$w' \to w s_{x',x}. \tag{2.20}$$

We denote the distribution function for the walker on $n-$th step as $P_n(x,w)$. It determines completely the wave function $\Psi_n(x)$:

$$\Psi_n(x) = \int dw w P_n(x,w). \tag{2.21}$$

On $n+1-$th step

$$P_{n+1}(x',w') = \sum_x \frac{p_{x,x'}}{b_x} P_n(x, \frac{w}{b_x s_{x',x}}) \tag{2.22}$$

Combining (2.22) and (2.21) we indeed recover (2.15).

One of the advantages of GFMC is the possibility to reduce the variance exploiting the information about the ground state, sometimes known a priori on physical grounds [58]. This is done by means of the *importance sampling transformation.* Consider slightly modified Green function:

$$\bar{G}_{x',x} = G_{x',x} \frac{\Psi_G(x')}{\Psi_G(x)} \tag{2.23}$$

The function $\Psi_G(x)$ is called guiding function and should be chosen as close as possible to the ground state and as simple as possible to evaluate numerically. Notice that this transformation does not change the spectrum of Hamiltonian, indeed if $\Psi(x)$ is an eigenstate of H then also $\Psi(x)\Psi_G(x)$ is an eigenstate of $\bar{H}$ with the same eigenvalue. The estimate of ground state energy after n steps is given by:

$$E_n = \frac{\langle \Psi_G | H | \Psi_0 \rangle}{\langle \Psi_G | \Psi_0 \rangle} = \frac{\langle w \bar{E}_x \rangle}{\langle w \rangle} = \frac{\sum_x E_x w_x}{\sum_x w_x} \tag{2.24}$$

where $\bar{E}_x$ is the local energy after importance sampling transformation: $\bar{E}_x = \sum_{x'} \bar{H}_{x',x}$.

If Ψ_G coincides with the ground state then local energy is just E_0 and the variance is identically zero - this is called *zero-variance property*. As in the case of Variation Monte Carlo, so called mixed average of any other observable can be computed in a similar way, namely introducing the quantity:

$$O_x = \frac{\sum_{x'} O_{x',x}\Psi_G(x')}{\Psi_G(x)} \tag{2.25}$$

then

$$O_n = \frac{\langle\Psi_G|O|\Psi_0\rangle}{\langle\Psi_G|\Psi_0\rangle} = \frac{\langle w\bar{O}_x\rangle}{\langle w\rangle}. \tag{2.26}$$

Very often, however, (almost in all physically interesting cases) for fermionic systems there is a kind of divergence, due to the nature of fermionic wave function to be antisymmetric under the permutation of the pair of electrons, which is manifested by the divergence of walker mean sign:

$$\bar{s}_n = \frac{\sum_x \int dw w P_n(x,w)}{\sum_x \int dw |w_x| P_n(x,w)} \tag{2.27}$$

This is the infamous *sign problem* and in this case $\bar{s}_n$ decreases exponentially to zero.

2.4 Fixed nodes approximation

In order to alleviate the sign problem so called *Fixed Node Approximation* (FN) [22] is used very often. The Green function for FN is designed after the importance sampling as follows:

$$\bar{G}^{FN}_{x',x} = \psi_G(x')(\Lambda\delta_{x',x} - \bar{H}^{FN}_{x',x})/\psi_G(x). \tag{2.28}$$

In (2.28) the effective Hamiltonian $\bar{H}^{FN}_{x',x}$ is defined as:

$$\bar{H}^{FN}_{x',x} = \begin{cases} H_{x',x} & \text{if } x' \neq x \text{ and } \psi_G(x')H_{x',x}/\psi_G(x) \geqslant 0 \\ 0 & \text{if } x' \neq x \text{ and } \psi_G(x')H_{x',x}/\psi_G(x) < 0 \\ H_{x,x} + \mathcal{V}_{sf}(x) & \text{if } x' = x \end{cases} \tag{2.29}$$

where the diagonal elements acquire so called *sign-flip* term:

$$\mathcal{V}_{sf}(x) = \sum_{\substack{\bar{H}_{x',x}>0 \\ \text{and } x' \neq x}} \bar{H}_{x',x}. \tag{2.30}$$

After the equilibration the walkers x will be distributed according to some function $\psi_{FN}(x)$. It is possible to prove [59] that the energy of ψ_{FN} is a variational upper bound for the ground state energy of initial Hamiltonian H.

2.5 Application of VMC to Jastrow-BCS wave function

Variational wave function used in the present thesis has the *Jastrow-BCS* form:

$$|\Psi_G\rangle = \mathcal{P}_N \exp\left(-\sum_i u_0 n_{i,\uparrow} n_{i,\downarrow} - \sum_{i \neq j} u(i-j) n_i n_j\right) \exp\left(-\sum_k f_k c^\dagger_{k,\uparrow} c^\dagger_{-k,\downarrow}\right) |0\rangle. \tag{2.31}$$

Here u_0 is Gutzwiller variational parameter, $u(i-j)$ - are that of Jastrow (which depend only on the distance $i-j$ for spatially isotropic systems) and $\mathcal{P}_N$ is the projector onto the subspace with fixed number of particles. f_k is the amplitude of Cooper pairs:

$$f_k = \frac{\Delta_k}{\epsilon_k + \sqrt{\epsilon_k^2 + \Delta_k^2}} \tag{2.32}$$

with Δ_k being the variational gap and ϵ_k - dispersion of free particles.

Our goal is to calculate the value of (2.31) on a given configuration x. Notice that Jastrow and Gutzwiller operators in the basis of states with definite coordinates and spins of electrons are just numbers, let us denote them $P_J(x)$ and $P_G(x)$. In general, to evaluate uncorrelated and non-superconducting wave function on a configuration x one usually constructs a *Slater determinant*, which contains as the columns one-electron orbitals and as the rows the positions of all the electrons. The use of BCS-type wave function would, in principle, imply the superposition of many Slater determinants, having different number of particles. To avoid this unnecessary

complication a trick is used known as *particle-hole transformation* on spin down electrons [60]:

$$\tilde{c}^{\dagger}_{i\downarrow} = (-1)^{i_x+i_y} c_{i\downarrow}, \quad \tilde{c}_{i\downarrow} = (-1)^{i_x+i_y} c^{\dagger}_{i\downarrow}$$
$$\tilde{c}^{\dagger}_{i\uparrow} = c^{\dagger}_{i\uparrow}, \quad \tilde{c}_{i\uparrow} = c_{i\uparrow}$$

where the factor $(-1)^{i_x+i_y}$ defines on a square 2D lattice two sublattices: one with $i_x + i_y$ even and another for which $i_x + i_y$ is odd. Such transformation is unitary and maps exactly the superconducting part of (2.31) into a *spin-density waves* state (SDW):

$$|\Psi_{SDW}\rangle = \prod_{\epsilon_k<\mu} \frac{1}{\sqrt{1+f_k^2}} (\tilde{c}^{\dagger}_{-(k+Q)\downarrow} + f_k \tilde{c}^{\dagger}_{k\uparrow}) |\tilde{0}\rangle \tag{2.33}$$

where $Q = (\pi, \pi)$, μ is the chemical potential of SDW state (SDW should always be at half-filling if we want $S_z = 0$ for initial fermions) and Δ_k becomes now an SDW gap. $|\tilde{0}\rangle = \prod_k c^{\dagger}_{-(k+Q)\downarrow}|0\rangle$ is the vacuum of new particles. Such state has definite number of particles and hence, can be represented by only one Slater determinant, but, instead, is not an eigenstate of $\hat{S}_z$ operator. Under particle-hole transformation the particles number operator becomes, up to a constant shift, the spin $\hat{S}_z$ one, and the state with N up spin and N down spin electrons on a lattice of M sites becomes a state with $N/2$ up spin electrons and $M - N/2$ those down.

The orbitals for the Slater determinant will be of the form:

$$\varphi_k(\mathbf{r}) = \frac{1}{\sqrt{1+f_k^2}} \left[\psi_k(\mathbf{r})|\uparrow\rangle + f_k \psi_{k+Q}(\mathbf{r})|\downarrow\rangle\right]. \tag{2.34}$$

Here $|\uparrow\rangle$ and $|\downarrow\rangle$ denote spin up and down respectively and $\psi_k(\mathbf{r}) \sim \exp(i\mathbf{k}\mathbf{r})$ are the orbitals with momentum k for the Fermi gas. Summarizing, we can write:

$$\Psi_G(x) = P_G(x) P_J(x) \det A \tag{2.35}$$

where $\det A$ is a Slater determinant and L is the number of sites:

$$\det A = \begin{vmatrix} \varphi_{k_1}(x_1) & \varphi_{k_2}(x_1) & \dots & \varphi_{k_L}(x_1) \\ \varphi_{k_1}(x_2) & \varphi_{k_2}(x_2) & \dots & \varphi_{k_L}(x_2) \\ \dots & \dots & \dots & \dots \\ \varphi_{k_1}(x_L) & \varphi_{k_2}(x_L) & \dots & \varphi_{k_L}(x_L) \end{vmatrix}. \tag{2.36}$$

In general, to implement the projection on fixed number of particles one has to apply the projector on every new configuration, generated with Monte Carlo. It can be proved, however, that we can reduce ourselves applying only two kinds of moves from x to x': hopping of particle with spin up or down and spin exchange between two sites (all the operations being accomplished in terms of new particles $\{\tilde{c},\ \tilde{c}^\dagger\}$). This is true because non-vanishing off-diagonal matrix elements $H_{x,x'}$, of a large class of Hamiltonian, including those used in the present thesis, are connected only by these two operations. Hence, choosing the initial state to be the eigenstate of the number of electrons operator, applying only the above mentioned moves, we will always stay in the subspace of the same number of electrons in the system.

The calculation of $\Psi_G(x)$ should require of the order of L^3 operations for every configuration. This can be reduced significantly by noting, that succeeding configurations x and x' are different only by the values of one or two columns and rows, all the rest of matrix being the same. This allows us *to update determinant*, instead of recalculating it [59], thus saving of the order of L^2 operations. In a similar way also can be updated $P_G(x)P_J(x)$.

2.6 Stochastic minimization

The search of the best variational wave function among a given class of functions can be viewed as a kind of power method. To see that let us rewrite (2.31) in slightly different manner[61]:

$$|\Psi_{var}\rangle = \mathcal{P}_N \exp\left(-\sum_{i=0}^{M} \alpha_i \hat{\Theta}_i\right) \exp\left(-\sum_{k\in BZ} f_k c^\dagger_{k,\uparrow} c^\dagger_{-k,\downarrow}\right) |0\rangle. \tag{2.37}$$

Here $\mathcal{P}_N$ is the projector onto a subspace with N particles, α_0 is the Gutzwiller variational parameter, α_1 the nearest neighbor Jastrow parameter *etc.* We exhaust all M distances possible on a sample of given size. In addition, we have superconducting variational parameters which, in principle, can also extend to all possible

distances compatible to a given symmetry (s, extended s, d *etc*) so that we have additional set of variational parameters $\{f_k\}_{k\in BZ}$. Therefore we add them to the set of α as α_i at $M < i < M+N$. For example: $\Theta_0 = \sum_i n_{i,\uparrow}n_{i,\downarrow}$, $\Theta_1 = \sum_{<ij>} n_i n_j$ and $\Theta_i = c^\dagger_{k_i,\uparrow}c^\dagger_{-k_i,\downarrow}$ for $M < i < M+N$.

The minimum condition for (2.37) reads:

$$\langle\Psi_G|\Theta_i H|\Psi_G\rangle = E_{min}\langle\Psi_G|\Theta_i|\Psi_G\rangle, \tag{2.38}$$

which can be interpreted as Schrödinger equation, projected onto subspace of $\{\Theta_i|\Psi_G\rangle\}$. We can adopt the previously introduced power method projecting, however, every time the result onto $\{\Theta_i|\Psi_G\rangle\}$. The variation of (2.37) reads:

$$\begin{aligned}&|\Psi_G(x,\alpha_0+\delta\alpha_0,\alpha_2+\delta\alpha_2,\ldots,\alpha_{M+N}+\delta\alpha_{M+N})\rangle \approx \\ &(1+\sum_{i=0}^{M+N}\hat{\theta}_i\delta\alpha_i)|\Psi_G(x,\alpha_0,\alpha_2,\ldots,\alpha_{M+N})\rangle.\end{aligned} \tag{2.39}$$

From the other hand we get: $\hat{G}|\Psi_G\rangle = (\Lambda - \hat{H})|\Psi_G\rangle$.

$$\Lambda(1-\frac{1}{\Lambda}\hat{H})|\Psi_G\rangle \tag{2.40}$$

Combining (2.39) and (2.40) and projecting the result onto $\{|\Theta_i\Psi_G\rangle\}$ we obtain the system of equations for $\delta\alpha_i$, which move variational parameters towards the minimum:

$$\sum_i \delta\alpha_i\langle\Theta_i\Theta_j\rangle = -\frac{1}{\Lambda}\langle\Theta_j H\rangle. \tag{2.41}$$

In principle all f_k can be optimized with this algorithm, however, in this thesis we assumed nearest neighbor d-wave pairing and thus all f_k become dependent on one only parameter Δ_{var}:

$$f_k = \frac{\Delta_k}{\varepsilon_k + \sqrt{\varepsilon_k^2+\Delta_k^2}}, \tag{2.42}$$

where $\Delta_k = \Delta_{var}\varphi_k$.

2.7 Finite size tilted lattices

Imagine a lattice, cut as in Fig.2.1. In such *tilted lattice* the number of sites is $N_{sites} = 2n^2$ for n natural. Tilting of the lattice gives an opportunity to study the systems with the sizes intermediate with respect to those of the simple square lattice where $N_{sites} = n^2$. On small clusters also the possibility to have so called *closed shell* is very important, since open shells have large degeneracies. Tilted lattices give somewhat better doping of their closed shells then the square ones. In thermodynamic limit nothing should depend on boundary conditions thus we can study tilted lattices exactly as the usual square ones. In the present thesis we used the following sizes $N_{sites} = 50,\ 98,\ 162,\ 242$ corresponding to $n = 5,\ 7,\ 9,\ 11$. To avoid the competition with magnetic phases we used in most of the cases the doping $\delta = 0.16$ if it is not specified otherwise. Due to specific boundary conditions the momentum quantization for tilted lattices is different from that for square ones:

$$k_1 = \frac{2\pi}{N_{sites}}(n_x k + n_y l) \tag{2.43}$$

$$k_2 = \frac{2\pi}{N_{sites}}(n_x k - n_y l) \tag{2.44}$$

where n_x and n_y are the sides of the lattice: $n_x^2 + n_y^2 = N_{sites}$ (in our case $n_x = n_y$) and k and l are the integers so that k_1 and k_2 fill the first Brillouin zone.

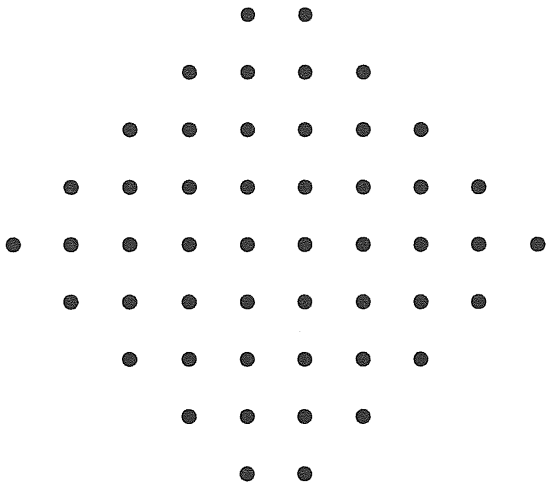

Figure 2.1: Tilted lattice of 50 sites.

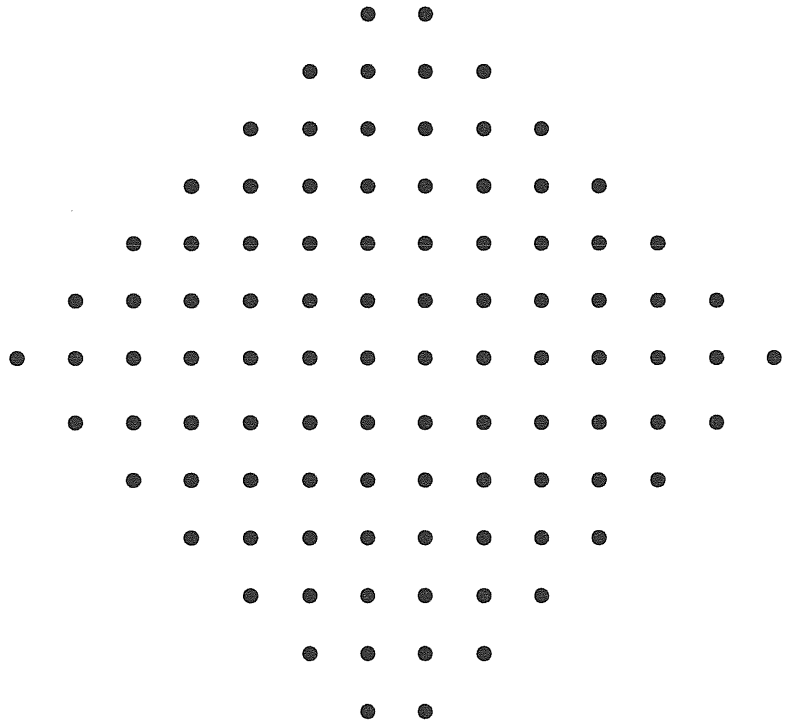

Figure 2.2: Tilted lattice of 98 sites.

Chapter 3

Exchange correlation energy in $d-$wave superconductors

3.1 Correlation energy in Low-T_C superconductors

Within the standard BCS theory of superconductivity, the Hartree-Fock (HF) condensation energy E^{HF}_{cond}, namely the difference between the HF energies of a normal Fermi liquid and a superconductor, is approximately given by $\frac{\Delta^2}{\epsilon_F}$, and is negligible if compared to the whole HF energy, as it is shown in the following table:

Element	$\frac{\Delta^2}{\epsilon_F^2}$
Al	$2.23 \cdot 10^{-10}$
Pb	$1.97 \cdot 10^{-8}$
Zn	$1.67 \cdot 10^{-10}$
Sn	$3.16 \cdot 10^{-10}$

On the other hand, a sizable contribution to the cohesive energy of a metal comes from the so-called *correlation energy* gain E_{corr}, defined by the energy difference between the true cohesive energy and that one calculated within the HF approximation. Being the various estimates of E_{corr} in a normal metal, which can be obtained with better approximations than the simple HF theory, much larger than E^{HF}_{cond}, it is legitimate to wonder about the order of magnitude and the sign of the condensation energy contribution due to E_{corr}.

The answer to this question is partly known. Indeed the largest amount of correlation energy gain comes from the long wavelength behavior of the longitudinal dielectric constant[62], specifically from the transfer of spectral weight of the particle-hole long wavelength excitations from small frequencies to the plasmon pole. Since the superconductor has the same long wavelength longitudinal dielectric properties of the normal phase, this contribution to the correlation energy does not change in the superconducting phase.

The high-T_c materials differ from the standard low-T_c superconductors in many respects, but mainly because of the role played by short range correlations, what is generally called the Hubbard U. Indeed, just to avoid the strong short range repulsion, the cuprates become d-wave superconductors. In view of the above discussion, it is clear in this case that an important contribution to the correlation energy should also come from the short range behavior. In other words, the justification of the stability of a strongly correlated d-wave superconductor can not avoid a comparison between the short range contribution to the correlation energy with that one of the normal phase. This is the actual scope of the present work.

We consider for simplicity a nearest-neighbor tight binding model on a square lattice,

$$H_0 = -t \sum_{<ij>} \sum_{\sigma} c^{\dagger}_{i\sigma} c_{j\sigma}, \tag{3.1}$$

where $c^{\dagger}_{i\sigma}$ ($c_{i\sigma}$) is the fermion creation (annihilation) operator at site i with spin σ. The short range correlation is modeled by an on site repulsion

$$H_{int} = U \sum_{i} n_{i\uparrow} n_{i\downarrow},$$

being $n_{i\sigma} = c^{\dagger}_{i\sigma} c_{i\sigma}$. Since our scope is only to investigate the screening properties of a d-wave superconductor, we also assume the existence of the attractive term

$$H_{d-SC} = W \sum_{i,\sigma} K_{i\sigma} K_{i-\sigma} \tag{3.2}$$

where

$$K_{i\sigma} = \sum_{\vec{\delta}} (c^{\dagger}_{i\sigma} c_{i+\delta\sigma} + c^{\dagger}_{i+\delta\sigma} c_{i\sigma}) f(\delta) \tag{3.3}$$

is the kinetic energy for the $i-th$ site, summed over all the nearest neighbors with phase prefactor:

$$f(\vec{\delta}) = \begin{cases} +1 & \text{for} \quad \vec{\delta} = \pm \vec{a}_x \\ -1 & \text{for} \quad \vec{\delta} = \pm \vec{a}_y \end{cases} \tag{3.4}$$

which stabilizes, within the Hartree-Fock approximation, a d-wave superconducting wave function, without specifying which mechanism mediates the attraction. The above $t-U-W$ Hamiltonian has been introduced in [63] as a trial model to study, with the aid of quantum Monte Carlo, the interplay between superconductivity and antiferromagnet at half filling. In addition, in [64] the Bethe-Salpeter equation for the effective interaction was also solved within Random Phase Approximation. It was shown that this effective interaction, developed on the antiferromagnetic background, has attractive regions, compatible with the $d-$wave symmetry of the gap.

In the $U-W$ plane, we define a generic path $U(s)$ and $W(s)$ parametrized by the variable s which joins the points $(U,W)=(0,0)$ at $s=0$ to the actual values of these parameters at $s=1$. The correlation energy may be determined through

$$\begin{aligned} E_{corr} &= E_0 - E_{HF} + \int_0^1 ds \, \langle \frac{\partial H}{\partial s} \rangle \\ &= E_0 - E_{HF} + \int_0^1 ds \, \langle \frac{\partial H}{\partial U} \rangle \frac{\partial U}{\partial s} + \langle \frac{\partial H}{\partial W} \rangle \frac{\partial W}{\partial s}, \end{aligned} \tag{3.5}$$

being E_0 and E_{HF} the non interacting and the HF energies, respectively. We notice that

$$\frac{1}{N}\frac{\partial H}{\partial U} = \frac{1}{4N}\sum_i \left(n_{i\uparrow}+n_{i\downarrow}\right)^2 - \left(n_{i\uparrow}-n_{i\downarrow}\right)^2 \equiv \frac{1}{4N}\sum_i n_i^2 - \sigma_i^2, \tag{3.6}$$

where N is the number of sites, can be written through the fluctuation-dissipation theorem as

$$\frac{1}{N}\frac{\partial H}{\partial U} = \frac{1}{4}n^2 + \frac{1}{4N}\sum_q \int \frac{d\omega}{2\pi} \coth\left(\frac{\beta\hbar\omega}{2}\right) \left[\mathcal{I}m\kappa(\omega,q) - \mathcal{I}m\chi(\omega,q)\right] \tag{3.7}$$

being n the electron density per site and $\kappa(\omega,q)$ and $\chi(\omega,q)$ the charge and spin density-density correlation functions at frequency ω and momentum q, calculated at temperature β^{-1}. The above expression clearly shows that the repulsive part of the correlation energy gain is obtained by suppressing charge while enhancing spin excitations. Analogously for H_{d-SC} term:

$$H_{d-SC} = \frac{1}{N}\frac{\partial H}{\partial W} = \frac{1}{4N}\sum_q \int \frac{d\omega}{2\pi} \coth\left(\frac{\beta\hbar\omega}{2}\right) \left[\mathcal{I}m\tilde{\kappa}(\omega,q) - \mathcal{I}m\tilde{\chi}(\omega,q)\right]$$

where

$$\begin{cases} \tilde{\kappa}(t,q) = -i\theta(t)\langle[K_q(t), K_{-q}(0)]\rangle \\ \tilde{\chi}(t,q) = -i\theta(t)\langle[\Lambda_q(t), \Lambda_{-q}(0)]\rangle \end{cases}$$

$$\begin{cases} K_q = \frac{1}{N}\sum_k (c^\dagger_{k\uparrow}c_{k+q\uparrow} + c^\dagger_{k+q\downarrow}c_{k\downarrow})F(k,q) \\ \Lambda_q = \frac{1}{N}\sum_k (c^\dagger_{k\uparrow}c_{k+q\uparrow} - c^\dagger_{k+q\downarrow}c_{k\downarrow})F(k,q) \end{cases}$$

K_q and Λ_q are the analogues of charge and spin density operators for H_{d-SC}, and $F(k,q) = \varphi(k) + \varphi(k+q) = \cos k_x - \cos k_y + \cos(k_x + q_x) - cos(k_y + q_y)$. We calculate the above correlation functions by means of the so-called time-dependent Hartree-Fock approximation (TDHF). Namely, we solve the Heisenberg equations of motion of particle-hole (p-h) excitation operators (where particle and hole refer to the Hartree-Fock ground state) by approximating the commutators between p-h operators with their expectation values on the HF wave-function. At the BCS level:

$$\begin{aligned} \alpha_k &= \cos\theta_k c_{k\uparrow} - \sin\theta_k c^\dagger_{-k\downarrow} \\ \beta_k &= \sin\theta_k c_{k\uparrow} + \cos\theta_k c^\dagger_{-k\downarrow} \end{aligned} \tag{3.8}$$

are the solutions of the BCS self-consistency equations for the $t-U-W$ model:

$$1 = -\frac{2W}{V}\sum_k \frac{\varphi_k^2}{E_k}, \tag{3.9}$$

where $\varphi_k = \cos k_x - \cos k_y$ and $E_k = \sqrt{(\epsilon_k - \mu)^2 + \Delta_k^2}$. The Hartree-Fock Hamiltonian is

$$H^{HF} = \sum_k E_k(\alpha_k^\dagger \alpha_k - \beta_k^\dagger \beta_k)$$

in the way that α-band is always empty and β-band is always filled. We define the bosonic operators

$$\begin{aligned} b_{kq} &= \beta^\dagger_{k+q}\alpha_k \\ b^\dagger_{kq} &= \alpha^\dagger_k \beta_{k+q} \end{aligned}$$

One can see that $\langle [b_{kq}, b^\dagger_{k'q'}]\rangle = \delta_{k,k'}\delta_{q,q'}$, if averaged on the HF ground state. We can define the operators $X_{k;q} = \frac{1}{\sqrt{2}}\Phi_k\sigma_1\Phi_{k+q}$ and $P_{k;q} = \frac{1}{\sqrt{2}}\Phi_k\sigma_2\Phi_{k+q}$, where $\Phi_k = \binom{\alpha_k}{\beta_k}$ - is the Nambu spinor, σ_i Pauli matrices $i = 0,1,2,3$ being σ_0 identity. $P_{k;q}$ and $X_{k;q}$ commute like generalized coordinate and momentum operators, i. e.

$$\langle [P_{k;q}, X^\dagger_{k';q'}]\rangle = i\delta_{k,k'}\delta_{q,q'}.$$

3.2 Time-dependent Hartree-Fock approximation

In this section we introduce the TDHF approach for the Hubbard Hamiltonian and solve it analytically for spin and charge susceptibilities. We then refer to Appendix A, where it is described how, in an analogous way, both susceptibilities can be found for the full $t-U-W$ Hamiltonian, solving the TDHF equations numerically. Within the TDHF method (for the derivation and discussion of the validity of TDHF see the excellent book of Pines and Nozieres [65]) the non-interacting

Hartree-Fock Hamiltonian is just a Hamiltonian of a system of free, non-coupled harmonic oscillators with frequencies $\omega_{k;q} = E_k + E_{k+q}$:

$$H_{free} = \frac{1}{2}\sum_{kq} \omega_{k;q}\left(X_{k;q}X^{\dagger}_{k;q} + P_{k;q}P^{\dagger}_{k;q}\right)$$

The introduction of Hubbard interaction term leads to the mixing of X_{kq} and P_{kq} with different k:

$$\begin{aligned} H_{int-Hubb} = \frac{U}{2N}\sum_{kpq} \\ \left[\cos\left(\theta_{k+q}+\theta_k\right)\cos\left(\theta_{p+q}+\theta_p\right) + \sin\left(\theta_{k+q}+\theta_k\right)\sin\left(\theta_{p+q}+\theta_p\right)\right] X_{k;q}X^{\dagger}_{p;q} \\ + \left[\cos\left(\theta_{k+q}-\theta_k\right)\cos\left(\theta_{p+q}-\theta_p\right) e \sin\left(\theta_{k+q}-\theta_k\right)\sin\left(\theta_{p+q}-\theta_p\right)\right] P_{k;q}P^{\dagger}_{p;q} \end{aligned} \tag{3.10}$$

To solve the TDHF equations means to diagonalize the Hamiltonian

$$H_{free} + H_{int-Hubb} \equiv \frac{1}{2}\sum_{k,p,q}\left(A_{k;p}(q)X_{k;q}X^{\dagger}_{p;q} + B_{k;p}(q)P_{k;q}P^{\dagger}_{p;q}\right). \tag{3.11}$$

We are interested in the fluctuations around ground state of the original Hamiltonian and they are just the zero-oscillations of eigenmodes:

$$E_{fl} = \frac{1}{4N}\sum_{q}\int \frac{d\omega}{2\pi}\coth\left(\frac{\hbar\beta\omega}{2}\right)\left[\mathcal{I}m\kappa(\omega,q) - \mathcal{I}m\chi(\omega,q)\right]$$

Since the $A_{k;p}(q)$ and $B_{k;p}(q)$ are real and the TDHF Hamiltonian is bilinear in $X_{k;q}$ and $P_{k;q}$ the diagonalization could be performed as if $X_{k;q}$ and $P_{k;q}$ would be the coordinates and momenta of the real classical oscillator, *i.e.* not operators but just number. The exact diagonalization could be accomplished only for finite systems, when we have finite matrices $A_{k;p}(q)$ and $B_{k;p}(q)$. However, if we do not need such complete information about the system but just the two-particles response functions, it is possible to derive a relatively simple system of equations connecting $\kappa(\omega,q)$ and $\chi(\omega,q)$. Namely, if we denote:

$$J_{X,c}(q) = \frac{1}{V}\sum_k X_{k;q}\cos\left(\theta_{k+q}+\theta_k\right), \tag{3.12}$$

$$J_{X,s}(q) = \frac{1}{V}\sum_k X_{k;q}\sin\left(\theta_{k+q}+\theta_k\right), \tag{3.13}$$

$$J_{P,c}(q) = \frac{1}{V}\sum_k P_{k;q}\cos\left(\theta_{k+q}-\theta_k\right), \tag{3.14}$$

$$J_{P,s}(q) = \frac{1}{V}\sum_k P_{k;q}\sin\left(\theta_{k+q}-\theta_k\right), \tag{3.15}$$

then the interaction Hamiltonian could be written as

$$H_{int-Hubb} = \frac{U}{2}\sum_q \left\{-\hat{J}_{P,s}\hat{J}(q)^\dagger_{P,s}(q) + \hat{J}_{P,c}(q)\hat{J}^\dagger_{P,c}(q) + \hat{J}_{X,s}(q)\hat{J}^\dagger_{X,s}(q) + \hat{J}_{X,c}(q)\hat{J}^\dagger_{X,c}(q)\right\}$$

The Heisenberg equations of motion:

$$\begin{cases} \frac{\partial H}{\partial X^\dagger_{kq}} = -\dot{P}_{kq} \\ \frac{\partial H}{\partial P^\dagger_{kq}} = \dot{X}_{kq} \end{cases} \tag{3.16}$$

solved with respect to $X_{kq}(\omega)$ and $P_{kq}(\omega)$ - Fourier components are:

$$\begin{aligned} X_{k;q} &= -\mathrm{i}\frac{\omega U\cos\left(\theta_{k+q}-\theta_k\right)}{\omega^2_{k;q}-\omega^2}J_{P,c} + \mathrm{i}\frac{\omega U\sin\left(\theta_{k+q}-\theta_k\right)}{\omega^2_{k;q}-\omega^2}J_{P,s} \\ &- \frac{\omega_{k;q}U\sin\left(\theta_{k+q}+\theta_k\right)}{\omega^2_{k;q}-\omega^2}J_{X,s} - \frac{\omega_{k;q}U\cos\left(\theta_{k+q}+\theta_k\right)}{\omega^2_{k;q}-\omega^2}J_{X,c} \end{aligned} \tag{3.17}$$

$$\begin{aligned} P_{k;q} &= -\frac{\omega_{k;q}U\cos\left(\theta_{k+q}-\theta_k\right)}{\omega^2_{k;q}-\omega^2}J_{P,c} + \frac{\omega_{k;q}U\sin\left(\theta_{k+q}-\theta_k\right)}{\omega^2_{k;q}-\omega^2}J_{P,s} \\ &+ \mathrm{i}\frac{\omega U\sin\left(\theta_{k+q}+\theta_k\right)}{\omega^2_{k;q}-\omega^2}J_{X,s} + \mathrm{i}\frac{\omega U\cos\left(\theta_{k+q}+\theta_k\right)}{\omega^2_{k;q}-\omega^2}J_{X,c}. \end{aligned} \tag{3.18}$$

These equations of motion describe an unperturbed system and the obvious solution is just $P_{k;q} = 0$ and $X_{k;q} = 0$. Because we need the response functions for density-density and spin-spin fluctuations it is necessary to perturb these degrees of freedom by some external source terms. In the formalism of Nambu spinors and TDHF the charge and spin densities are expressed as follows:

$$\rho(q) = \sum_k \Psi_k^\dagger \sigma_3 \Psi_{k+q} = -\sqrt{2} \sum_k \sin(\theta_{k+q} + \theta_k) X_{k;q} = -\sqrt{2} J_{X,s} \tag{3.19}$$

$$\sigma_z(q) = \sum_k \Psi_k^\dagger \sigma_0 \Psi_{k+q} = -i\sqrt{2} \sum_k \sin(\theta_{k+q} - \theta_k) P_{k;q} = -i\sqrt{2} J_{P,s} \tag{3.20}$$

and hence the terms coupling ρ_q and σ_q respectively are:

$$\begin{aligned} \rho(q) V_q &= -\sqrt{2} \sum_k V_q \sin(\theta_{k+q} + \theta_k) X_{kq} = \\ &- \sqrt{2} J_{X,s} V_q = \sum \lambda^X_{kq} X_{kq} \end{aligned} \tag{3.21}$$

$$\begin{aligned} \sigma_z(q) H_q &= -i\sqrt{2} \sum_k H_q \sin(\theta_{k+q} + \theta_k) P_{kq} = \\ &- i\sqrt{2} J_{X,s} H_q = \sum \lambda^P_{kq} P_{kq}, \end{aligned} \tag{3.22}$$

where

$$\begin{cases} \lambda^X_{k;q} = -\sqrt{2} V_q \sin(\theta_{k+q} + \theta_k) \\ \lambda^P_{k;q} = -\mathrm{i}\sqrt{2} H_q \sin(\theta_{k+q} + \theta_k) \end{cases} \tag{3.23}$$

obey the self-conjugation condition:

$$\begin{cases} \lambda^X_{k;q} = (\lambda^X_{k+q;-q})^* \\ \lambda^P_{k;q} = (\lambda^P_{k+q;-q})^* \end{cases} \tag{3.24}$$

The term (3.21) should be added to the full Hamiltonian (3.11), when determining κ, while (3.22) is for χ. Combining (3.2), (3.17) and (3.18) with source terms one can derive a system of algebraic equations, relating quantities J at fixed q and ω. From the symmetry considerations one can prove that when perturbing $\rho(q)$ then $J_{Ps} = 0$, while for $\sigma_z(q)$ $J_{Xs} = 0$.

The solutions of such equations will be proportional to the source terms and the coefficients will be just the appropriate susceptibilities:

$$\kappa(q,\omega) = \left.\frac{\delta\rho(q,\omega)}{\delta V_q}\right|_{\substack{\lambda^X_{kq}\neq 0 \\ \lambda^P_{kq}=0}} \qquad \chi(q,\omega) = \left.\frac{\delta\sigma_z(q,\omega)}{\delta H_q}\right|_{\substack{\lambda^P_{kq}\neq 0 \\ \lambda^X_{kq}=0}} \tag{3.25}$$

For the Hubbard model the equations of TDHF for susceptibilities could be resolved analytically since we have the system of only 3 linear equations. For the sake

of convenience, in view of further summation over $i\omega$ it is helpful to derive all the susceptibilities as functions of imaginary Matsubara frequencies:

$$\begin{aligned} &\frac{1}{4N}\sum_q \int \frac{d\omega}{2\pi} \coth\left(\frac{\hbar\beta\omega}{2}\right)[\mathcal{I}m\kappa(\omega,q) - \mathcal{I}m\chi(\omega,q)] = \\ &\frac{T}{4N}\sum_q \sum_{\{\omega_n\}} [\kappa(\omega_n,q) - \chi(\omega_n,q)]\,. \end{aligned} \tag{3.26}$$

The RPA expressions for the density-density and spin-spin correlation functions for the case of only Hubbard interaction are:

$$\kappa^{RPA}(q,\omega) = -2\frac{\kappa^{HF}(q,\omega) + G(q,\omega)}{1 + U(\kappa^{HF}(q,\omega) + G(q,\omega))} \tag{3.27}$$

$$\chi^{RPA}(q,\omega) = -2\frac{\chi^{HF}_{zz}(q,\omega)}{1 - U\chi^{HF}(q,\omega)} \tag{3.28}$$

where

$$\kappa^{HF}(q,\omega) = \frac{1}{N}\sum_{k\in BZ} \frac{\omega_{kq}\sin^2(\theta_{k+q} + \theta_k)}{\omega^2 + \omega^2_{kq}} \tag{3.29}$$

$$\chi^{HF}(q,\omega) = \frac{1}{N}\sum_{k\in BZ} \frac{\omega_{kq}\sin^2(\theta_{k+q} - \theta_k)}{\omega^2 + \omega^2_{kq}} \tag{3.30}$$

ω being on imaginary axis and $G(q,\omega)$ expressed in terms of the following sums:

$$G(q,\omega) = U\frac{S_5^2(1+US_1) - S_3^2(1+US_4) - 2S_3S_2S_5U}{U^2S_2^2 + (1+US_1)(1+US_4)}, \tag{3.31}$$

$$S_1(q,\omega) = \frac{1}{N}\sum_{k\in BZ} \frac{\omega_{kq}\cos^2(\theta_{k+q} + \theta_k)}{\omega^2 + \omega^2_{kq}} \tag{3.32}$$

$$S_2(q,\omega) = \frac{1}{N}\sum_{k\in BZ} \frac{\omega\cos(\theta_{k+q} + \theta_k)\cos(\theta_{k+q} - \theta_k)}{\omega^2 + \omega^2_{kq}} \tag{3.33}$$

$$S_3(q,\omega) = \frac{1}{N}\sum_{k\in BZ} \frac{\omega_{kq}\cos(\theta_{k+q} + \theta_k)\sin(\theta_{k+q} + \theta_k)}{\omega^2 + \omega^2_{kq}} \tag{3.34}$$

$$S_4(q,\omega) = \frac{1}{N}\sum_{k\in BZ} \frac{\omega_{kq}\cos^2(\theta_{k+q} - \theta_k)}{\omega^2 + \omega^2_{kq}} \tag{3.35}$$

$$S_5(q,\omega) = \frac{1}{N}\sum_{k\in BZ} \frac{\omega\cos(\theta_{k+q} - \theta_k)\sin(\theta_{k+q} + \theta_k)}{\omega^2 + \omega^2_{kq}}. \tag{3.36}$$

In (3.32-3.36) we used θ_k defined as in (3.8):

$$\cos 2\theta_k = -\frac{\varepsilon_k - \mu}{E_k}, \qquad \sin 2\theta_k = \frac{\Delta_k}{E_k}.$$

In the case of added H_{d-SC} term the latter is represented in terms of J operators as follows:

$$H_{d-SC} = \frac{W}{N}\sum_q \Big\{ -J_{FP,s}(q)J^\dagger_{FP,s}(q) + J_{FX,s}(q)J^\dagger_{FX,s}(q) + \tag{3.37}$$
$$J_{\varphi\varphi P,c}(q)J^\dagger_{P,c}(q) + J_{P,c}(q)J^\dagger_{\varphi\varphi P,c}(q) + J_{\varphi P,c}(q)J^\dagger_{\varphi_1 P,c}(q) + J_{\varphi_1 P,c}(q)J^\dagger_{\varphi P,c}(q) +$$
$$J_{\varphi\varphi X,c}(q)J^\dagger_{X,c}(q) + J_{X,c}(q)J^\dagger_{\varphi\varphi X,c}(q) + J_{\varphi X,c}(q)J^\dagger_{\varphi_1 X,c}(q) + J_{\varphi_1 X,c}(q)J^\dagger_{\varphi X,c}(q)\Big\}$$

being J operators, apart from those defined by (3.12-3.15) are the following:

$$J_{FX,s}(q) = \frac{1}{V}\sum_k F(k,q)X_{k;q}\sin\left(\theta_{k+q}+\theta_k\right), \tag{3.38}$$

$$J_{FP,s}(q) = \frac{1}{V}\sum_k F(k,q)P_{k;q}\sin\left(\theta_{k+q}-\theta_k\right), \tag{3.39}$$

$$J_{\varphi\varphi P,c}(q) = \frac{1}{V}\sum_k \varphi(k)\varphi(k+q)P_{k;q}\cos\left(\theta_{k+q}-\theta_k\right), \tag{3.40}$$

$$J_{\varphi\varphi X,c}(q) = \frac{1}{V}\sum_k \varphi(k)\varphi(k+q)X_{k;q}\cos\left(\theta_{k+q}+\theta_k\right), \tag{3.41}$$

$$J_{\varphi P,c}(q) = \frac{1}{V}\sum_k \varphi(k)P_{k;q}\cos\left(\theta_{k+q}-\theta_k\right), \tag{3.42}$$

$$J_{\varphi X,c}(q) = \frac{1}{V}\sum_k \varphi(k)X_{k;q}\cos\left(\theta_{k+q}+\theta_k\right), \tag{3.43}$$

$$J_{\varphi_1 P,c}(q) = \frac{1}{V}\sum_k \varphi(k+q)P_{k;q}\cos\left(\theta_{k+q}-\theta_k\right), \tag{3.44}$$

$$J_{\varphi_1 X,c}(q) = \frac{1}{V}\sum_k \varphi(k+q)X_{k;q}\cos\left(\theta_{k+q}+\theta_k\right), \tag{3.45}$$

where $\varphi(k) = \cos k_x - \cos k_y$ and $F(k,q) = \varphi(k+q)+\varphi(q)$. An efficient algorithm, which allows to solve TDHF equations for the susceptibilities numerically in the case of an interaction of arbitrary form and which was used in the present Chapter is described in Appendix A. Notice that TDHF is identical to the so called Generalized Random Phase Approximation [65].

3.3 Results

The BCS wave function

$$|\Psi_{BCS}\rangle = \prod_k \left(u_k + v_k c^\dagger_{k\uparrow} c^\dagger_{-k\downarrow}\right)|0\rangle$$

does not conserve the number of particles. On the other hand, the number operator $\hat{N}$ commutes with the Hamiltonian. Therefore the exact charge density susceptibility at $q = 0$, defined by

$$\kappa(t,0) = -\mathrm{i}\theta(t)\langle\left[\hat{N}(t), \hat{N}(0)\right]\rangle = -\mathrm{i}\theta(t)\langle\left[\hat{N}, \hat{N}\right]\rangle \tag{3.46}$$

is identically zero. The charge susceptibility, calculated within BCS Hartree-Fock does not fulfill this requirement: expression (3.29) at $q = 0$ gives

$$\kappa^{HF}(0,\omega) = \frac{1}{N}\sum_{k\in BZ} \frac{2E_k \sin^2 2\theta_k}{\omega^2 + E_k^2} \neq 0.$$

This is because we have broken the U(1) symmetry in BCS allowing a class of wave functions non conserving the number of particles and thus not satisfying the rule (3.46). Taking into account quantum fluctuations as it is done within TDHF permits to obtain a susceptibility, obeying (3.46). To see that let us rewrite the Heisenberg equations of motion for $X_{k,0}$ (3.16) in the presence of W part (3.37) at $q = 0$ with a source term coupled to the density:

$$\begin{aligned} -\ \omega X_{k,0} &= 2E_k P_{k',0} + \frac{U}{V}\sum_{k'} P_{k',0} \\ +\ \frac{2W}{V}&\left(\varphi_k^2 \sum_{k'} P_{k',0} + \sum_{k'} \varphi_{k'}^2 P_{k',0} + 2\varphi_k \sum_{k'} \varphi_{k'} P_{k',0}\right). \end{aligned} \tag{3.47}$$

Remembering the definition of charge density in TDHF (3.19) we get

$$\kappa^{RPA}(0,\omega) = \frac{\rho(q)}{V_q} = \frac{2\sqrt{2}}{\omega}\sum_{k'} \varphi_{k'} P_{k',0}\Delta\left[1 + \frac{2W}{V}\sum_k \frac{\varphi_k^2}{E_k}\right] = 0$$

which implies $\kappa^{RPA}(0,\omega) = 0$, since the expression in brackets is just the self-consistency condition (3.9). Here Δ is the amplitude of BCS gap $\Delta_k = \Delta(\cos k_x - \cos k_y)$. Thus in TDHF the correct behavior of the charge density susceptibility around the point $q \to 0$ is restored, which helps to avoid unphysical results in calculation of the correlation energy.

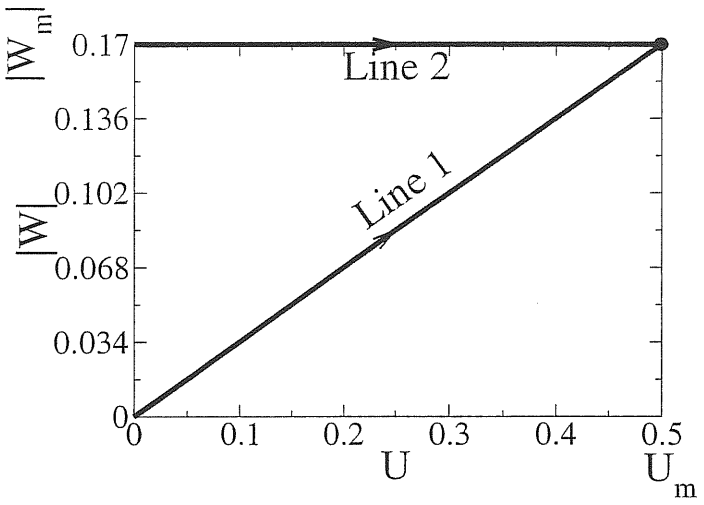

Figure 3.1: The paths in the $U-W$ plane we have used in calculation of the exchange correlation energy at the point $U = 0.5t$, $W = -0.17t$ (solid circle at the right top of the figure) according to (3.5). Values are in units of t.

Since TDHF is a weak coupling theory we are constrained to work in the region of Hamiltonian parameters U and W, when the latters can be considered as the a perturbation to the free electron system, described by the kinetic energy. In addition we have to avoid the values of doping very close to half filling, since in that case even small U can turn the system into the antiferromagnetic insulator. On the other hand, since we expect the condensation energy change due to correlations to be very small, compared to the BCS condensation energy Δ^2/ε_F, which in turns is a small quantity, then W, governing the BCS gap should not be too small i) to allow the BCS gap solution on a system of a given finite size and ii) to permit the effect to be observed numerically. Based on the above considerations we have chosen the following range of parameters: $0 < U < 0.5t$, $-0.17t < W < 0$ and the doping $\delta = 0.20$. In this range we calculate the integrals in $U - W$ plane as described in the previous section along the paths shown of Fig.3.1. line 1 is the simplest possible path, which joins the points $U = 0$, $W = 0$ and $U = 0.5t$, $W = -0.17t$, being in the latter the maximal effect, while in the former identically zero. The second line on Fig.3.1 serves to study the influence of changing only U on the correlation energy, since Δ, depending only on W remains constant.

After integrating out the frequency in (3.7) we have the difference of correlation functions depending on q. In the rest of this Chapter for brevity we shall call this

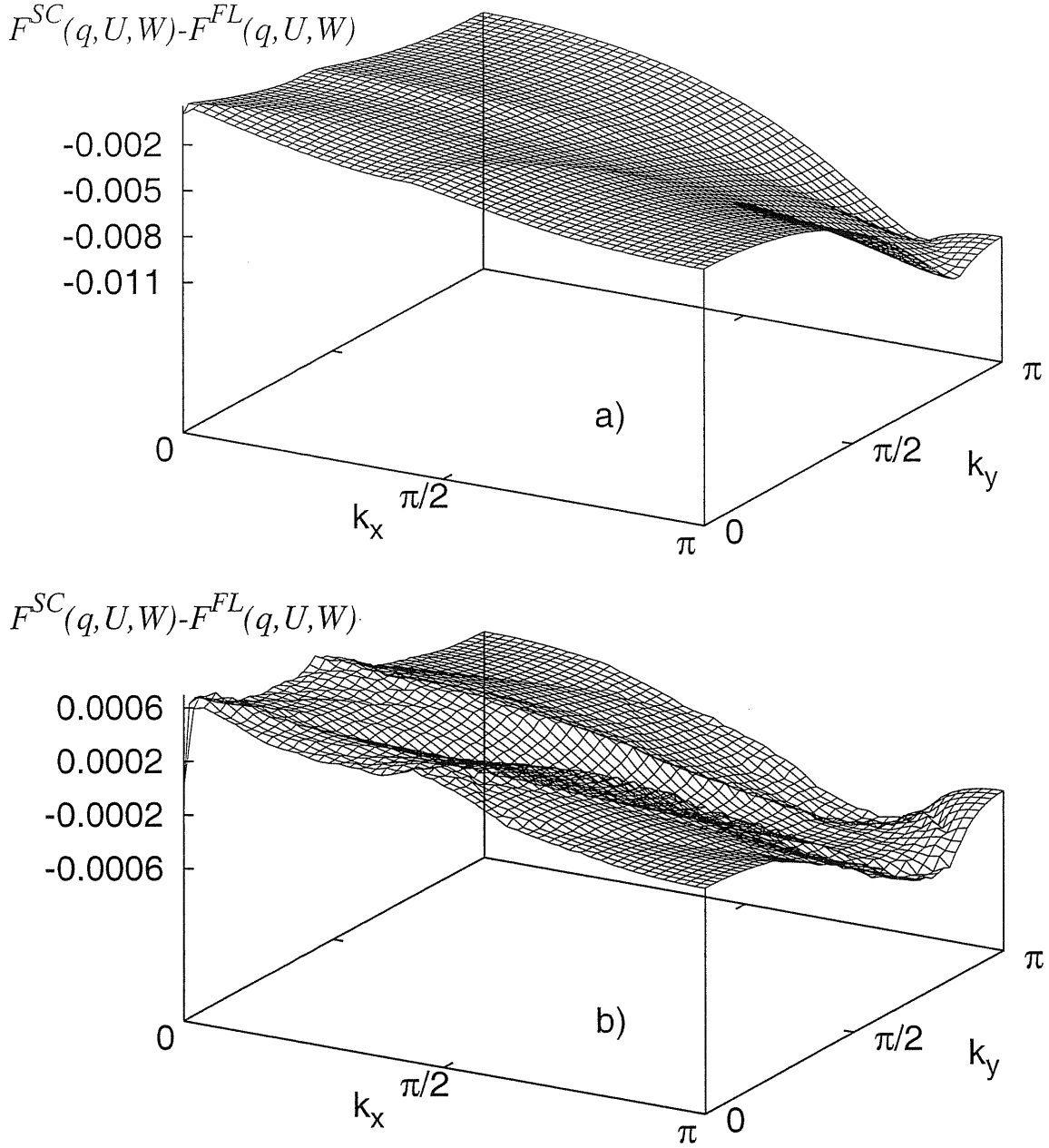

Figure 3.2: a) Correlation energy $F(q,U,W)$ as a function of momentum q for the superconducting state as calculated in TDHF, $U = 0.5t$, $\delta = 0.20$ $W = -0.17t$. The values plotted for $F(q,U,W)$ are the deviation from the bare value $(\frac{\pi}{2})^2$. b) Difference in correlation energy between superconducting and Fermi liquid states at the same values of Hamiltonian parameters as in a).

difference $F(q,U,W)$:

$$F(q,U,W) \equiv \frac{1}{4}\int \frac{d\omega}{2\pi} \coth\left(\frac{\beta\hbar\omega}{2}\right) \left[\mathcal{I}m\kappa(\omega,q) - \mathcal{I}m\chi(\omega,q)\right]. \tag{3.48}$$

Its value should then be summed over all momenta and integrated along the appropriate path in the $U-W$ plane. Studying the q dependence of $F(q,U,W)$ allows to reveal the momenta which have the dominant contribution to the correlation energy. At fixed W, since the Hubbard repulsion does not affect the d-wave superconductivity, but only the chemical potential, we have Δ also fixed. We got for $U = 0.5t$, $W = -0.17t$ and $\delta = 0.20$ following values of BCS parameters: $\mu = -0.4352t + U(1-\delta)^2/4$, $\Delta = 0.026489t$.

The q dependence of $F(q,U,W)$ for the superconducting "parent" state is shown on Fig. 3.3a). That of Fermi liquid one is very similar and their difference is presented on Fig. 3.3b). The most contributing part is that near the nesting vector $\vec{Q} = (\pi,\pi)$, which at finite doping splits into two incommensurate vectors. This clearly shows that the fluctuations in the spin channel dominate the correlation energy in Hubbard model within TDHF, both in superconducting and in Fermi liquid states. At $q = 0$ we have $F(q,U,W) = 0$ in both states, as the gauge invariance implies. Fig. 3.3b) shows that the superconductor gains energy in TDHF, since the integral difference $\int \mathrm{d}^2q(F^{SC}(q,U,W) - F^{FL}(q,U,W))$ is negative. By the opening of a superconducting gap the correlation energy is enhanced in the vicinity of $\vec{Q}$, while near to $q = 0$ the effect is opposite. As we have already mentioned the enhancement of charge fluctuations through (3.7) makes the superconductor to loose the energy respect to the Fermi liquid, while the opposite happens with the spin fluctuations. Such an enhancement in the charge channel occurs because putting an attractive interaction into TDHF allows a competition also against a charge ordered phase, whose enhanced correlations are observed in the charge density susceptibility of the superconductor. These correlations will finally lead to a charge ordering instability on long distances upon further increase of $|W|$. Since in the real materials there is also the residual long range Coulomb interaction, our results at small q might be an artifact of the oversimplified model. We emphasize, however, that the enhanced charge fluctuations can not turn the overall sign of the "correlation part" of the condensation energy due to Hubbard interaction. On the contrary, the spin fluctuations due to the proximity of an antiferromagnetic state, known to be well reproduced by the Hubbard model, lower the correlation energy in TDHF.

We proceed now to the analysis of the integral contribution to the exchange correlation energy. We are interested in its numerical value at the point $U = 0.5t$, $W =$

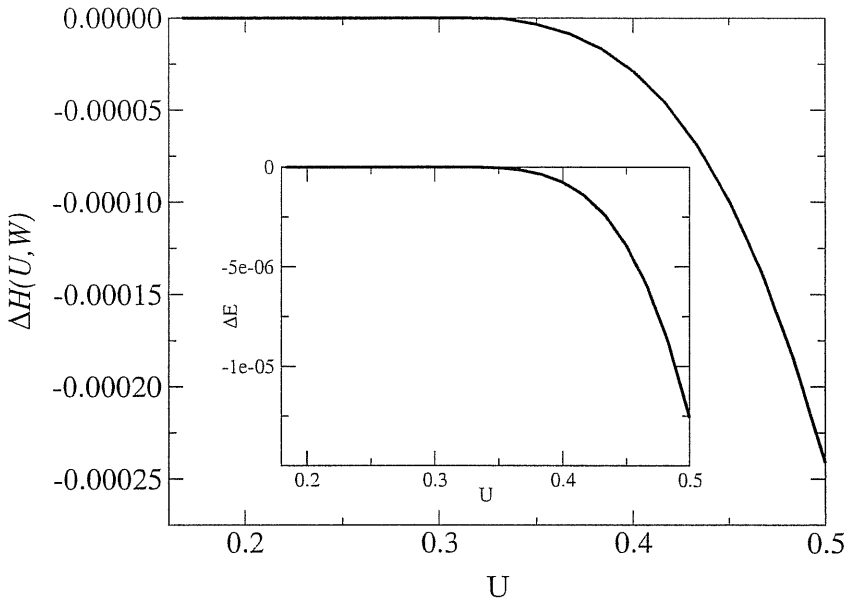

Figure 3.3: Correlation functions difference $\Delta H(U,W)$ between superconducting and normal states as a function of U along the line 1 on the Fig. 3.1. $\delta = 0.20$, U and W change from $(U = 0,\ W = 0)$ to $(U = 0.5t,\ W = -0.17t)$.

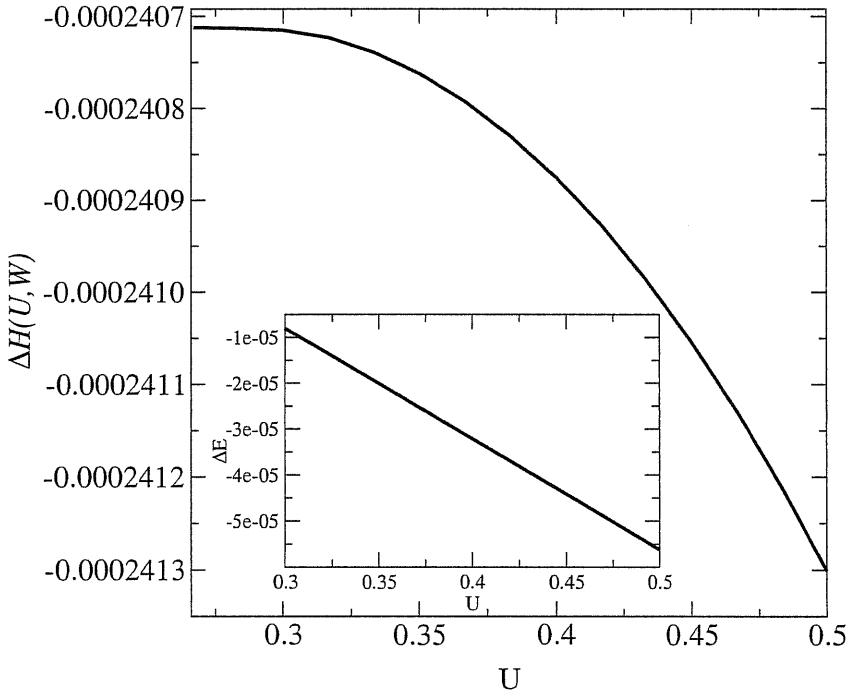

Figure 3.4: Correlation functions difference $\Delta H(U,W)$ between superconducting and normal states as a function of U along the line 2 on the Fig. 3.1. $\delta = 0.20$, U and W change from $(U = 0,\ W = -0.17t)$ to $(U = 0.5t,\ W = -0.17t)$.

$-0.17t$ as well as in its behavior upon varying U and W. In the underlying Hartree-Fock state the superconducting gap depends only on W. Therefore when both U and W are changed there are two quantities which affect the correlation energy: U and Δ. To study both possibilities, in addition to the line 1, where U and W are changed linearly to each other, we consider also the line 2, where W and hence Δ remains constant.

We define the exchange correlation part of the condensation energy ΔE as follows:

$$\Delta E = \int_S \mathrm{d}s \Delta H(U(s), W(s)), \tag{3.49}$$

where

$$\Delta H(U, W) \equiv \int \mathrm{d}^2 q \left\{ F^{SC}(q, U, W) - F^{FL}(q, U, W) \right\}. \tag{3.50}$$

Here the path S is either line 1 or line 2. The plots of $\Delta H(U, W)$ along the lines 1 and 2 as a function of U are shown on main panels of Fig. 3.3 and Fig. 3.4 respectively, while the results of integration along S are shown on the insets. Comparing these two figures it is clear that both U and Δ contribute to lower the correlation energy, being a pronounced tendency to gain the energy at fixed Δ just upon increase of U, as it can be seen from the Fig. 3.4.

To get more quantitative insight, we compare the value of ΔE to the that of the BCS condensation energy ΔE^{BCS}. The latter is defined as the difference between the ground state energy of BCS Hamiltonian:

$$\hat{H}^{HF} = \frac{1}{V} \sum_k (\varepsilon_k - \mu)(c^\dagger_{k\uparrow} c_{k\uparrow} + c^\dagger_{-k\downarrow} c_{-k\downarrow}) + 4W\Delta_1 \frac{1}{V} \sum_k \varphi_k (c^\dagger_{k\uparrow} c^\dagger_{-k\downarrow} + c_{-k\downarrow} c_{k\uparrow}) \tag{3.51}$$

with optimized Δ and that of $\Delta = 0$, at the same value of doping. Here

$$\Delta_1 = \frac{1}{4V} \sum_k \frac{\Delta \varphi_k^2}{E_k} \tag{3.52}$$

- is the BCS order parameter. On Fig. 3.5 we plot both ΔE and ΔE^{BCS}, measured along the line 1.

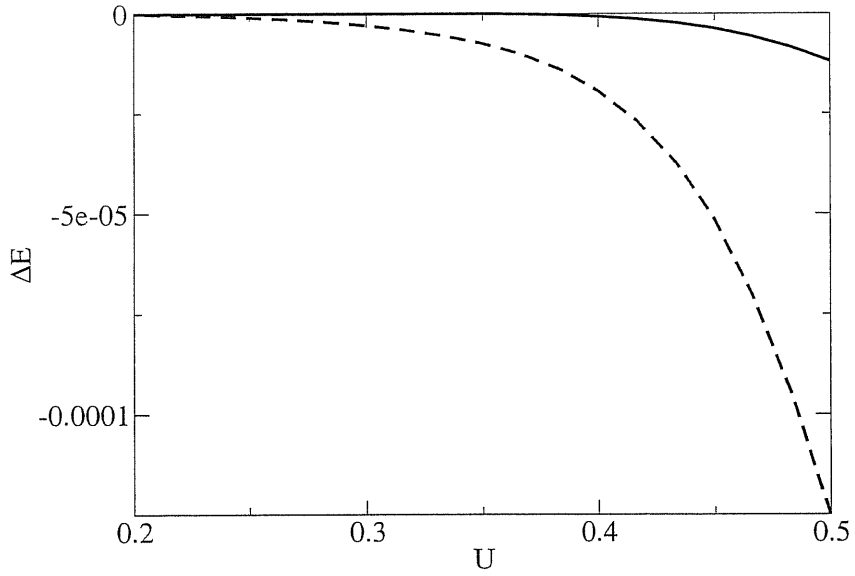

Figure 3.5: Exchange correlation energy ΔE (solid line) against the BCS condensation energy ΔE^{BCS} (dashed line) along the line 1 on the Fig. 3.1.

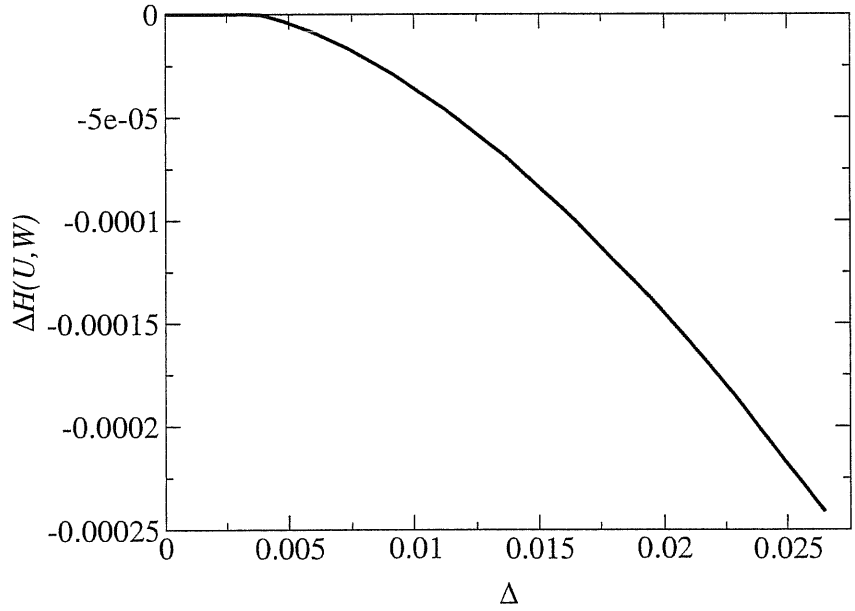

Figure 3.6: Correlation functions difference $\Delta H(U, W)$ between superconducting and normal states as a function of superconducting gap Δ along the line 1 on the Fig. 3.1. $\delta = 0.20$, U and W change from ($U = 0$, $W = 0$) to ($U = 0.5t$, $W = -0.17t$).

While the former remains always small, compared to the latter, as it is needed for the weak coupling TDHF method to be valid, it gives however a sensible contribution to

the overall energy gain of the superconductor. For example at $U = 0.5t$, $W = -0.17t$ we have $\Delta E/\Delta E^{BCS} \sim 10^{-1}$. To complete our analysis we present on Fig. 3.6 the dependence of $\Delta H(U, W)$ on the BCS gap Δ along the line 1, which shows that the above quantity is very sensible to the the gap change.

3.4 Conclusions

In this Chapter we have considered the influence of the exchange correlation energy on the total energy balance in BCS type d-wave superconductor. We used the so called Time-Dependent Hartree-Fock Approximation, which is identical to the generalized Random Phase Approximation, to treat the interaction in the $t - U - W$ model. The above exchange correlation energy was compared in both superconducting and Fermi-liquid states in the region of Hamiltonian parameters where the interactions U and W can be considered weak and the above TDHF method is applicable. We have found that the exchange correlations lower the energy of the superconductor, and this effect comes from the enhancement of the spin correlations in the vicinity of $\vec{Q} = (\pi, \pi)$. Numerical value of the exchange correlation energy gain in the superconductor at $U = 0.5t$ and $W = -0.17t$ is only an order of magnitude smaller than the appropriate condensation energy in BCS. This means that the presence of Hubbard repulsion enforces the stability of a d-wave superconductor if the correlations are taken into account. This effect was shown also to increase by increasing U.

We can formally write down the ground state of a system, containing the quantum fluctuations around the Hartree-Fock state as a state with zero-point motion of harmonic oscillators $\tilde{X}_{kq}$, $\tilde{P}_{kq}$ - eigenmodes of (3.10) plus (3.2):

$$|\Psi_{RPA}\rangle = \prod_{k,q} \exp\left\{\mathrm{i}\gamma_{kq}(\tilde{P}^{\dagger}_{kq}\tilde{X}_{kq} + \tilde{X}^{\dagger}_{kq}\tilde{P}_{kq})\right\}|BCS\rangle. \tag{3.53}$$

After some algebra it can be rewritten in terms of the original α and β operators from page 36 as follows:

$$|\Psi_{RPA}\rangle = \prod_{q,q'} \exp\left\{-\zeta(q,q')n^{\alpha}_{q}n^{\beta}_{q'}\right\}|BCS\rangle \tag{3.54}$$

with some other coefficient $\zeta(q, q')$ and e.g.

$$n^{\alpha}_{q} \equiv \sum_{k} \alpha^{\dagger}_{k}\alpha_{k+q}. \tag{3.55}$$

Written in this form it resembles a well known Jastrow correlated BCS wave function (see the next Chapters):

$$|\Psi_{\rm Jastrow}\rangle = \exp\left\{-\sum_q v_q n_q n_{-q}\right\}|BCS\rangle. \tag{3.56}$$

We expect therefore, that our results for small U can be qualitatively confirmed by using the above Jastrow wave function.

Chapter 4

Increasing $d-$wave superconductivity by on site repulsion

4.1 Introduction

The interplay between strong correlation and superconductivity is one of the major problems raised by the discovery of cuprate High-T_c materials. In the present chapter we address the question of what influence could have a repulsion of the form:

$$H_U = \sum_{ij} U_{ij} n_i n_j \tag{4.1}$$

with a large on-site component $U_{ii} = U$, on a system which does have an explicit attraction, parametrized by a coupling V_{SC}. Within the conventional BCS theory for phonon-mediated weak coupling superconductivity, a repulsive interaction is likely to depress T_c. Indeed, according to Landau Fermi liquid theory, the attractive coupling in the presence of strong repulsion would acquire an additional renormalization (we neglect that one induced by the same attraction, which we assume to be small) :

$$V^*_{SC} \to Z^2 \Gamma_V V_{SC} \tag{4.2}$$

where Γ_V includes vertex corrections and

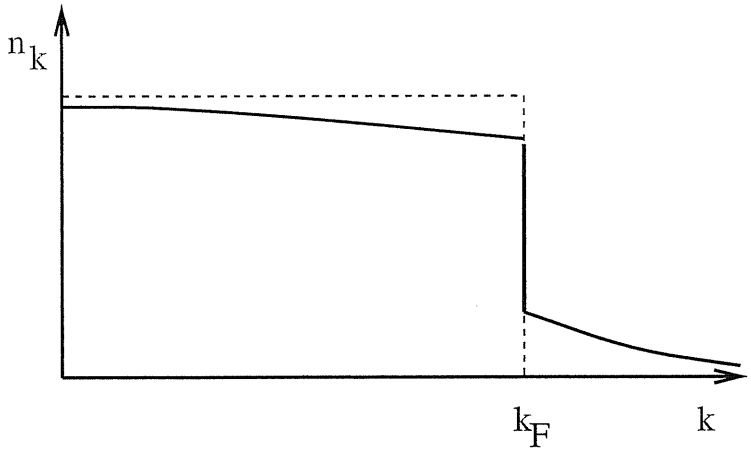

Figure 4.1: The momentum distribution jump for the interacting (full line) and noninteracting (dashed line) cases.

$$Z = \left(1 - \frac{\partial \Sigma(k_F, 0)}{\partial \omega}\right)^{-1} \tag{4.3}$$

is the *quasiparticle wave function renormalization*, $\Sigma(k, \omega)$ being the electron self-energy defined through one-particle Green function, namely

$$G(k, \mathrm{i}\omega) = \frac{1}{\mathrm{i}\omega - \varepsilon_k^0 - \Sigma(k, \omega)}. \tag{4.4}$$

Here ε_k^0 and k_F are respectively the dispersion and Fermi momentum of non-interacting system. The parameter $Z < 1$ is also the jump in the interacting momentum distribution, see Fig.4.1. For a strongly correlated system one expects $Z \ll 1$.

Another consequence of repulsion which is relevant for superconductivity is the *quasiparticles effective mass* enhancement:

$$m_* = \frac{m}{Z}\left(1 + \frac{1}{m k_F}\frac{\partial \Sigma(k_F, 0)}{\partial k}\right). \tag{4.5}$$

Typically $m/Z \geq m_* > m$, being the former an equivalence only if the self-energy is momentum independent.

The dimensionless parameter which measures the strength of the attractive interaction between electrons is the product of the renormalized interaction amplitude

times the quasi-particle *density of states at the Fermi level* $V_{SC}^{*}\rho_{*} = \lambda_{*}$. In the presence of strong repulsion, the latter is increased with respect to its non interacting value ρ_0 according to $\rho_{*} = \rho_0 m_{*}/m > \rho_0$. Therefore

$$\lambda_{*} = \lambda_0 \, Z^2 \, \Gamma_V \, \frac{m_{*}}{m}. \tag{4.6}$$

If vertex corrections are negligible with respect to the strong wave-function renormalization, i.e. $\Gamma_V \sim 1$ while $Z \ll 1$, then

$$\lambda_{*} \ll \lambda_0,$$

implying a pronounced suppression of the attraction strength.

As we discussed in Chapter 2, one has also to consider the residual repulsion among quasiparticles, V_C. When the superconductivity is concerned, the strength of this repulsion is parametrized by the dimensionless Coulomb pseudo potential $\mu \equiv V_C \rho_0$. Even if RPA-screened, the Coulomb interaction may be still much stronger than the electron-phonon attraction. However, taking into account *retardation effects* leads to an additional screening which takes advantage of the degrees of freedom at higher energy scales than the typical one, defined as ω_c in Chapter 2, below which the attraction is effective. By summing up ladder-type diagrams for the residual Coulomb interaction, one shows [66] that the actual repulsion experienced by the low-energy electrons is much lower:

$$\mu_{*} = \frac{\mu_0}{1 + \mu_0 \log\left(\frac{\omega_c}{\varepsilon_F}\right)}. \tag{4.7}$$

Here ε_F is the Fermi energy. One expect that, upon increase of repulsion, the Coulomb pseudo potential among quasiparticles increases, hence $\lambda_{*} - \mu_{*}$ diminishes even more pushing T_c down.

By solving a model for alkali doped fullerenes within dynamical mean field theory, it has been recently argued[67] that there exist attractive channels for which vertex corrections may compensate the wave-function renormalization factor leading to

$$\lambda_0 \to \frac{m_{*}}{m}\lambda_0 > \lambda_0,$$

which may indeed lead to an enhancement of T_c by increasing U. The main ingredient was identified into a pairing mechanism not involving the charge density operator, which is mostly subject to the renormalization induced by U, but other

internal degrees of freedom, like the spin (or the orbital index, if orbital degeneracy is present), unveiling a kind of spin-charge separation even within Landau Fermi liquid theory.

This proposal is not far in spirit from the original Resonating Valence Bond (RVB) scenario for High-T_c superconductivity in the t-J model[9]. There superconductivity occurs naturally upon doping since the parent insulating state is well described by an RVB state: the spin-singlet valence-bond pairs naturally evolve into Cooper pairs. They can propagate around the lattice only through the empty sites left behind by the holes. This constraint easily explains a superfluid density proportional to the hole doping. Moreover, although at small doping superconductivity is suppressed, the energy scale associated to the binding energy of the valence-bond pairs remains finite, which is advocated to explain the experimentally observed pseudo-gap phase of High-T_c materials[68, 61].

Within the Fermi liquid framework, the constraint of no double occupancy appears to renormalize the quasiparticle hopping to a value $Zt \simeq 2\delta t$, δ being the doping, while leaving untouched the quasiparticle attraction, here provided by the super-exchange J. The superconducting phase of the t-J model can be approached either from the half-filled anti-ferromagnetic Mott insulator upon increasing doping or at finite doping by decreasing temperature. In both cases, even though the $T = 0$ superconductor might still be described in terms of Landau-Bogoliubov quasiparticles, in the RVB language spinon-holon confined objects, the relevant excitations above T_c or in the close vicinity to the half-filled anti-ferromagnet do not necessarily look as conventional quasiparticles.

For this reason, in this work we shall try to understand whether this strongly correlated d-wave superconductor can be approached at zero temperature starting from a weakly correlated regime, where standard many-body techniques and the well established Landau Fermi liquid theory should apply.

We consider an extended Hubbard model in two-dimensions away from half-filling,

$$\begin{aligned}\hat{H} &= -t\sum_{<ij>}\sum_{\sigma}\left(c^{\dagger}_{i\sigma}c_{j\sigma}+H.c.\right)+U\sum_{i}n_{i\uparrow}n_{i\downarrow} \\ &\quad +J\sum_{<ij>}\left(\vec{S}_i\cdot\vec{S}_j-\frac{1}{4}n_in_j\right)+V\sum_{<ij>}n_in_j, \qquad (4.8)\end{aligned}$$

where, in addition to the on-site repulsion, we add a nearest neighbor spin-exchange and a charge-repulsion term, with strengths J and V, respectively. These nearest-neighbor interactions compete, J favoring a d-wave singlet pairing away from half-

filling while V opposing against it. For $V = 0$ and U strictly equal to ∞, (4.8) reduces to the standard t-J model, which also corresponds to the large U limit of the pure Hubbard model, in which case $J \to 4t^2/U$. However, contrary to the latter, model (4.8) possesses undoubtedly a d-wave superconducting phase at weak coupling (U, V and J all much smaller than t) also within the Hartree-Fock approximation. Indeed one can show that J provides a d-wave pairing mechanism with $\lambda_0 = J\rho_0$, while V an opposing Coulomb pseudo potential, $\mu_0 = V\rho_0$, being d-wave not sensible to the on-site repulsion U. Therefore, at least for weak coupling, if $J > V$ superconductivity occurs, otherwise a normal metal is more stable.

For this reason model (4.8) is more suitable to address the issue of electron-electron correlation effects on d-wave superconductivity. Moreover, since V involves charge-density while J spin-density operators, the presence of both gives the opportunity to test if U indeed induces different renormalization factors on charge with respect to spin vertices.

4.2 Results of VMC

A variational approach which was shown to correctly reproduce both the weak [69] and the strong [70] coupling limits of the Hubbard model appears well suited for model (4.8) too. It consists in searching by a variational Monte Carlo (VMC) technique for the best wave function of the form

$$|\Psi\rangle = A\hat{P}_{\mathrm{N}}\hat{P}_{\mathrm{Jastrow}}\hat{P}_{\mathrm{G}}|\Psi_{BCS}\rangle \tag{4.9}$$

where A is a normalization factor, $|\Psi_{BCS}\rangle$ a BCS wave-function [71] projected by $\hat{P}_{\mathrm{N}}$ onto a fixed number of particles, with a d-wave gap-function $\Delta_k = \Delta_{var}(\cos k_x - \cos k_y)$, being Δ_{var} a variational parameter, $|0\rangle$ is the vacuum. $\hat{P}_{\mathrm{G}}$ is a Gutzwiller projector:

$$\hat{P}_{\mathrm{G}} = \prod_n (1 - \alpha_0 n_{n,\uparrow} n_{n,\downarrow}), \tag{4.10}$$

whereas $\hat{P}_{\mathrm{Jastrow}}$ a long-range Jastrow factor which enforces the correct long-wavelength behavior of the structure factors (see Appendix B):

$$\hat{P}_{\mathrm{Jastrow}} = e^{-\alpha_1 \sum_{<ij>} n_i n_j - \alpha_2 \sum_{<<ij>>} n_i n_j - \ldots}, \tag{4.11}$$

where "..." stands for the summation over next, next-next, etc. nearest neighbor sites (i.e. all those possible on a finite size sample).

The method is based on the Stochastic Reconfiguration (SR) technique [70], which allows to minimize the energy of a variational wave function containing even a large number of parameters.

To get further insight from the numerics, we compare the results with those obtained by the *Gutzwiller approximation*, described below, for the variational wavefunction without the long-range Jastrow factor and the projector onto a fixed number of particles.

In Fig. 4.2 we plot the variational parameter Δ_{var} as a function of U for $J = 0.2t$, $\delta = 0.16$ and for different values of V. For $J > V$, Δ_{var} starts finite at $U = 0$ and increases with U. For $V > J$, $\Delta_{var} = 0$ at small U, in agreement with the Hartree-Fock results. More remarkably above a critical U_c a finite Δ_{var} appears. Namely, the normal metal at $V > J$ turns into a superconductor by increasing the on-site repulsion. Both results can be explained within the Fermi liquid picture provided by the Gutzwiller approximation, according to which the effective J_* acting between the quasiparticles stays essentially un-renormalized when U increases, contrary to V_*, which is substantially suppressed with respect to its bare value V. Therefore, as U increases for $J > V$, the quasiparticle bandwidth gets reduced, the attraction staying un-renormalized, so that the dimensionless coupling λ_* increases, hence Δ_{var}. If $J < V$, a normal metal is stable until $V_* > J_* \simeq J$, after which superconductivity gets in. In our numerical study we have found that the inclusion of the long range Jastrow factor (4.11) considerably improves the simpler Gutzwiller wave function and allows larger values of Δ_{var}. However, as shown in Fig. 4.2b the qualitative behavior of Δ_{var} vs. U is reproduced already by Gutzwiller approximation.

4.3 Gutzwiller approximation

When dealing with Gutzwiller type variational wave function, the approximation, described below and called *Gutzwiller approximation* (GA) appears to be extremely useful. There is no rigorous justification of using it for any finite-dimensional system, but at least for two dimensions the empirical observation is that GA works surprisingly well [72]. In his original paper Gutzwiller [73] has proposed to treat the variational wave function

$$|\Psi_G\rangle = \prod_k (1 - g n_{\uparrow,k} n_{\uparrow,k}) \, |\Psi_0\rangle \tag{4.12}$$

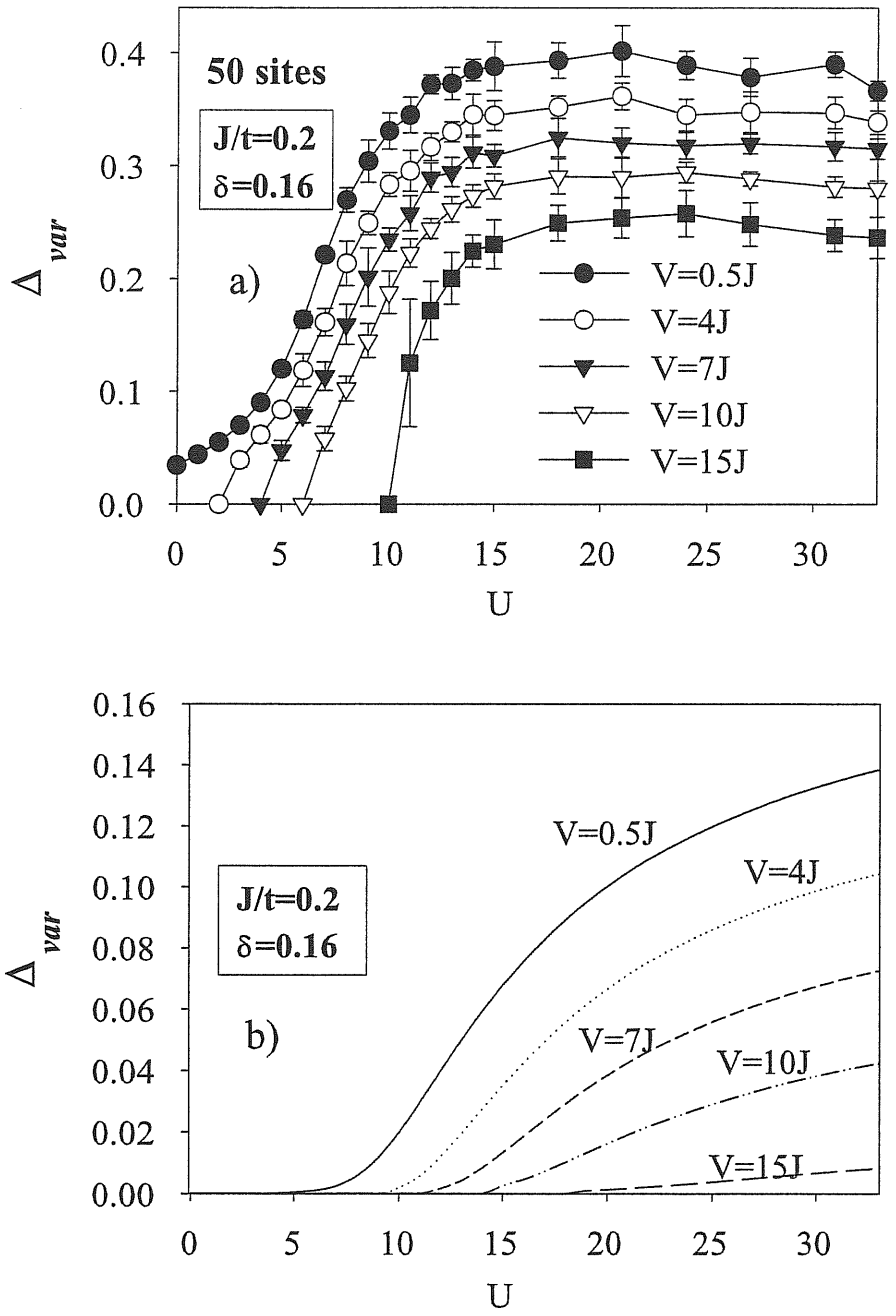

Figure 4.2: Variational gap as function of U for different values of V within variational Monte Carlo a) and GA b).

approximately, as if there were no spatial correlations in the system. Here $|\Psi_0\rangle$ is the "uncorrelated" wave function e.g. BCS wave function. Resulting picture becomes site-independent and the local probabilities of finding spin up/down or both of them on a given site are determined from pure combinatorial counting. Vollhardt and Metzner [75] and Gebhard [74] have developed analytical approaches for treating the correlation functions averaged on Gutzwiller wave function. They have constructed the perturbation expansion in powers of $g^2 - 1$ (g from (4.12)). These methods appeared to be significantly simplified in the limit of infinite dimensions [75], [74], when the self-energy becomes momentum-independent. It was proved that GA becomes exact for Gutzwiller variational wave function when $d \to \infty$. The action of Gutzwiller (density-density suppressing) correlation in this limit is reduced to the multiplication of a given correlation function by a factor depending on variational parameter. Since in infinite dimensions there is a simple relation between variational parameter g and the probability of double occupancy d the later is usually used as a variational parameter.

We consider the Hubbard model with $2n$ electrons per site, n therefore being the filling. We define as $0 < d < n$ the probability $P_2(d)$ of having a doubly occupied site, hence $P_0(d) = 1-2n+d$ is the probability of an empty site and $P_1(d) = (2n-2d)$ the probability of single occupancy. If $T_0(n)$ is the non interacting average value of the hopping energy, then, within the Gutzwiller approximation, the average value of the Hamiltonian as function of the variational parameter d is

$$E(d) = ZT_0(n) + Ud \tag{4.13}$$

where

$$Z = \frac{P_1(d)}{2n(1-n)}\left[\sqrt{P_0(d)} + \sqrt{P_2(d)}\right]^2 \tag{4.14}$$

Notice that the non interacting probabilities are $P_0(0) = (1-n)^2$, $P_1(0) = 2n(1-n)$ and $P_2(0) = n^2$ so that for those values $Z = 1$ as it should be. The best d is obtained by the condition that the total free energy be minimal.

If a nearest neighbor exchange

$$J \sum_{<ij>} \vec{S}_i \vec{S}_j, \tag{4.15}$$

is present so to induce a $d-$wave BCS instability with order parameter

$$\Delta = |\langle c^{\dagger}_{i,\uparrow} c^{\dagger}_{j,\downarrow} \rangle|, \tag{4.16}$$

its average value within the Gutzwiller approximation is

$$-3J \left(\frac{P_1(d)}{P_1(0)} \right)^2 (r_1^2 + \Delta^2) \tag{4.17}$$

where, if we suppose the non interacting electrons dispersion and $d-$wave gap function respectively:

$$\begin{aligned} \xi_k &= -2(t + Jr_1)(\cos k_x + \cos k_y) - \mu = -2(t + Jr_1)\psi_k - \mu \\ \Delta_k &= w(\cos k_x - \cos k_y) = w\phi_k \end{aligned}$$

then Δ is the following function of variational parameters:

$$\Delta = \frac{1}{4V} \sum_k \phi_k \sin 2\theta_k \tag{4.18}$$

and for r_1 we have the following self-consistent equation:

$$r_1 = \frac{1}{4V} \sum_k \psi_k \cos 2\theta_k \tag{4.19}$$

Here

$$\sin 2\theta_k = \frac{\Delta_k}{\sqrt{\Delta_k^2 + \xi_k^2}}; \qquad \cos 2\theta_k = -\frac{\xi_k}{\sqrt{\Delta_k^2 + \xi_k^2}}$$

$$\phi_k = \cos k_x - \cos k_y; \qquad \psi_k = \cos k_x + \cos k_y$$

The non interacting BCS kinetic energy is expressed through the variational parameters as follows:

$$T_0(w, d) = -8tr_1 \tag{4.20}$$

Apart from, this we have the condition that the average number of particles per site be constant:

$$2n = \frac{1}{V}\sum (1 + \cos\theta_k)\,. \tag{4.21}$$

Summarizing, we have to minimize the total energy:

$$E(w,d) = -8tZ(d)r_1(w,d) + Ud - 3J\left(\frac{P_1(d)}{P_1(0)}\right)^2 (r_1^2(w,d) + \Delta^2(w,d)) \tag{4.22}$$

subject to the conditions on r_1 and μ

$$r_1(w,d) = \frac{1}{4V}\sum_k \psi_k \cos 2\theta_k$$

$$2n = \frac{1}{V}\sum (1 + \cos\theta_k)$$

and depending on the following function Δ:

$$\Delta(w,d) = \frac{1}{4V}\sum_k \phi_k \sin 2\theta_k. \tag{4.23}$$

Notice that, if a nearest neighbor repulsion:

$$W\sum_{<ij>} n_i n_j \tag{4.24}$$

is included to prevent superconductivity, then $\xi_k \to -2(t + (\frac{3}{4}J + W)r_1)\psi_k - \mu$ and the total energy will be:

$$\begin{aligned} E(w,d) &= -8tZ(d)r_1(w,d) + Ud - 3J\left(\frac{P_1(d)}{P_1(0)}\right)^2 (r_1^2(w,d) + \Delta^2(w,d)) \\ &- 4W\left(\frac{n(1-2n)+d}{n(1-2n)+n^2}\right)^2 (r_1^2(w,d) - \Delta^2(w,d)) \end{aligned}$$

The model (4.8) corresponds to $W = V - \frac{1}{4}J$. Let us mention that in, terms of W, superconductivity should vanish at weak-coupling when $W = \frac{3}{4}J$.

On the contrary, in Gutzwiller approximation, if we consider the limit $U \to \infty$ we can put $d = 0$ and renormalized interactions will be $J^* = J\frac{1}{(1-n)^2}$ and $W^* = W\left(\frac{1-2n}{1-n}\right)^2$ (or $W^* = (W - \frac{J}{4})\left(\frac{1-2n}{1-n}\right)^2$ if we are dealing with $t-J$ model) . In this limit the minimization procedure reduces to the solution of usual BCS equations for one only parameter Δ and, as we know, the critical W^* is found from the condition that $W^* = \frac{3}{4}J^*$ which for $t-J$ gives

$$W_C = \frac{J}{4}\left(\frac{3}{(1-2n)^2} + 1\right)$$

For underdopped system with $2n = 0.84$ we find $W_C = 29.55J$ instead of $W_C^{BCS} = 0.75$!

4.4 Results from GA

Within the GA it is possible to study explicitly the competing influence of both J and V on superconductivity. Let us consider the superconducting contributions to the uncorrelated expectation values for nearest neighbor sites i and j,

$$\langle \Psi_{BCS}|n_i n_j|\Psi_{BCS}\rangle_{sc} = 2\Delta_{SC}^2 \tag{4.25}$$

$$\langle \Psi_{BCS}|\vec{S}_i \cdot \vec{S}_j|\Psi_{BCS}\rangle_{sc} = -\frac{3}{2}\Delta_{SC}^2, \tag{4.26}$$

where $\Delta_{SC} = |\langle \Psi_{BCS}|c_{i\sigma}^\dagger c_{j-\sigma}^\dagger|\Psi_{BCS}\rangle|$ is the order parameter of the uncorrelated wave function. In the case of Eq.(4.25), this term derives from configurations in which i and j are both singly occupied, both doubly occupied or one singly and the other doubly occupied, with weights δ^2, $(1-\delta)^2$ and $2\delta(1-\delta)$, respectively, where δ is the doping. On the contrary, Eq.(4.26) has contribution only by configurations where both sites are singly occupied. In the limit of very large U, the configurations with doubly occupied sites are projected out, hence only the contributions from singly occupied sites survive in Eqs. (4.25) and (4.26). This implies that (4.25) gets a reduction factor δ^2 relatively to (4.26), so that the actual condition for superconductivity at $U \to \infty$ reads approximately

$$\frac{3}{4}J > \delta^2\left(V - \frac{1}{4}J\right).$$

Since, in the same limit, the wave function renormalization $Z \simeq 2\delta$, we indeed recover the desired Fermi liquid result that interactions involving the charge density

operators get renormalized down by a factor Z^2 with respect to those involving spin operators. The above discussion also shows that not all the pairing mechanisms are equally equipped against on-site repulsion. Indeed a weak coupling d-wave superconductivity might be stabilized even by a negative V at $J = 0$: an explicit attraction between charges. However, for increasing U, the effective strength of this attraction would decrease as Z^2 so that $\lambda_* \sim Z\lambda_0$, hence T_c would go down.

4.5 Long-range order parameter

The behavior of the variational gap Δ_{var} as shown in Fig. 4.2 suggests a crossover from weak to strong coupling superconductivity as U increases. This is manifest by comparing Fig. 4.3a with Fig. 4.3b.

In the latter the variational energy gap is displayed for several U's, while in the former we plot the true long range order parameter Δ_{LRO} in the correlated wave function. Δ_{LRO} is estimated on a finite cluster through the pair-pair correlation function f as follows:

$$\Delta_{LRO} = \frac{1}{2}\sqrt{f - f_{\rm norm}},$$

where

$$f \equiv \sum_{\sigma,\sigma'} < c^{\dagger}_{\vec{x},\ \sigma} c^{\dagger}_{\vec{x}\pm\vec{1},-\sigma} c_{\vec{y}\pm\vec{1},-\sigma'} c_{\vec{y},\ \sigma'} >, \tag{4.27}$$

being evaluated at the maximum distance $|\vec{x} - \vec{y}|$ available on a given size. Notice that f includes normal contributions f_{norm}, which nevertheless vanish in the infinite size limit. In order to improve the quality of any finite size analysis, one should estimate f_{norm} to get a meaningful value of the true long range order parameter. We decided to approximate f_{norm} by the value of f calculated with the optimized wave function having the same form (4.9) with the variational parameter Δ_{var} equal to zero (see inset Fig.4.3a). After this subtraction, size effects are acceptable, at least for our qualitative analysis (see Fig.4.3a).

The crossover region where the gap Δ_{var} rapidly moves from small BCS-like values to much larger values corresponds to a maximum of the true order parameter, as one would expect in the intermediate region between weak to strong coupling superconductivity. The notably difference with the latter is that in our model the crossover does not occur by varying the bare attraction λ, but by increasing the repulsion U.

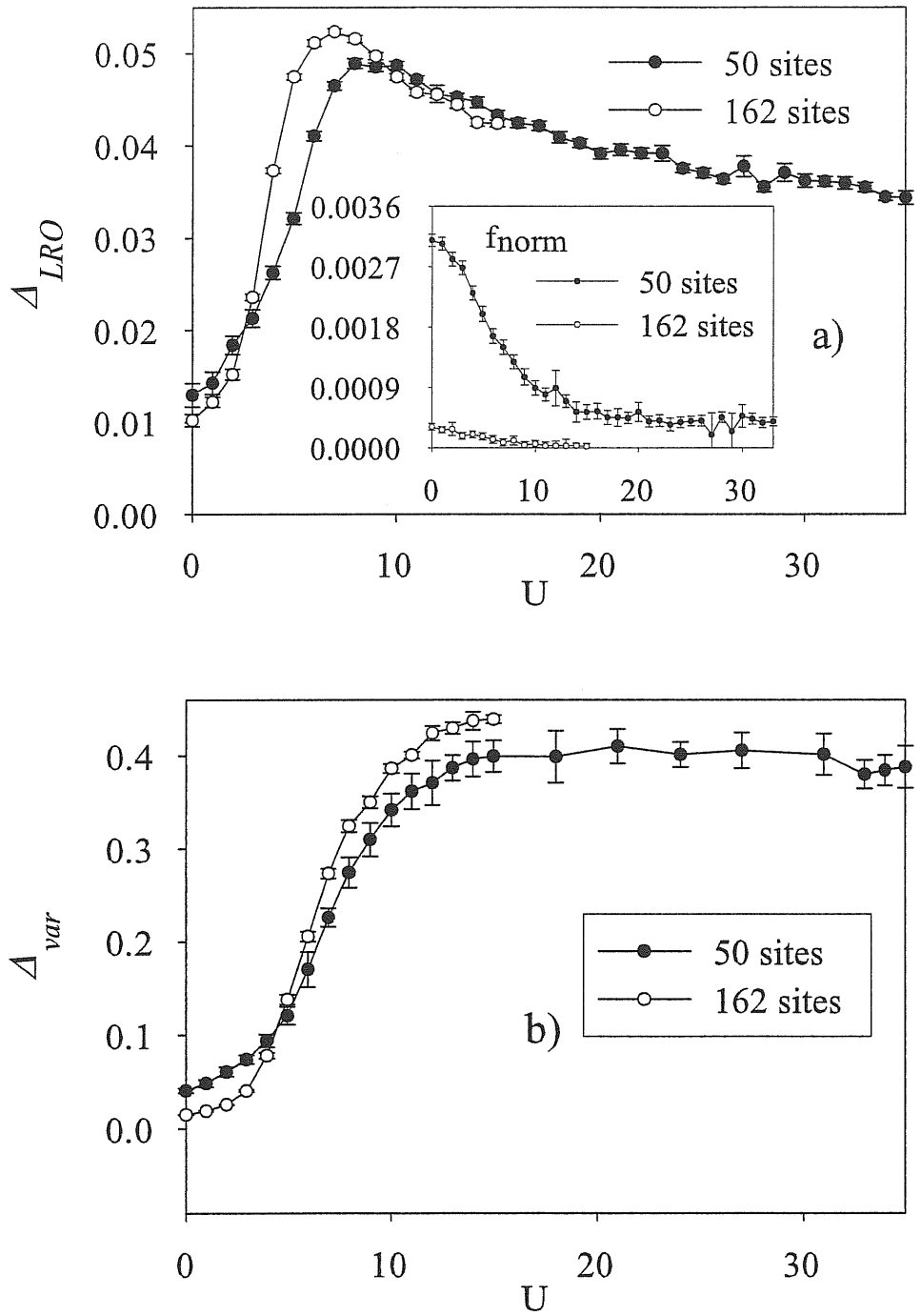

Figure 4.3: Superconducting order parameter Δ_{LRO} a), and the variational gap Δ_{var} b), as a function of U at $V = 0$, $J/t = 0.2$, $\delta = 0.16$. The inset in a) shows the long distance pairing correlations for the non-superconducting state (see text).

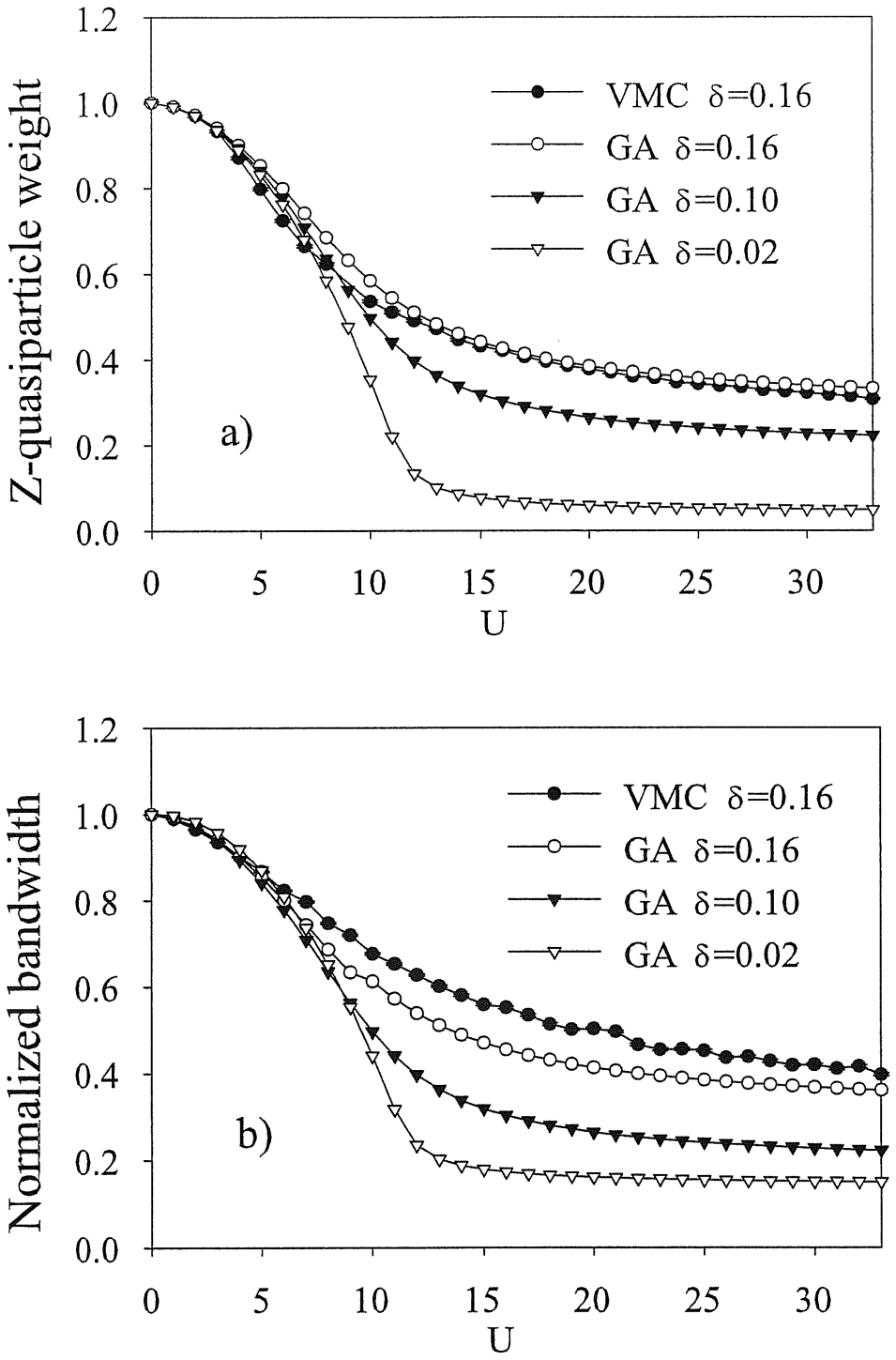

Figure 4.4: Panel a): wave-function renormalization Z as calculated through the jump in the momentum distribution along the nodal direction. Finite size scaling from 50 to 162 is used to evaluate the jump Z in the thermodynamic limit for the VMC. Panel b): quasiparticle bandwidth normalized to its uncorrelated value. The VMC refers to the 50 site cluster, as finite size effects are small. $V = 0$ and $J/t = 0.2$ for both figures.

The different behavior of the variational gap with respect to the true order parameter, which has been associated with the behavior of the pseudo-gap versus T_c in the cuprates[61, 68], has a clear explanation within the GA, where Δ_{LRO} is suppressed by the factor Z with respect to the uncorrelated Δ_{SC}. Indeed, as shown in Fig. 4.4a, the quasiparticle residue Z, defined as the jump in the momentum distribution function along the nodal directions, is a decreasing function of U tending to $Z \sim 2\delta$ as $U \to \infty$.

However, as shown in Fig. 4.4b, Z is not the reduction factor of the full quasiparticle bandwidth, which gets contributions also from J and V. Again, this is an obvious result in the GA where the Hartree-Fock decoupling of the nearest neighbor interactions effectively generate hopping terms. In spite of that, the charge current vertex is still determined by the true hopping t, hence gets suppressed by a factor $Z \simeq 2\delta$. On the contrary, spin current vertex does include a contribution from J and survives against the strong wave function renormalization Z.

4.6 Conclusions

In this Chapter we have considered $t-U-J$ model in the crossover region from weak to strong coupling, by varying U. We have shown that strong short range correlations enhance or suppress pairing correlations if they primarily involve spin or charge degrees of freedom, respectively. This behavior is manifest at strong U, in agreement with slave boson approaches[76] and numerical calculations[23, 61, 68], but starts to appear already at weak coupling. Indeed, a recent calculation within the Random Phase Approximation (Chapter 3) shows that the d-wave superconducting phase of model (4.8) at $V = 0$ gains more exchange-correlation energy than a normal metal, thus supporting the results here obtained by variational Monte Carlo.

Chapter 5

Superconductivity in the Hubbard model

5.1 Introduction

As it was already mentioned in Chapter 1, the one-band Hubbard model is often casted [79] as an adequate model to describe the low-energy physics of cuprates. On the other hand, it is not at all clear if the very Hubbard model exhibits a superconducting behavior in any range of parameters, in particular for the range relevant to cuprates (*i.e.* doping $\delta \sim 15 \div 20\%$ and $U \sim 4 \div 12t$). Indeed, although the Hubbard model has been extensively studied for long time, the definitive answer to the question if it could have a superconducting ground state for some values of parameters is still controversial. The presence of superconductivity has been predicted by various analytical approaches, while usually denied by the numerical methods.

Within the *FLEX* or fluctuation exchange approximation [80] a so called conserving approximation, *i.e.* satisfying the total number of particle, energy and momentum conservation lows may be constructed. By examining the spectral function it was indeed speculated in [21] the presence of a superconducting gap with the ratio $2\Delta_k/T_c \sim 10$ and $T_c = 0.027t$ for $\langle n \rangle = 0.875$ and $U/t = 6$. However the FLEX method, as an approximation based on a perturbative expansion in U, breaks down in the strong coupling regime when U is of the order of the free electron bandwidth $U \sim 8t$.

In Renormalization Group studies [19, 81] a $d-$wave instability has also been

observed. It shows up by a divergence of the pair-pair susceptibility as the infrared cutoff Λ_c approaches zero. Nevertheless, the complexity of RG equations in [19, 81] impose to use one-loop approximation, which has limited the conclusions only to the weak-coupling limit $U \lesssim t$.

Calculations within the Dynamical Mean Field Theory (DMFT) [82] can be performed in the strong coupling regime and in the thermodynamic limit. Although, due to the lack of spatial correlations one can not observe the nonlocal order parameter like in the case of $d_{x^2-y^2}$-wave superconductivity. Recently it was claimed to observe the $d_{x^2-y^2}$ instability due to repulsive interaction in Hubbard model within Dynamical Cluster Approximation [83], supposed to be a generalization of DMFT to include the spatial correlations, but these results have been strongly criticized [84].

The possibility to have a Kohn-Luttinger [89] type of superconductivity, at least in the weak-coupling limit, has been recently advocated in [20]. By applying a canonical transformation on the Hubbard model, supplied with small next nearest neighbor hopping t', the latter model was shown to reduce to an effective model containing an attractive term of the order of $U^2/8t$. This attraction was then treated within the BCS approach. The results suggest $\Delta_{\max} = 0.0023t$ and $T_c = 0.0013t$ for $\langle n \rangle = 0.8$, $t'/t = 0.3$.

However, all the above results are not easily confirmed by the numerical methods. In particular, within Quantum Monte Carlo (QMC) the conclusions are quite quite controversial. For example, by measuring the effective interaction constants one can conclude that the net interaction between electrons is attractive [85, 86], but the temperatures reached by QMC are much higher than the presumed T_c. On the contrary, measurements of the *long range order parameter* [87, 88] show that the latter is zero within the error-bars, again for temperatures accessible by QMC.

In the present Chapter we report the results of QMC variational study of superconductivity in the one-band Hubbard model by analyzing the long range order parameter, the condensation amplitude and the condensation energy, introduced in Section 1.1.1. We present also a comparison of these results with those of *exact* Lanczos diagonalization technique for small-size clusters as well as the results of Fixed Node approximation for the clusters of bigger sizes.

5.2 Results of VMC

In VMC we use the same variational wave function as in the previous Chapter:

$$|\Psi\rangle = A\hat{P}_{\rm N}\hat{P}_{\rm Jastrow}\hat{P}_{\rm G}|\Psi_{BCS}\rangle, \tag{5.1}$$

where $\hat{P}_{\rm N}$ is the projector onto subspace with N particles, $\hat{P}_{\rm Jastrow}$ a Jastrow correlation part and $|\Psi_{BCS}\rangle$ the BCS variational state with $d-$wave gap: $\Delta_k = \Delta_{var}(\cos k_x - \cos k_y)/2$. We used doping $\delta = 0.16$ to be sure that there is no competition with spin ordering (see [71]). When Δ_{var} is zero in (5.1) and away from half filling, $|\Psi\rangle$ describes a Fermi-liquid metal while for finite Δ_{var} it is a superconductor. Therefore, within the variational approach we can compare physical properties of both states. For instance we can calculate the condensation energy, defined as $\Delta E \equiv E_{var}|_{\Delta_{opt}} - E_{var}|_{\Delta=0}$: Fermi liquid phase will be unstable with respect to the superconducting pairing if $\Delta E < 0$.

We have mentioned in Section 1.2.2, that the Hubbard model at the BCS level does not contain any attraction of the right symmetry to give rise to the $d-$wave superconductivity. It is therefore surprising, that supplied with the Gutzwiller and Jastrow correlators it manages to do so with bigger variational gap for bigger repulsion. On Fig. 5.1 we plot Δ_{var} as a function of U for the systems, containing 50, 98, 162 and 242 sites. The value of the gap at large U remains approximately constant by increase of the system size. The possibility to have non zero variational gap at finite U is non trivial and was first realized in [90], although with only Gutzwiller plus BCS variational wave function and smaller values of Δ_{var}. We conclude, therefore, that the correlations between electrons described by the long range Jastrow factors enhances the variational gap by an order of magnitude. In addition, the Jastrow variational wave function correctly reproduces the long range behavior of the static structure factor (see Appendix B) and provides lower variational energies, representing thus a better approximation to the ground state than the one used in [90]. The reason why a superconducting state has lower energy is still unclear: it appears that in a way the state with non zero BCS gap manages to suppress density fluctuations more effectively than a Fermi liquid, as it can be seen from the Table 5.1.

The crossover from small to large values of U is manifested by almost an order of magnitude increase in Δ_{var}. This effect was studied in [91] and has been explained in the previous Chapter as due to the band narrowing effect.

The results for the variational gap are in agreement with the behavior of the

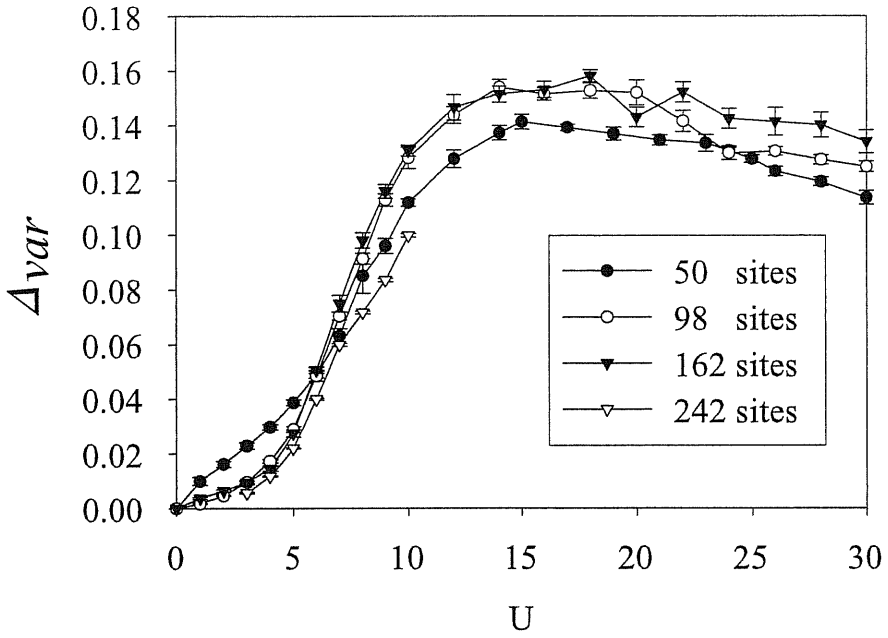

Figure 5.1: Variational superconducting gap for the Hubbard model at $\delta = 0.16$ as a function of U and for different system sizes.

Table 5.1: Optimal values of the Gutzwiller (α_0), nearest (α_1), next-nearest (α_2) and next-next-nearest (α_3) neighbor Jastrow variational parameters for the system of 50 sites at $U/t = 10$ and $\delta = 16\%$ and for both SC and FL states.

	α_0	α_1	α_2	α_3
SC	-1.732	-0.316	-0.158	-0.096
FL	-1.720	-0.273	-0.118	-0.084

condensation energy, which we define as above. On Fig. 5.2 we show ΔE for different system sizes. It has a broad minimum in the region $U \sim 10 \div 15t$, which is similar to what Δ_{var} shows. Being rather large at large U ΔE is, however, very small when $U \to 0$, which suggests a crossover from weak to strong coupling. From this point of view the results presented in this Chapter are very similar qualitatively to those from the previous Chapter. We would like to emphasize, however, that in the case of the pure Hubbard model we do not have any explicit attraction.

The long range order parameter Δ_{LRO} on a finite cluster is defined through the

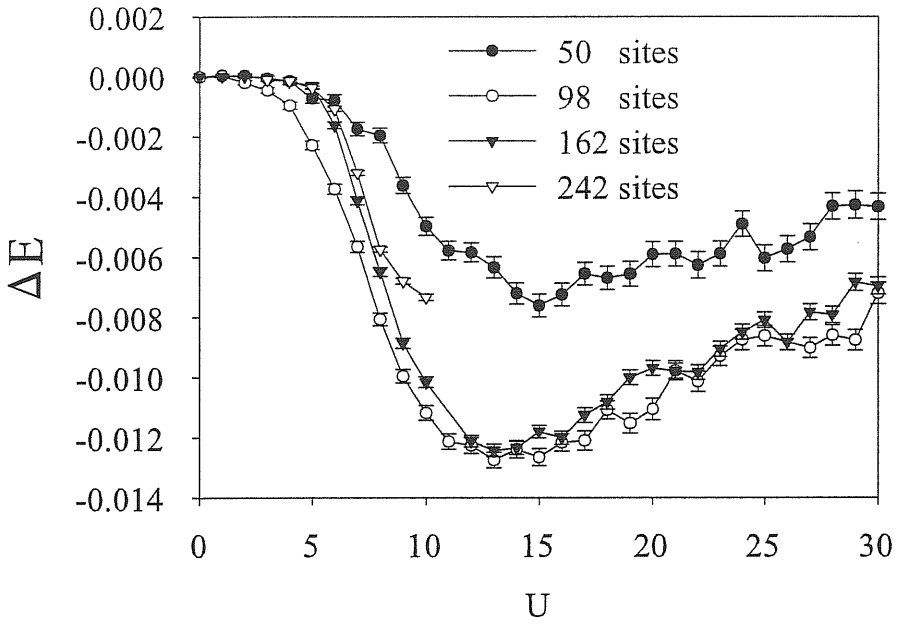

Figure 5.2: Condensation energy, defined as the energy difference between two variational states: $\Delta E = E_{SC} - E_{FL}$ for different values of cluster sizes. $\delta = 0.16$.

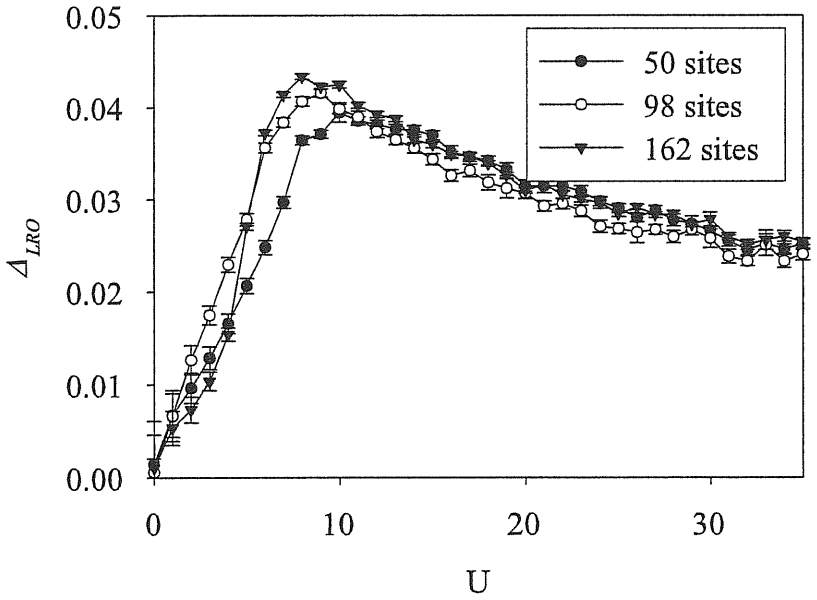

Figure 5.3: Long-range order parameter Δ_{LRO}, defined to eliminate the normal (non superconducting) contributions (see in the text) as a function of U for different system sizes. $\delta = 0.16$.

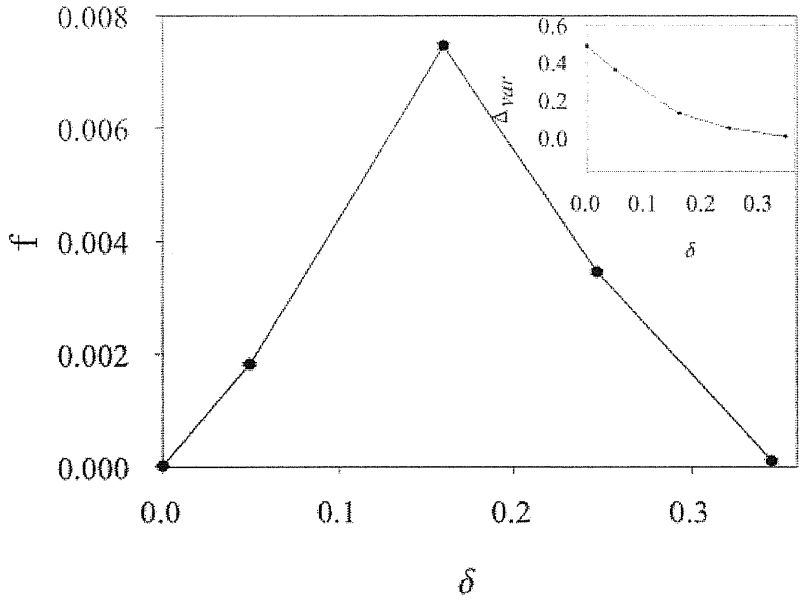

Figure 5.4: Doping dependence of the pairing correlation function for the system of 162 site at $U = 10t$ and $\delta = 0.16$. In the inset: on the contrary variational gap Δ_{var} increases monotonically when approaching half filling.

maximum distance limit of pair-pair correlation function $f(x, y)$:

$$f(x,y) \equiv \sum_{\sigma,\sigma'} \langle c^{\dagger}_{\vec{x},\,\sigma} c^{\dagger}_{\vec{x}\pm\vec{1},-\sigma} c_{\vec{y}\pm\vec{1},-\sigma'} c_{\vec{y},\,\sigma'} \rangle. \tag{5.2}$$

In the presence of long range order the $\lim_{|x-y|\to\max} f(x, y)$ should be finite and proportional to the square of the order parameter Δ. As in the previous Chapter, to get rid of the normal contributions we define Δ_{LRO} as the square root of the difference between the values of f in the superconducting and the Fermi-liquid states:

$$\Delta_{LRO} = \frac{1}{2}\sqrt{f - f_{norm}}. \tag{5.3}$$

At small, U Δ_{LRO} starts linearly and has rather sharp maximum at $U/t = 8 \div 10$. At large U it slows down and saturates at $U \to \infty$. The doping dependence of the pair-pair correlation function f is quite peculiar (Fig. 5.4): at large enough U at half filling it is zero as well as at large doping $\delta \sim 0.33$ and is maximal at $\delta \sim 0.16$, which agrees with the existence of optimal doping in cuprates. On the other hand the variational gap Δ_{var} does not show such behavior at all: instead it is a decreasing function of doping, as shown in the inset of Fig. 5.4.

5.3 What beyond VMC?

The results of the previous Section suggest that there is quite strong tendency towards superconductivity in the Hubbard model. Simple variational wave function (5.1) gains energy from opening a d-wave gap. The variational Monte Carlo clearly overestimates superconductivity. For example in [87] it was shown within the Constrained Path Monte Carlo technique the absence of the off diagonal long range order in the range of $U < 4t$, contrary to our results. We will see, however, that the application of the Fixed Node approximation, used to improve the variational state, confirms the results of [87] at $U < 6t$.

In general, if one has an arbitrary many-body state on a finite lattice, as obtained *e.g.* from QMC simulations or from the exact diagonalization, it is quite difficult to decide if it is superconducting or not: if the pair-pair correlation function is not monotonous around the maximal distances on a given size, then the off diagonal long range order parameter can not be safely determined. But even if the pair-pair correlation function is monotonous, one needs high precision calculations to reveal a small order parameter, since the measured quantity is supposed to be proportional to the square of the small of the latter. In principle there are two ways to go beyond the variational approach. One is to consider as large as possible for Monte Carlo clusters and apply some approximate method, which allows to improve the variational results. In the present Chapter we use the Fixed Node approximation. Another way is to exploit the exact Lanczos diagonalization technique for small cluster sizes (at most 18 sites for Hubbard model). But, as it was already pointed out, there is not enough information in such small systems to determine the long range order parameter; *e.g.* in the system of 18 site there are only 3 points to guess Δ_{LRO} from the behavior of f as defined in (5.2). In this situation, in order to minimize size effects, we calculate the real space order parameter, defined as the condensation amplitude (1.9) between the states with N and $N+2$ particles.

Comparison with Fixed Node approximation

By construction within FN the nodal structure of the wave function remains unchanged, while the amplitudes of the configurations which do not cause any sign problem are rearranged in a way to lower the variational energy (see Section 2.4). This means that the superconducting state will become after the application of FN a state which can be considered as a "better approximated superconducting

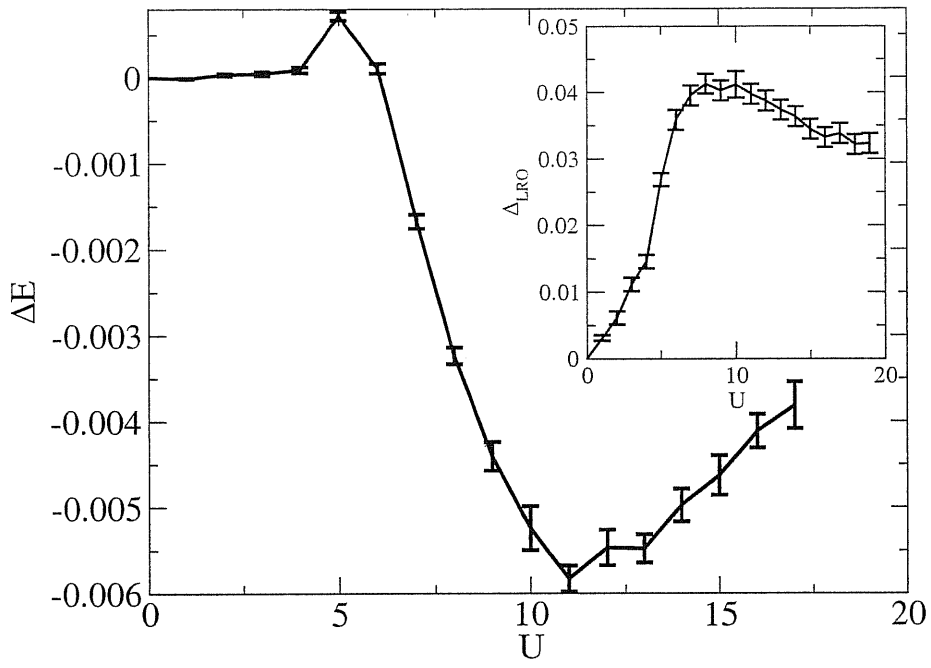

Figure 5.5: Condensation energy in the FN approximation, defined as the difference $\Delta E^{FN} = E_{SC}^{FN} - E_{FL}^{FN}$ for the system of 162 sites at $\delta = 0.16$. Notice, that for $U \leq 6t$ ΔE^{FN} is positive, which implies that superconductor is unfavorable at those U. In the inset: Δ_{LRO}, calculated for the same case in FN is almost unchanged (compare to Fig. 5.3).

state" and the Fermi liquid one will become a "better approximated Fermi liquid". We can therefore once again define the condensation energy in FN approximation: $\Delta E^{FN} = E_{SC}^{FN} - E_{FL}^{FN}$. On the system of 162 sites at the doping $\delta = 0.16$ ΔE^{FN} shows that indeed at large U the variational approach overestimates the condensation energy by approximately the factor of two (compare Fig. 5.5 and Fig. 5.2). More surprisingly, at small values of Hubbard interaction ΔE^{FN} becomes positive, which means that at these U the Fermi liquid state is more stable than the superconductor. The onset of the superconductivity occurs only at $U \sim 7t$ and has a maximum at $U \sim 10 \div 13t$.

On the other hand the long range order parameter appears almost unchanged in FN with respect to VMC (see the inset on Fig. 5.5). This happens because FN, improving much the variational energy, leaves unchanged the nodal structure of the wave function and thus the correlation functions.

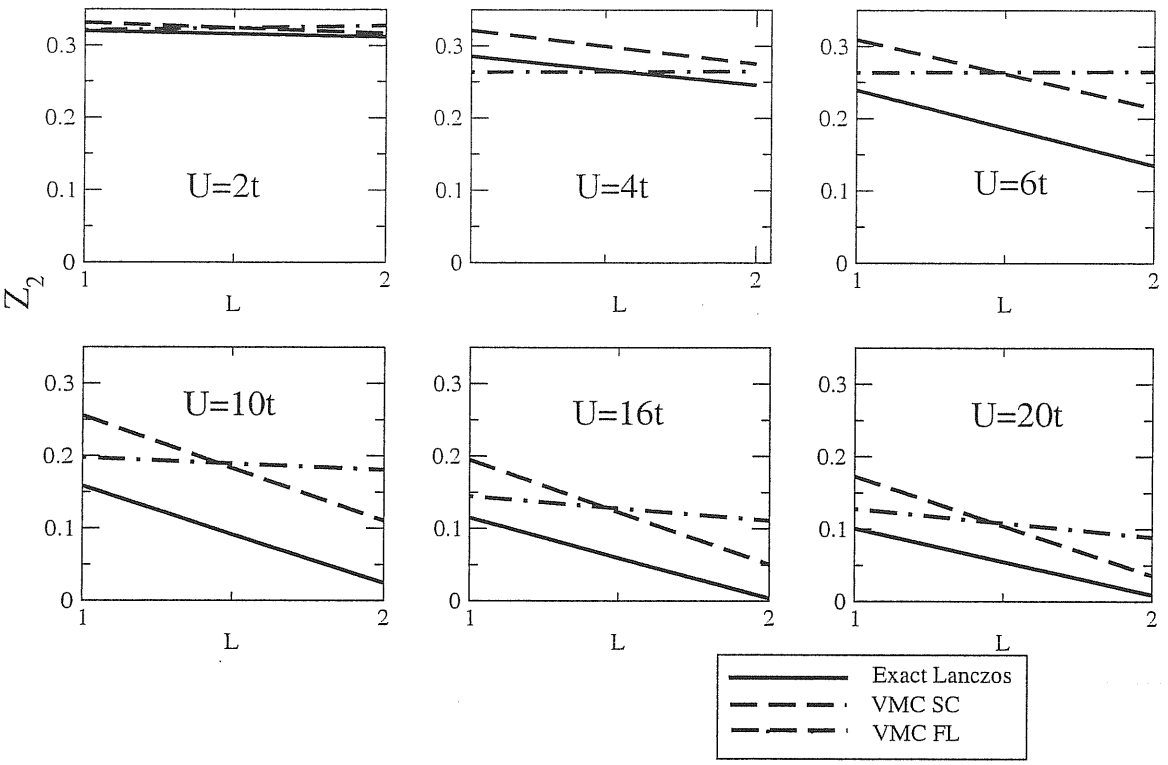

Figure 5.6: Order parameter $Z_2(L)$ at $L = 1, 2$ for VMC superconducting (dashed line) and Fermi-liquid (dashed-dotted line) states as compared with the exact Lanczos diagonalization values (solid line) for the system of 18 site at different values of U. Notice the different slope of the FL line respect to SC and exact ones.

Comparison with exact diagonalization

To estimate the precision of our variational approach we calculate the order parameter in the real space $Z_2(i-j)$ for the system of 18 sites in both superconducting and Fermi-liquid states and compare it to the values obtained with the help of Lanczos diagonalization [92].

The order parameter Z_2 is defined in the real space as follows:

$$Z_2(i-j) \equiv \langle \Psi_{var}(N+2) | \left(c^\dagger_{i,\uparrow} c^\dagger_{j,\downarrow} + c^\dagger_{j,\uparrow} c^\dagger_{i,\downarrow} \right) | \Psi_{var}(N) \rangle \tag{5.4}$$

and for translationally invariant system depends only on the difference $i-j$ between two sites $i = (i_x, i_y)$ and $j = (j_x, j_y)$. $Z_2(i-j)$ as a function of $i-j$ is flat for Fermi-liquid, but has a maximum at some distance $i-j$ for the superconductor (in the case of (5.1) with nearest neighbors correlated BCS part, the maximum should correspond to $|i-j| = \pm 1$). In (5.4) we assumed, for simplicity, that both wave

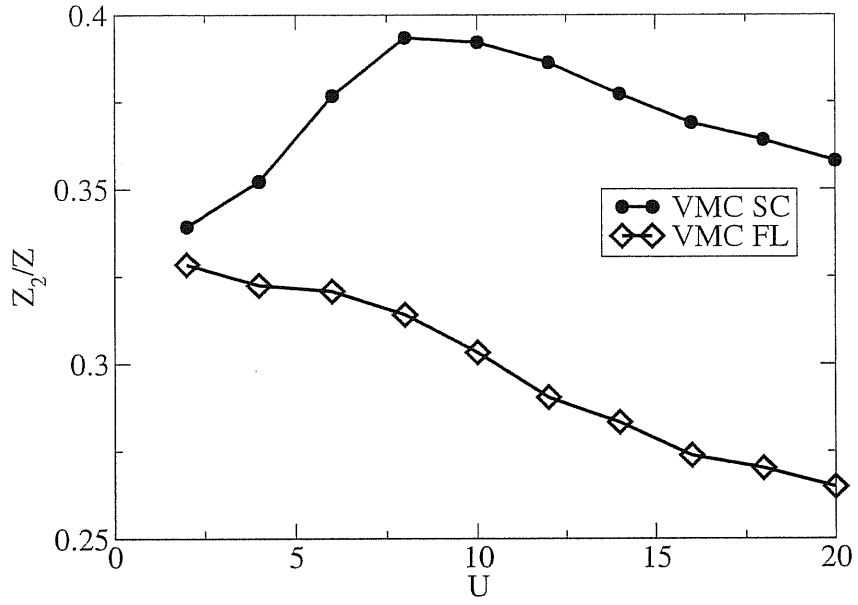

Figure 5.7: Ratio $Z_2(a)/Z(M)$ as a function of U within VMC for the system of 18 sites. The curve with circles represents VMC superconducting state, while that one with diamonds - VMC Fermi liquid. Error-bars are smaller then the symbols.

functions are normalized. In practice it is not the case with Monte Carlo simulations. In Appendix C we describe the way to calculate Z_2 in the case when the wave function is not normalized in VMC. Notice that $Z_2(i-j)$ is non zero also in the non superconducting state, since the two states $|\Psi_{var}(N+2)\rangle$ and $c^\dagger_{i,\uparrow}c^\dagger_{j,\downarrow}|\Psi_{var}(N)\rangle$ have always a finite overlap. We compare the values of $Z_2(L)$ for the system of 18 sites both for VMC SC and VMC FL states as well as for the exact one. The results of such comparison for different values of U are shown on Fig. 5.6. On such a system we have two separation distances along *e.g.* x axis, compatible with d-wave symmetry: a and $2a$, where a is the lattice spacing. Up to $U = 20t$ the values of Z_2 for Fermi liquid state is approximately distance independent, while for the superconducting state as well as for the exact one it is not the case. Indeed, both go almost parallel to each other, which suggests, that the VMC SC state captures correctly the order parameter, although overestimating it.

Such overestimation comes from the fact, that simple VMC does not have enough tools to follow the strong quasiparticle weight renormalization Z, which occurs in the Hubbard model at large U. As usual, within Landau Fermi liquid theory (see the Section 4.1) in the presence of a strong interaction, the value of the one-body correlation function such as Z_2 acquires the renormalization factor of Z. If the

latter is overestimated within our variational approach ($Z_{VMC} > Z_{exact}$), then the overall result for Z_2 is larger then the exact value even though the most important quantity Z_2/Z might be close to its exact counterpart. In other words we have to calculate the order parameter in terms of the dressed quasiparticles $\tilde{c}_{k\sigma} \simeq c_{k\sigma}/\sqrt{Z}$, rather than the bare ones [93]. In this Chapter we define Z in the way similar to the definition of Z_2:

$$Z(k) \equiv \langle \Psi_{var}(N+1)|c^{\dagger}_{k,\sigma}|\Psi_{var}(N)\rangle^2. \tag{5.5}$$

We choose $M \equiv (\pi, 0)$ to estimate quasiparticle weight. Details of the calculations of Z are presented in Appendix C. To illustrate the idea of the dressed quasiparticles on Fig. 5.7 we plot the ratio $Z_2(a)/Z(M)$ for the nearest neighbors distance as a function of U for the system of 18 sites, as calculated by VMC in both superconductor and Fermi liquid. Indeed, the VMC SC curve shows a maximum around $U \sim 7 \div 13t$, while the Fermi liquid state become more and more suppressed upon increasing U. Therefore our calculations of the order parameter for the dressed quasiparticles qualitatively distinguish superconducting and Fermi liquid states. Calculation of the quantity $Z_2(a)/Z(M)$ by means of the exact diagonalization for 18 sites could finally shed light on this topic and argue in favor of our variational state or rule it out. This work is in progress.

5.4 Conclusions

In this Chapter we considered the possibility of a superconducting ordering in the repulsive Hubbard model at zero temperature. Our variational Monte Carlo studies revealed a non trivial superconducting variational state, which is stabilized by means of supplying the BCS wave function with Jastrow and Gutzwiller correlators. This state was shown to be robust with respect to the increase of the system size. Various quantities characterizing this state have been calculated, among them the condensation energy, long range order parameter, and the order parameter in real space, Z_2. The methods we used to examine the superconductivity in Hubbard model beyond VMC range from Fixed Node approximation to the exact diagonalization technique. All these data suggest that in the strong coupling limit of the Hubbard model and the doping $\delta \sim 0.16$ there is superconductivity. The maximal strength of the order parameter was observed in the range of $U/t \sim 9 \div 15$. It was shown that, though in the VMC the quasiparticle weight Z is overestimated, the order parameter of the dressed quasiparticles in the superconducting state exhibits the maximum at

the above mentioned region of U, while in the Fermi liquid state it becomes gradually suppressed when increasing U. In addition, our FN results suggest that in the Hubbard model within the range of $5 < U/t < 7$ there should be a transition from a Fermi liquid to a strongly coupled superconductor. The strong quasiparticle renormalization Z expected in the low doping Hubbard model, may explain why the superconducting order parameter Z_2 measured with the bare quasiparticles, is so small but nevertheless different from that of the Fermi liquid as we tried to show in this Chapter. Our results clarify, therefore, the controversial conclusions on the superconductivity in the Hubbard model, based on previous studies [87, 86].

Conclusions

In the present thesis we have addressed the question of a influence of repulsive Hubbard interaction on d-wave superconductivity. We started by considering the effect of the above interaction on already formed Cooper pairs, as a result of an explicit attraction W favoring d-wave pairing, and we ended up by studying the Hubbard interaction itself as a source of superconducting instability. The Hubbard model is often considered as a relevant model for High-T_c materials, although it does not include any explicit pairing mechanism. Numerous analytical and numerical approaches did not give so far the definitive answer to the question about the presence of superconductivity in the repulsive Hubbard model. On the other hand, even though the attraction in the cuprates is supplied by some other mechanism, it is still very important to study the role of the strong on site repulsion, since the latter appears to be the fingerprint of High-T_c's. Here we have studied both the pure Hubbard model and the Hubbard model with an added (small) attractive term by using a variety of semi-analytical and numerical methods such as Time Dependent Hartree-Fock approximation (TDHF), Gutzwiller approximation (GA), Variational Monte Carlo (VMC), Fixed Node approximation (FN).

For a superconducting transition to occur it is of crucial importance to check thoroughly the energy balance between normal and superconducting states. BCS theory provides only the lowest order condensation energy, which does not include the correlations effects. We have calculated the exchange correlation energy due to the Hubbard repulsion with the help of TDHF. Both in superconducting and Fermi-liquid states within region where both interactions U and W can be considered weak and TDHF method is applicable. We have found that the exchange correlations lower the energy of the superconductor, and this effect comes mainly from the enhancement of the spin correlations in the vicinity of $\vec{Q} = (\pi, \pi)$. The numerical value of the exchange correlation energy gain in the superconductor at $U = 0.5t$ and $W = -0.17t$ is only an order of magnitude smaller than the BCS condensation energy. This suggests that the presence of the Hubbard repulsion enforces

the stability of a d-wave superconductor compared to a Fermi liquid. This effect was shown also to increase by increasing U.

These weak coupling results have been confirmed also in the intermediate and strong coupling regimes. We have studied by VMC on the Hubbard model in the presence of an explicit nearest neighbor exchange J, favoring away from half filling d-wave superconductivity, competing against a nearest neighbor repulsion V. We have demonstrated that strong short range correlations enhance or suppress pairing correlations if they primarily involve spin or charge degrees of freedom, respectively. We have succeeded in interpreting these results by means of the simple analytic GA. The above enhancement was shown to come from the fact that, at large U, the configurations involving doubly occupied sites become highly suppressed, hence the effective quasiparticle band gets shrinked. The density of states at the Fermi level increases, leading to the increase of variational gap. This behavior is manifest at strong U, in agreement with slave boson approaches[76] and numerical calculations[23, 61, 68], but starts to appear already at weak coupling. The true order parameter Δ_{LRO}, defined through the long distance behavior of the pair pair correlation function, appears to have a maximum region at $U/t = 7 \div 10$, while the variational gap remains constant.

The above results led us to the decision to look for the superconductivity in the Hubbard model itself. By means of the variational Monte Carlo we have found non trivial superconducting variational state, which is stabilized by supplying the BCS wave function with Jastrow and Gutzwiller correlators. This state was shown to be robust with respect to increasing the system size. Various quantities characterizing this state have been calculated, among them the condensation energy, the long range order parameter, and the order parameter in real space, Z_2. The methods we used to examine superconductivity in the Hubbard model beyond VMC range from Fixed Node approximation to the exact diagonalization technique. All the data suggest that in the strong coupling limit of the Hubbard model and for doping $\delta \sim 0.16$ there is superconductivity. The maximal strength of the order parameter was observed in the range of $U/t \sim 9 \div 15$. In addition, our FN results suggest that in the Hubbard model within the range of $5 < U/t < 7$ there should be some transition from a Fermi liquid to a strongly coupled superconductor.

Acknowledgments

First of all it is a pleasure for me to thank my scientific advisers Michele Fabrizio and Sandro Sorella. Everything, that I learned in SISSA is due to their patience and ability to explain complicated notion of strongly correlated electronic systems in a comprehensive way. To stay in the place like SISSA would be impossible without such a great personality as Erio Tosatti, to whom I am very thankful. I would like to thank also Richard Hlubina and Shiwei Zhang for the enlightening discussions of our results on Hubbard model. I am very grateful to Federico Becca for explaining me Sandro's programs and for giving me his results on exact diagonalization. My roommates from "ufficio 27" of SISSA, Paola, Lorenzo and Tanya deserve a special thank for nice company during all these years apart from the fruitful scientific (and not only) conversations. I am very grateful to Davide Ceresoli and Ugo Tartaglino for the ocean of computer information I learned from them. A particular thank to Tanya, who sustained me a lot during this last period of my Ph.D.

Appendix A

Details of the algorithm, resolving TDHF equations for susceptibilities

Let us determine the spin and charge susceptibilities for the case of a general Hamiltonian, containing coupled harmonic oscillators:

$$H_1 = \frac{1}{2}\sum_{k,q}\omega_{k,q}\left(X^{\dagger}_{k,q}X_{k,q} + P^{\dagger}_{k,q}P_{k,q}\right)$$
$$+\frac{1}{2}\sum_{i=1}^{M}\sum_{k,k',q}\alpha_i(q)f_i(k,q)f_i(k',q)X^{\dagger}_{k,q}X_{k',q}+\frac{1}{2}\sum_{i=1}^{M}\sum_{k,k',q}\beta_i(q)g_i(k,q)g_i(k',q)P^{\dagger}_{k,q}P_{k',q}.$$

Here $\alpha_i(q)$ and $\beta_i(q)$ include the interaction constants with signs, $f_i(k,q)$, $g_i(k,q)$ and $\alpha_i(q)$ and $\beta_i(q)$ for the model under consideration will be given at the end of this Appendix. We introduce shorthand notations:

$$J_i(q) = \frac{1}{V}\sum_{k} f_i(k,q)X_{k,q}, \qquad K_i(q) = \frac{1}{V}\sum_{k} g_i(k,q)P_{k,q} \tag{A.1}$$

and the source terms for both spin and charge densities just as in (3.25):

$$H = H_1 - \sqrt{2}\sum_{q} V_q J_0(q) - \mathrm{i}\sqrt{2}\sum_{q} H_q K_0(q). \tag{A.2}$$

Here we put the quantity $\sum_k \sin(\theta_{k+q}+\theta_k)X_{k,q}$, which is proportional to the charge density to $J_0(q)$ and $\sum_k \sin(\theta_{k+q}-\theta_k)P_{k,q}$ to $K_0(q)$.

As in (3.17) and (3.18) we express $P_{k,q}$ and $X_{k,q}$ in terms of $J_i(q)$ and $K_i(q)$:

$$\begin{aligned} X_{kq} = & - \frac{\omega_{k,q}}{\omega_{k,q}^2+\omega^2}\sum_{i,q}\alpha_i(q)f_i(k,q)J_i(q) - \frac{\omega}{\omega_{k,q}^2+\omega^2}\sum_{i,q}\beta_i(q)g_i(k,q)K_i(q) \\ & + \frac{\omega_{k,q}}{\omega_{k,q}^2+\omega^2}\sqrt{2}V_q f_0(k,q) + \frac{\omega}{\omega_{k,q}^2+\omega^2}\mathrm{i}\sqrt{2}H_q g_0(k,q) \end{aligned} \tag{A.3}$$

$$\begin{aligned} P_{kq} = & - \frac{\omega_{k,q}}{\omega_{k,q}^2+\omega^2}\sum_{i,q}\beta_i(q)g_i(k,q)K_i(q) + \frac{\omega}{\omega_{k,q}^2+\omega^2}\sum_{i,q}\alpha_i(q)f_i(k,q)J_i(q) \\ & + \frac{\omega_{k,q}}{\omega_{k,q}^2+\omega^2}\mathrm{i}\sqrt{2}H_q g_0(k,q) + \frac{\omega}{\omega_{k,q}^2+\omega^2}\sqrt{2}V_q f_0(k,q). \end{aligned} \tag{A.4}$$

Substituting (A.3) and (A.4) into (A.1) we obtain the system of equations for $J_i(q)$ and $K_i(q)$:

$$K_l = -\sum_i C_{li}K_i + \sum_i D_{li}J_i + \mathrm{i}\sqrt{2}H_q\nu_l - \sqrt{2}V_q\epsilon_l \tag{A.5}$$

$$J_l = -\sum_i B_{li}J_i - \sum_i A_{li}K_i + \mathrm{i}\sqrt{2}H_q\mu_l + \sqrt{2}V_q\xi_l, \tag{A.6}$$

where we introduced the following matrices and rows:

$$\begin{aligned} A_{li} &= \frac{1}{V}\sum_k \frac{\omega}{\omega_{k,q}^2+\omega^2}f_l(k,q)g_i(k,q)\beta_i(q) \\ B_{li} &= \frac{1}{V}\sum_k \frac{\omega_{k,q}}{\omega_{k,q}^2+\omega^2}f_l(k,q)f_i(k,q)\alpha_i(q) \\ C_{li} &= \frac{1}{V}\sum_k \frac{\omega_{k,q}}{\omega_{k,q}^2+\omega^2}g_l(k,q)g_i(k,q)\beta_i(q) \\ D_{li} &= \frac{1}{V}\sum_k \frac{\omega}{\omega_{k,q}^2+\omega^2}g_l(k,q)f_i(k,q)\alpha_i(q) \end{aligned}$$

and

$$\epsilon_l = \frac{1}{V}\sum_k \frac{\omega}{\omega_{k,q}^2+\omega^2} f_0(k,q)g_l(k,q), \qquad \mu_l = \frac{1}{V}\sum_k \frac{\omega_{k,q}}{\omega_{k,q}^2+\omega^2} g_0(k,q)f_l(k,q)$$

$$\nu_l = \frac{1}{V}\sum_k \frac{\omega_{k,q}}{\omega_{k,q}^2+\omega^2} g_1(k,q)g_l(k,q), \qquad \xi_l = \frac{1}{V}\sum_k \frac{\omega}{\omega_{k,q}^2+\omega^2} f_1(k,q)f_l(k,q).$$

Let us consider first the case of charge susceptibility: $H_q = 0$ and $V_q \neq 0$. In vector notations we have:

$$\vec{K} = -\mathbf{C}\vec{K} + \mathbf{D}\vec{J} - \sqrt{2}V_q\vec{\epsilon} \tag{A.7}$$

$$\vec{J} = -\mathbf{B}\vec{J} - \mathbf{A}\vec{K} + \sqrt{2}V_q\vec{\xi}. \tag{A.8}$$

This linear system can be easily solved for $J_0(q)$, which is proportional to the density operator $\rho_q \sim \sqrt{2}J_0(q)$ and $\rho_q = \kappa(\omega,q)V_q$:

$$\kappa(\omega,q) = -2\frac{\det \mathbf{\Gamma}_1}{\det \mathbf{\Gamma}}, \tag{A.9}$$

where

$$\mathbf{\Gamma} = \mathbf{E} + \mathbf{B} + \mathbf{A}(\mathbf{E}+\mathbf{C})^{-1}\mathbf{D} \tag{A.10}$$

and $\mathbf{\Gamma}_1$ is $\mathbf{\Gamma}$ with the first row put equal to:

$$\vec{Z} = \vec{\xi} + \mathbf{A}(\mathbf{E}+\mathbf{C})^{-1}\vec{\epsilon}. \tag{A.11}$$

Analogously for the second case, when $H_q \neq 0$ and $V_q = 0$ we have:

$$\chi(\omega,q) = -2\frac{\det \mathbf{\Delta}_1}{\det \mathbf{\Delta}}, \tag{A.12}$$

$$\mathbf{\Delta} = \mathbf{E} + \mathbf{C} + \mathbf{D}(\mathbf{E}+\mathbf{B})^{-1}\mathbf{A} \tag{A.13}$$

and $\mathbf{\Delta}_1$ has $\vec{Y}$ as the first row:

$$\vec{Y} = \vec{\nu} + \mathbf{D}(\mathbf{E}+\mathbf{B})^{-1}\vec{\mu}. \tag{A.14}$$

For the $t-U-W$ model, introduced in Chapter 3 coefficients $\alpha_i(q)$, $\beta_i(q)$, $f_i(k,q)$ and $g_i(k,q)$ are:

$$\begin{aligned}
\alpha_1 &= U & \beta_1 &= -U \\
\alpha_2 &= U-2W & \beta_2 &= U-2W \\
\alpha_3 &= 2W & \beta_3 &= -2W \\
\alpha_4 &= 2W & \beta_4 &= 2W \\
\alpha_5 &= -2W & \beta_5 &= -2W \\
\alpha_6 &= 2W & \beta_6 &= 2W \\
\alpha_7 &= -2W & \beta_7 &= -2W \\
\alpha_8 &= -2W & \beta_8 &= -2W
\end{aligned}$$

$$\begin{aligned}
f_1(k,q) &= \sin(\theta_{k+q}+\theta_k) & g_1(k,q) &= \sin(\theta_{k+q}-\theta_k) \\
f_2(k,q) &= \cos(\theta_{k+q}+\theta_k) & g_2(k,q) &= \cos(\theta_{k+q}-\theta_k) \\
f_3(k,q) &= F(k,q)\sin(\theta_{k+q}+\theta_k) & g_3(k,q) &= F(k,q)\sin(\theta_{k+q}-\theta_k) \\
f_4(k,q) &= (\varphi(k)\varphi(k+q)+1)\cos(\theta_{k+q}+\theta_k) & g_4(k,q) &= (\varphi(k)\varphi(k+q)+1)\cos(\theta_{k+q}-\theta_k) \\
f_5(k,q) &= \varphi(k)\varphi(k+q)\cos(\theta_{k+q}+\theta_k) & g_5(k,q) &= \varphi(k)\varphi(k+q)\cos(\theta_{k+q}-\theta_k) \\
f_6(k,q) &= F(k,q)\cos(\theta_{k+q}+\theta_k) & g_6(k,q) &= F(k,q)\cos(\theta_{k+q}-\theta_k) \\
f_7(k,q) &= \varphi(k)\cos(\theta_{k+q}+\theta_k) & g_7(k,q) &= \varphi(k)\cos(\theta_{k+q}-\theta_k) \\
f_8(k,q) &= \varphi(k+q)\cos(\theta_{k+q}+\theta_k) & g_8(k,q) &= \varphi(k+q)\cos(\theta_{k+q}-\theta_k)
\end{aligned}$$

and the functions $F(k,q)$ and $\varphi(k)$ are introduced in the Chapter 3.

Appendix B

Jastrow variation wave function and structure form-factor

A variational wave function containing Jastrow prefactors, which describe the correlations among all the sites possesses an important property which regards the behavior of the static structure form factor. Suppose that $|\Psi_0\rangle$ is the exact ground state of the system with the energy E_0. One can consider a state $|\Psi_q\rangle \equiv n_q|\Psi_0\rangle$ with the Fourier-transformed density n_q at arbitrary q as a variational and respectively $E_q = \langle\Psi_q|H|\Psi_q\rangle/\langle\Psi_q|\Psi_q\rangle$ as a variational energy. Then necessarily $E_q > E_0$. Notice that the normalization $\langle\Psi_q|\Psi_q\rangle = S(q)\langle\Psi_0|\Psi_0\rangle$ - is proportional to the static form factor. It is easy to show that the following identity holds:

$$[n_q[n_{-q}H]] = n_q n_{-q}H + Hn_q n_{-q} - n_q H n_{-q} - n_{-q}Hn_q \tag{B.1}$$

Plugging it into the definition of E_q and noting that the double commutator is merely a number ($[n_q[n_{-q}H]] = T_0(2-\cos q_x - \cos q_y) \equiv f(q)$ for the Hubbard model, where T_0 is the kinetic energy of non-interacting electron gas) we have for $S(q)$

$$S(q) = \frac{f(q)}{2(E_q - E_0)} \tag{B.2}$$

Consider now a variational wave function containing Jastrow correlators for all pairs of sites:

$$|\Psi_{var}\rangle = \exp\left(-\sum_{i\neq j} u_{i,j}n_i n_j\right)|\Phi\rangle \tag{B.3}$$

where $|\Phi\rangle$ could be whatever state with definite number of particles. The expectation value of the energy $E_{var} = \langle\Psi_{var}|H|\Psi_{var}\rangle/\langle\Psi_{var}|\Psi_{var}\rangle$, $E_{var} > E_0$. Here $u_{i,j}$ are the variational coefficients which depend only on the difference $|i-j|$ and should be determined by minimizing energy. The sum in the exponential of (B.3) can be represented in momentum space as follows:

$$\sum_q \phi(q) n_q n_{-q} \equiv \sum_q \{(u(1)\psi_1(q) + u(2)\psi_2(q) + ... + u(n)\psi_n(q)\} n_q n_{-q}$$

where e.g. $u(2)$ is the Jastrow parameter for the next nearest neighbors and $\psi_1(q) = \cos q_x + \cos q_y$ and $\psi_2(q) = 2\cos q_x \cos q_y$ etc. are the Fourier transforms of hopping to the appropriate distances.

The condition of the extremum reads:

$$\frac{\partial E_{var}}{\partial u(i)} = 0.$$

We have a set of equations for E_{var}:

$$E_{var} = \frac{1}{2} \frac{\langle\Psi_{var}| \sum_q \psi_i(q) \left[n_q n_{-q} H + H n_q n_{-q}\right] |\Psi_{var}\rangle}{\langle\Psi_{var}| \sum_q \psi_i(q) n_q n_{-q} |\Psi_{var}\rangle}, \text{ for all } 1 \leq i \leq n \qquad \text{(B.4)}$$

Using (B.1) once again we have for $S^J(q) = \langle\Psi_{var}|n_{-q}n_q|\Psi_{var}\rangle/\langle\Psi_{var}|\Psi_{var}\rangle$ - the structure factor of our variational Jastrow wave function and for the variational energy $E_q^J = \langle\Psi_{var}|n_{-q}Hn_q|\Psi_{var}\rangle/\langle\Psi_{var}|n_{-q}n_q|\Psi_{var}\rangle$ - an analog of E_q:

$$0 = \sum_q \psi_i(q) \left\{ \left(E_{var} - E_q^J\right) S^J(q) - \frac{f(q)}{2} \right\}, \text{ for all } 1 \leq i \leq n \qquad \text{(B.5)}$$

Since (B.5) holds for the whole set of functions $\psi_i(q)$ which constitute the complete set of basis functions on a lattice of a given size the only way for (B.5) to hold is that the expression in braces if identically zero. Thus we arrive to:

$$S^J(q) = \frac{f(q)}{2(E_q^J - E_{var})} \qquad \text{(B.6)}$$

which is of the same form as (B.2). We emphasize that the function Φ could be whatever correlated wave function which preserves the number of particles and does

not depend explicitly on Jastrow parameters. It could be, in particular, the BCS wave function, projected on a subspace with fixed number of particles:

$$|\Phi_{BCS}\rangle = P_{\mathrm{N}} \prod_{k} \left(u_k + v_k c^{\dagger}_{k,\uparrow} c^{\dagger}_{-k,\downarrow} \right) |0\rangle \tag{B.7}$$

Therefore the static structure form factor on the variational wave function (B.3) obeys the same kind of relation (B.6) as on the exact wave function (B.2).

Appendix C

Details of calculations of Z and Z_2

In order to calculate Z_2, defined in the real space as

$$Z_2(i-j) \equiv \langle \Psi_{var}(N+2)|c^\dagger_{i,\uparrow}c^\dagger_{j,\downarrow}|\Psi_{var}(N)\rangle, \tag{C.1}$$

within the Variational Monte Carlo, we make use of the particle-hole transformation (2.33), after which the operator $c^\dagger_{i,\uparrow}c^\dagger_{j,\downarrow}$ becomes $\tilde{c}^\dagger_{i,\uparrow}\tilde{c}_{j,\downarrow}(-1)^j$ and conserves the number of particles. The above correlation function should be calculated between the state with $N/2+1$ up and $M-N/2-1$ down and the state with $N/2$ up and $M-N/2$ down spins. We neglect the difference between the variational parameters of the two states and therefore:

$$Z_2(i-j) = (-1)^j \frac{\langle \Psi_{var}(N+2)|\tilde{c}^\dagger_{i,\uparrow}\tilde{c}_{j,\downarrow}|\Psi_{var}(N)\rangle}{\langle \Psi_{var}(N+2)|\Psi_{var}(N+2)\rangle^{\frac{1}{2}}\langle \Psi_{var}(N)|\Psi_{var}(N)\rangle^{\frac{1}{2}}} \tag{C.2}$$

because the wave functions are not normalized. To avoid calculation of normalizations in (C.2) we calculate:

$$\begin{aligned} A(i-j) &= \frac{\langle \Psi_{var}(N)|\tilde{c}^\dagger_{i,\uparrow}\tilde{c}_{j,\downarrow}|\Psi_{var}(N)\rangle}{\langle \Psi_{var}(N)|\Psi_{var}(N)\rangle} \\ B(i-j) &= \frac{\langle \Psi_{var}(N+2)|\tilde{c}^\dagger_{j,\downarrow}\tilde{c}_{i,\uparrow}|\Psi_{var}(N+2)\rangle}{\langle \Psi_{var}(N+2)|\Psi_{var}(N+2)\rangle} \end{aligned} \tag{C.3}$$

so that (C.2) is just the square root of the product of the two:

$$Z_2(i-j) = (-1)^j \sqrt{A(i-j)B(i-j)}. \tag{C.4}$$

During the Monte Carlo sampling of $\Psi_{var}(N)$ it is approximated by the sum of the walkers:

$$|\Psi_{var}(N)\rangle \approx \sum_x |x\rangle\langle x|\Psi_{var}(N)\rangle. \tag{C.5}$$

Hence e.g. $A(i-j)$ is given by:

$$A(i-j) = \sum_x \frac{\langle\Psi_{var}(N)|\tilde{c}^\dagger_{i,\uparrow}\tilde{c}_{j,\downarrow}|x\rangle}{\langle\Psi_{var}(N)|x\rangle} P_x^N, \tag{C.6}$$

where

$$P_x^N = \frac{\langle\Psi_{var}(N)|x\rangle^2}{\sum_{x'}\langle\Psi_{var}(N)|x'\rangle^2}. \tag{C.7}$$

The ratio $\langle\Psi_{var}(N)|\tilde{c}^\dagger_{i,\uparrow}\tilde{c}_{j,\downarrow}|x\rangle/\langle\Psi_{var}(N)|x\rangle$ in (C.6) can be easily calculated: configuration $|x'\rangle \equiv \tilde{c}^\dagger_{i,\uparrow}\tilde{c}_{j,\downarrow}|x\rangle$ differs from $|x\rangle$ by adding an up spin on the site i and removing of a down spin from site j. Therefore we can use standard folmulae to update determinant (see page 28). Jastrow factors, defined as

$$J_N(x) = \exp\left(\frac{1}{2}\sum_{k,l} v(k-l)n_k n_l\right), \tag{C.8}$$

will also contribute to the above ratio:

$$\frac{J_N(x')}{J_N(x)} = \exp\left(\sum_{k\neq i} v(i-k)n_k - \sum_{k\neq j} v(j-k)n_k\right). \tag{C.9}$$

Calculation of $Z(i)$, defined as:

$$Z(i) \equiv \langle\Psi_{var}(N+1)|c^\dagger_{i,\uparrow}|\Psi_{var}(N)\rangle^2, \tag{C.10}$$

is a bit more involved. Here, for convenience we work with spin up electrons. Once again we introduce two quantities:

$$C(i) = \frac{\langle \Psi_{var}(N+1)|c^{\dagger}_{i,\uparrow}|\Psi_{var}(N)\rangle}{\langle \Psi_{var}(N)|\Psi_{var}(N)\rangle}$$
$$D(i) = \frac{\langle \Psi_{var}(N)|c_{i,\uparrow}|\Psi_{var}(N+1)\rangle}{\langle \Psi_{var}(N+1)|\Psi_{var}(N+1)\rangle} \quad . \tag{C.11}$$

so that $Z(i) = C(i)D(i)$. We need to evaluate the overlap between the two wave functions in (C.11): $\langle \Psi_{var}(N+1)|$ and $c^{\dagger}_{k,\uparrow}|\Psi_{var}(N)\rangle$. On every configuration $|x\rangle$, generated in Monte Carlo, we calculate

$$C(i) = \sum_x \frac{\langle \Psi_{var}(N+1)|c^{\dagger}_{i,\uparrow}|x\rangle}{\langle \Psi_{var}(N)|x\rangle} P^N_x, \qquad D(i) = \sum_x \frac{\langle \Psi_{var}(N)|c_{i,\uparrow}|x\rangle}{\langle \Psi_{var}(N+1)|x\rangle} P^{N+1}_x \quad . \tag{C.12}$$

Similarly to the previous case of Z_2, the ratios of the Slater determinants in (C.12) can be easily calculated without evaluation of both determinants. Let us denote as $\{\varphi_j(r)\}$ the orbitals of the above Slater determinants. Then the wave function $|\Psi_{var}(N)\rangle$ will have N lowest orbitals filled with N particles, while $|\Psi_{var}(N+1)\rangle$ will have one more orbital with another particle on it. We denote this extra orbital as $\varphi_{N+1}(r)$.

We consider first the evaluation of $C(i)$. The value of $|\Psi_{var}(N)\rangle$ on a given configuration $|x\rangle$ is given by: $\langle \Psi_{var}(N)|x\rangle = J_N(x) \det S_1$ while $\langle \Psi_{var}(N+1)|x\rangle = J_{N+1}(x) \det S_2$ where

$$S_1 = \begin{pmatrix} \varphi_1(x_1) & \varphi_2(x_1) & \dots & \varphi_N(x_1) \\ \varphi_1(x_2) & \varphi_2(x_2) & \dots & \varphi_N(x_2) \\ \dots & \dots & \dots & \dots \\ \varphi_1(x_{i-1}) & \varphi_2(x_{i-1}) & \dots & \varphi_N(x_{i-1}) \end{pmatrix}$$

and

$$S_2 = \begin{pmatrix} \varphi_1(x_1) & \varphi_2(x_1) & \dots & \varphi_N(x_1) & \varphi_{N+1}(x_1) \\ \varphi_1(x_2) & \varphi_2(x_2) & \dots & \varphi_N(x_2) & \varphi_{N+1}(x_2) \\ \dots & \dots & \dots & \dots & \dots \\ \varphi_1(x_{i-1}) & \varphi_2(x_{i-1}) & \dots & \varphi_N(x_{i-1}) & \varphi_{N+1}(x_{i-1}) \\ \varphi_1(x_i) & \varphi_2(x_i) & \dots & \varphi_N(x_i) & \varphi_{N+1}(x_i) \end{pmatrix}$$

and $J_N(x)$ are the Jastrow functions, as before. The ratio in the first expression of (C.12) is equal to $\det S_2/\det S_1$ times the ratio $J_{N+1}(x)/J_N(x)$, which is merely

$$\frac{J_{N+1}(x)}{J_N(x)} = \exp\left(\sum_{k\neq i} v(i-k)n_k + \frac{1}{2}v(0)\right) \tag{C.13}$$

in this case. Here $v(0)$ is the Gutzwiller variational parameter, while $v(i-k)$, when $k \neq i$ are the Jastrow ones. The two matrices differ by one row and one line, therefore it is clear that during the calculation of determinants one essentially has to do almost the same job twice. To save computational time we express $\det S_2$ in terms of the auxiliary matrix Σ_2:

$$\Sigma_{2kl} = \begin{cases} S_{1kl}, & \text{if} \quad k,l \leq N+1 \\ \varphi_N(x_i) & \text{if} \quad k,l = N+1 \\ 0 & \text{otherwise} \end{cases} \tag{C.14}$$

and

$$S_{2kl} = \Sigma_{2kl} + \delta_{l,N}(1-\delta_{k,i})\varphi_N(x_k) + \delta_{k,i}(1-\delta_{l,N})\varphi_k(x_i). \tag{C.15}$$

One can easily verify, that $\det \Sigma_2 = \det S_1 \varphi_{N+1}(x_i)$ and that

$$\det S_2 = \det S_1 \left(\varphi_N(x_i) - \sum_{k,l}^{N} \varphi_k(x_i) S^{-1}_{2k,l} \varphi_N(x_l)\right). \tag{C.16}$$

This is because $\Sigma_2^{-1} S_2$ is the matrix of rank 2 with two eigenvalues, whose product is

$$\varphi_{N+1}(x_i)^{-1}\left(1 - \sum_{k,l}^{N} \varphi_k(x_i) S^{-1}_{2k,l} \varphi_N(x_l)\right). \tag{C.17}$$

Let us evaluate now $D(i)$. We follow the same strategy as before, but express everything in terms of S_2. For this case we find:

$$\frac{\det S_1}{\det S_2} = \sum_l S^{-1}_{2i,l} \varphi_N(x_l) \tag{C.18}$$

and the ratio of the Jastrow factors:

$$\frac{J_N(x)}{J_{N+1}(x)} = \exp\left(\sum_{k\neq i} -v(i-k)n_k - \frac{1}{2}v(0)\right). \tag{C.19}$$

Bibliography

[1] J. Bardeeen, L. N. Cooper and J. R. Schrieffer Phys. Rev. **108**, 1175 (1957).

[2] L.N. Cooper, Phys. Rev. **104**, 1189 (1956).

[3] P.W. Anderson, Phys. Rev. **110**, 827 (1958); *ibid.* **130**, 439 (1963).

[4] A. B. Migdal, Zh. Experim. i Teor. Fiz. 34, 1438 (1958); (Soviet Phys. JETP 7, 996 (1958)).

[5] G. M. Eliashberg, Zh. Experim. i Teor. Fiz. **38**, 966 (1960) (Soviet. Phys. JETP **11**, 696 (1960)).

[6] B. Batlogg, Phys. Today **44**, No. 6, p.44, (1991).

[7] J. G. Bednortz and K. A. Muller, Z. Phys. **B** - Condensed Matter **64**, 189 (1986).

[8] For a recent review see: T. Timusk and B. Statt, Rep. Prog. Phys. **62**, 61 (1999).

[9] P.W. Anderson, Science **235**, 1196 (1987); G. Baskaran, Z. Zou, and P.W. Anderson, Solid State Comm. **63**, 973 (1987).

[10] J. R. Schrieffer, X. G. Wen and S. C. Zhang, Phys. Rev. B **39**, 11663 (1989).

[11] P. Lee, cond-mat/0307508 and references therein.

[12] J. Schmalian, D. Pines and B. Stojkovic, Phys. Rev. B **60**, 667 (1999).

[13] V. J. Emery, S. A. Kivelson, J. M. Tranquada, Proc. Natl. Acad. Sci. USA **96**, 8814 (1999).

[14] S. Sachdev, Science **288**, 475 (2000); C. Di Castro, L. Benfatto, S. Caprara, C. Castellani and M. Grilli, Physica C **341**, 1715 (2000).

[15] C. C. Tsuei, D. M. Newns, C. C. Chi and P. C. Pattnaik, Phys. Rev. Lett. **65**, 2724 (1990).

[16] D. M. Newns, H. R. Krishnamurthy, P. C. Pattnaik, C. C. Tsuei and C. L. Kane, Phys. Rev. Lett. **69**, 1264 (1992).

[17] P. Brusov, *Mechanisms of High Temperature Superconductivity*, (Rostov State University Publishing, Rostov on Don, 1999).

[18] P. W. Anderson and J. R. Schrieffer, Phys. Today, **44**, June 55, (1991).

[19] C. J. Halboth and W. Metzner, Phys. Rev. B 61, 7364 (2000).

[20] J. Mráz and R. Hlubina Phys. Rev. B **67**, 174518 (2003).

[21] C.-H. Pao and N.E. Bickers, Phys. Rev. B 51, 16310 (1995).

[22] D.F.B. ten Haaf, H.J.M. van Bemmel, J. M. J. van Leeuven, W. van Saarlos and D.M. Ceperley, Phys. Rev. B **51**, 13039 (1995).

[23] C. Gros, Phys. Rev. B **38**, 931 (1988).

[24] E. S. Heeb and T. M. Rice, Europhys. Lett. *27*, 673 (1994).

[25] M. Kohno, Phys. Rev. B *55*, 1435 (1997).

[26] C. T. Shih, Y. C. Chen, H. Q. Lin and T. K. Lee, Phys. Rev. Lett. *98*, 1294 (1998).

[27] H. Kamerling Onnes, *Leiden Comm.* 120b, 122b, 124c (1911).

[28] J. R. Schrieffer, *Theory of Superconductivity*, Benjamin, New-York, (1964).

[29] M. Tinkham, *Introduction to Superconductivity* McGraw-Hill, Inc. (1996).

[30] H. Frölich, Phys. Rev. **79**, 845 (1950).

[31] D. Pines, Phys. Rev. **109**, 280 (1958).

[32] P. G. de Gennes, *Superconductivity in Metals and Alloys,* W. A. Benjamin, New York (1966), reprinted by Addison-Wesley, Reading, MA, 1989, p. 102.

[33] A. Schilling, M. Cantoni, J. D. Guo and H. R. Ott, Nature **363**, 56 (1993).

[34] J.D. Jorgensen Phys. Today **44**, June, 34 (1991).

[35] See e.g. J. M. Tranquada *et al.* Phys. Rev. Lett. **60**, 156 (1988).

[36] G. Burns 1992, *High-Temperature Superconductivity* (Academic. New York).

[37] Yoji Koike, Y. Iwabuchi, S. Hosoya, N Kobayashi and T. Fukase, Physica C **159**, 105 (1989).

[38] S. Hoen et al., Phys. Rev. B **39**, 2269 (1989).

[39] M. K. Crawford et al., Phys. Rev. B **41**, 282 (1990).

[40] J. P. Franck, S. Harker and J. H. Brewer, Phys. Rev. Lett. *71* 283 (1993).

[41] For the review of proves for $d_{x^2-y^2}$ pairing see: D. Pines, Physica **B 199-200**, 300 (1994).

[42] B. Batlogg in *High Temperature Superconductivity, Proc. Los Alamos Symp., 1989*, eds. K.S. Bedell, D. Coffey, D.E. Meltzer, D. Pines, J.R. Schrieffer (Addison-Wesley, Reading Ma, Advanced Book Program, 1990), p.37.

[43] Y. Nakamura and S. Uchida, Phys. Rev. B **47**, 8369 (1993).

[44] H. Ding, T. Yokoya, J.C. Campuzano, T. Takahashi, M. Randeria, M. R. Norman, T. Mochiku, K. Kadowaki and J. Giapinzakis, Nature **382**, 51 (1996).

[45] M. R. Norman, H. Ding, M. Randeria, J.C. Campuzano, T. Yokoya, T. Takahashi, T. Takahashi, T. Mochiku, K. Kadowaki and D.G. Hinks, Nature **392**, 1587 (1998).

[46] V. J. Emery Phys. Rev. Lett. **58**, 2794 (1987).

[47] M. S. Hybertsen, M. Schlüter and N. E. Christensen, Phys. Rev. B **39**, 9028, (1989).

[48] F. C. Zhang and T. M. Rice, Phys. Rev. B **37**, 3759 (1988).

[49] F. C. Zhang and T. M. Rice, Phys. Rev. B **41**, 7243 (1990).

[50] P.W. Anderson, Science **235**, 1196 (1987).

[51] S. Sorella, G. B. Martins, F. Becca, C. Gazza, L. Capriotti, A. Parola, and E. Dagotto Phys. Rev. Lett. **88**, 117002 (2002).

[52] J. Hubbard, Proc. R. Soc. , London, Ser. A **276**, 238 (1963); M. C. Gutzwiller, Phys. Rev. Lett. **10**, 159 (1963); J. Kanamori, Prog. Theor. Phys. **30**, 275 (1963).

[53] S. Bacci, E. Galliano, R. Martin and J. Annett, Phys. Rev. B **44**, 7504 (1991).

[54] E. Dagotto Rev. Mod. Phys. **66**, 763 (1994).

[55] For a review on $t-J$ model see: T.M. Rice, *Strongly interacting Fermions and High T_c Superconductivity*, Les Houches, edited by B. Doucot and J. Zinn-Justin, Elsevier, North Holland (1991).

[56] N. Metropolis, A. W. Rosenbluth, M. N. Rosenbluth, A. H. Teller and E. Teller, J. Chem. Phys. 21, 1087 (1953).

[57] Monte Carlo Methods, v.1, M. H. Kalos, P. Whitlock, (Wiley-Interscience publication, 1986).

[58] D. M. Ceperley and M. H. Kalos, in *Monte Carlo Method in Statistical Physics,* edited by K. Binder (Springer-Verlag, Heidelberg, 1992).

[59] See e. g. M. Calandra Ph. D. Thesis, SISSA, (1999).

[60] H. Yokoyama and H. Shiba J. Phys. Soc. Jpn. **57**, 2482 (1988).

[61] S. Sorella, *et al.* Phys. Rev. Lett. **88**, 117002 (2002).

[62] P. Nozieres and D. Pines, Phys. Rev. **111**, 442 (1958).

[63] F. F. Assaad, M. Imada and D. J. Scalapino, Phys. Rev. B **56**, 15001 (1997).

[64] T. Exkl, E. Arrigoni, W. Hanke and F. F. Assaad, Phys. Rev. B **62**, 12395 (2000).

[65] D. Pines and P. Nozieres, The Theory of Quantum Liquids: Volume I, W. A. Benjamin, New York.(1966).

[66] See e.g. P. B. Allen and B. Mitrovic in Solid State Physics, **37**, 1 (1982).

[67] M. Capone, M. Fabrizio, C. Castellani, and E. Tosatti, Science **296**, 2364 (2002).

[68] A. Paramekanti, M. Randeria, and N. Trivedi, Phys. Rev. Lett. **87**, 217002 (2001).

[69] H. Yokoyama and H. Shiba, J. Phys. Soc. Jpn. **56** 1490 (1987), *ibid.* 3582.

[70] S. Sorella, Phys. Rev. B **64**, 024512 (2001).

[71] We have verified that this variational wavefunction is stable against a spin-density wave order parameter with corresponding magnetic Jastrow factors [69], in the hole doping region we have considered.

[72] P. G. J. van Dongen, F. Gebhard and D. Vollhardt Z. Phys. B **76**, 199(1989).

[73] M. C. Gutzwiller, Phys. Rev. A **137**, 1726(1965).

[74] F. Gebhard, Phys. Rev. B **41**,9452(1990).

[75] W. Metzner and D. Vollhardt Phys. Rev. B **37**,7382(1988).

[76] G. Kotliar and J. Liu, Phys. Rev. B **38**, 5142 (1988); P.A. Lee and X.G. Wen, Phys. Rev. Lett. **78**, 4111 (1997).

[77] F. C. Zhang cond-mat/0209272.

[78] R. B. Laughlin cond-mat/0209269.

[79] P.W. Anderson, *The Theory of Superconductivity in the High-Tc Cuprates* (Princeton University Press, Princeton, NJ, 1997).

[80] N.E. Bickers, D.J. Scalapino and S.R. White Phys. Rev. Lett. **62**, 961 (1989).

[81] A. Neumayr and W. Metzner, Phys. Rev. B 67, 035112 (2003).

[82] A. Georges, G. Kotliar, W. Krauth and M. J. Rozenberg, Rev. Mod. Phys. 68, 13 (1996).

[83] Th. Maier, M. Jarrel, Th. Pruschke and J. Keller, Phys. Rev. Lett. **85**, 1524 (2000).

[84] Gang Su, Phys. Rev. Lett. **86**, 3690 (2001).

[85] T. Huslein *et al.* Phys. Rev. B **54**, 16179 (1996).

[86] S. R. White, D. J. Scalapino, R. L. Sugar, N. E. Bickers and R. T. Scalettar Phys. Rev. B **39**, 839-842 (1989).

[87] S. Zhang, J. Carlson and J. Gubernatis Phys. Rev. Lett. **78**, 4486 (1997).

[88] G. Levine, W. Su and B. Friedman Phys. Rev. B **46**, 8421 (1992).

[89] W. Kohn and J.M. Luttinger, Phys. Rev. Lett. **15**, 525 (1965).

[90] K. Yamaji, T. Yanagisawa, T. Nakanishi, S. Koike, Physica C **304**, 225 (1998).

[91] E. Plekhanov, S. Sorella, M. Fabrizio Phys. Rev. Lett. **90**, 187004 (2003).

[92] F. Becca, Privat communication.

[93] E. Dagotto and J. R. Schrieffer, Phys. Rev. B **43**, 8705-8708 (1991).